Structural Performance of a Novel Sustainable and Demountable Composite Floor System - Recycled Aggregate Concrete-Steel Composite Beam Utilising Demountable Shear Connectors

WANG MINGDA
Chartered Engineer
MSc in Civil Engineering

Submitted in fulfilment of the requirements for the
Degree of Doctor of Philosophy

School of Engineering
College of Science & Engineering
University of Glasgow

March 2025

ABSTRACT

This study examines sustainable construction methods, particularly the reusing of steel beams and the recycling of concrete materials. This study specifically looks at how recycled aggregate concrete (RAC) and demountable shear connectors could be used in composite floor systems, an area that has yet to be looked into enough in the past. The demand for sustainable solutions in the construction sector is rising, and this research responds to that necessity by offering an innovative flooring system that integrates RAC with demountable shear connectors, specifically for application in temporary and short-term leasing structures.

A literature study on concrete microstructure indicated that residual mortar on recycled aggregate alters the interfacial transition zone (ITZ), influencing the mechanical properties of RAC. A review was conducted on the structural uses of RAC, encompassing RAC-filled steel tubes and composite slabs. For the development of the proposed innovative floor system, two types of demountable shear connectors were evaluated, with the bolted type chosen for its practicality. Bondek II was chosen for profiled steel decking because of its benefits and prevalent application in the local market. A study gap was identified: the majority of studies on RAC employ a fixed mix design, altering the percentage of recycled aggregate instead of sustaining a consistent goal concrete strength. This complicates the assessment of whether diminished structural resistance results from the utilisation of recycled aggregates or from a reduction in design strength relative to normal aggregate concrete (NAC). A fixed design strength approach was suggested to provide target strength by augmenting recycled aggregate replacement and diminishing the water-to-cement ratio. The primary scientific challenge is ascertaining the ideal water-to-cement ratio to facilitate recycled aggregates substitution and attain the requisite concrete strength.

Two main tests are proposed. The first assessment is the push-off test, frequently employed to assess the shear behaviour of shear connections. Two categories of push-off specimens have been developed, each comprising four identical geometries, distinguished by shear connector dimensions: M20 and M24. The M20 bolts are positioned in closer proximity to establish a complete connection, whilst

the larger M24 bolts are arranged at greater intervals for a partial connection. The recycled aggregate substitution ratio ranges from 0% to 30%, 70%, and 100%, delineating the four specimen categories. Test results demonstrate that the shear resistance of bolted connectors in RAC increases by up to 40% with a higher proportion of recycled aggregate, corresponding to a lower water-to-cement ratio. Full bending tests were performed to evaluate the overall structural performance of the proposed composite floor system. Five test specimens were produced and classified into two categories according to the size of the shear connectors. The first type employed M20 connectors at 200 mm intervals, aligning with the push-off test, and utilised three concrete mixtures: 0% recycled aggregate (baseline), 30%, and 100% replacement. The second variant employed M24 connectors at 400 mm intervals, adhering to the identical push-off test design, utilising two mixtures: 30% and 100% replacement. Test results indicate that composite beams with bolted connectors provide up to a 10% enhancement in flexural resistance in RAC relative to NAC.

Subsequent to testing, the pertinent codes were employed to compute resistances and juxtapose them with experimental outcomes. EC3 and EC4 appropriately forecasts shear resistance for bolted connectors in NAC but underestimates it in RAC by 16–51%. AISC and ACI provide more precise average projections; nonetheless, they yield unsafe estimates for NAC, underestimating by as much as 13%, and do not reliably identify the failure mode. Both EC4 and AISC accurately forecast the bending resistance of composite sections, with a mere 2% overestimation of NAC resistance. Nonetheless, they underestimate the bending resistance of RAC by as much as 9%, with AISC exhibiting better precision compared to EC4. Furthermore, the findings demonstrate that bending resistance predictions derived from push-off test data closely correspond with experimental bending test outcomes, indicating that push-off tests function as a reliable indirect approach for evaluating bending resistance with enhanced precision.

Table of Contents

ABSTRACT ..... **II**

LIST OF TABLES ..... **VII**

LIST OF FIGURES ..... **VIII**

PREFACE ..... **X**

ACKNOWLEDGEMENT ..... **XII**

AUTHOR'S DECLARATION ..... **XIII**

DEFINITIONS/ABBREVIATIONS ..... **XIV**

SYMBOLS ..... **XV**

1 INTRODUCTION **1**

1.1 BACKGROUND 1

1.2 RESEARCH OBJECTIVES 4

1.3 THESIS OUTLINE 5

2 LITERATURE REVIEW **7**

2.1 INTRODUCTION 7

2.2 RECYCLED AGGREGATE CONCRETE (RAC) 7

2.2.1 Microstructure *7*

2.2.2 Compressive strength *10*

2.2.3 Tensile, splitting tensile and flexural tensile strength *12*

2.2.4 Shear strength *14*

2.2.5 Elastic modulus *15*

2.2.6 Shrinkage and Creep *16*

2.2.7 Structural application *19*

2.3 DEMOUNTABLE SHEAR CONNECTOR 20

2.4 PROFILED STEEL DECKING 23

2.5 SUMMARY 26

3 PROPOSED SUSTAINABLE AND DEMOUNTABLE COMPOSITE FLOOR SYSTEM AND TESTING PLAN **28**

3.1 INTRODUCTION 28

3.2 PROPOSED SUSTAINABLE AND DEMOUNTABLE FLOOR SYSTEM 28

3.2.1 RAC *29*

3.2.2 Shear connectors *29*
3.2.3 Arrangement of shear connectors *33*
3.2.4 Assembling and disassembling *34*
3.2.5 Sustainability and circular economy *37*
3.3 Testing plan and specimen preparation 38
3.3.1 Push-off tests *38*
3.3.2 Four-point bending tests *41*
3.4 Summary 47
4 PUSH-OFF EXPERIMENTS AND NUMERICAL MODELLING 49
4.1 Introduction 49
4.2 Material tests 49
4.2.1 Concrete *49*
4.2.2 Steel *53*
4.3 Push-off tests 56
4.4 Discussion on test results 57
4.4.1 Failure modes *57*
4.4.2 Load-slip curves *66*
4.5 Numerical modelling programme 69
4.5.1 General *69*
4.5.2 Development of FE models *69*
4.5.3 Validation study *77*
4.6 Evaluation on design codes 80
4.6.1 Overview *80*
4.6.2 Evaluation on EN 1994-1-1 (EC4) and EN 1993-1-8 (2005) *81*
4.6.3 Evaluation on ANSI/AISC 360-16 (AISC) and ACI 318-19 (ACI) *85*
4.7 Summary 88
5 EXPERIMENTAL INVESTIGATION AND ANALYSIS OF FULL-SCALE BENDING TEST 89
5.1 Introduction 89
5.2 Full-scale four-point bending tests 89
5.3 Discussions on test results 92
5.3.1 Failure modes *92*
5.3.2 Load-deflection curves *95*
5.3.3 Slips *97*

5.3.4 Strain distributions *102*
5.3.5 Demountability *108*
5.4 EVALUATION ON DESIGN CODES 111
5.4.1 Overview *111*
5.4.2 Degree of connection *111*
5.4.3 Flexural resistance *112*
5.5 SUMMARY 116
6 CONCLUSIONS AND SUGGESTIONS FOR FUTURE WORK 117
6.1 CONCLUSIONS 117
6.2 SUGGESTIONS FOR FUTURE WORK 120
LIST OF REFERENCES 122

List of Tables

TABLE 3.1 SPECIFICATIONS OF PUSH-OFF TEST SPECIMENS AND TEST RESULTS 41
TABLE 3.2 DESIGN DETAILS OF COMPOSITE BEAM SPECIMENS 46
TABLE 4.1 PROPORTIONS OF CONCRETE MIXTURES (UNIT: KG/M^3) 51
TABLE 4.2 SUMMARY OF 7 DAYS AND 28 DAYS CONCRETE COMPRESSIVE STRENGTH 51
TABLE 4.3 KEY MATERIAL PROPERTIES OF CONCRETE 53
TABLE 4.4 MATERIAL PROPERTIES MEASURED FROM TENSILE COUPON TESTS 54
TABLE 4.5 DESIGN DETAILS OF PUSH-OFF TEST SPECIMENS AND TEST RESULTS 67
TABLE 4.6 MESH SIZE SUMMARY 75
TABLE 4.7 COMPARISON OF TEST FAILURE LOADS AND MODES WITH PREDICTED RESULTS FROM EN 1994-1-1 (2004) AND EN 1993-1-8 (2005) 84
TABLE 4.8 COMPARISON OF TEST FAILURE LOADS AND MODES WITH PREDICTED RESULTS FROM ANSI/AISC 360-16 (2016) AND ACI 318-19 (2019) 87
TABLE 5.1 KEY MATERIAL PROPERTIES OF CONCRETE 89
TABLE 5.2 FOUR-POINT BENDING TEST RESULTS 97
TABLE 5.3 COMPARISON OF TEST FAILURE LOADS WITH PREDICTED RESULTS FROM EN 1994-1-1 (2004) 114
TABLE 5.4 COMPARISON OF TEST FAILURE LOADS WITH PREDICTED RESULTS FROM ANSI/AISC 360-16 (2016) 114
TABLE 5.5 COMPARISON OF TEST FAILURE LOADS WITH PREDICTED RESULTS FROM PUSH-OFF TESTS 115

List of Figures

FIG. 1.1 INTERIOR WALLS WITH RAC 2
FIG. 2.1 INTERFACIAL TRANSITION ZONE 8
FIG. 2.2 MICROSTRUCTURE OF RAC PREPARED WITH RECYCLED AGGREGATE 9
FIG. 2.3 RECYCLED AGGREGATE CONTENT VS COMPRESSIVE STRENGTH 11
FIG. 2.4 RECYCLED AGGREGATE CONTENT VS UNIAXIAL TENSILE STRENGTH 12
FIG. 2.5 RECYCLED AGGREGATE CONTENT VS SPLITTING TENSILE STRENGTH 13
FIG. 2.6 RECYCLED AGGREGATE CONTENT VS FLEXURAL TENSILE STRENGTH 14
FIG. 2.7 RECYCLED AGGREGATE CONTENT VS SHEAR STRENGTH 15
FIG. 2.8 RECYCLED AGGREGATE CONTENT VS ELASTIC MODULUS 16
FIG. 2.9 RECYCLED AGGREGATE CONTENT VS DRYING SHRINKAGE 17
FIG. 2.10 RECYCLED AGGREGATE CONTENT VS SHRINKAGE DEFORMATION RELATIVE TO CONCRETE AGE 17
FIG. 2.11 RECYCLED AGGREGATE CONTENT VS CREEP DEFORMATION 18
FIG. 2.12 RECYCLED AGGREGATE CONTENT VS CREEP DEFORMATION RELATIVE TO CONCRETE AGE 18
FIG. 2.13 DIFFERENT TYPE OF DEMOUNTABLE CONNECTORS 21
FIG. 2.14 DIFFERENT GEOMETRIC VARIATIONS OF PROFILED STEEL DECKING 24
FIG. 2.15 THREE COMMON TYPES OF PROFILED STEEL DECKING 26
FIG. 3.1 PROPOSED FLOOR SYSTEM 28
FIG. 3.2 NELSON DEMOUNTABLE SHEAR CONNECTOR 30
FIG. 3.3 BOLTED SHEAR CONNECTOR 33
FIG. 3.4 DECKING WITH PREDRILLED HOLES 34
FIG. 3.5 STEEL BEAM WITH PREDRILLED HOLES ON TOP FLANGE 35
FIG. 3.6 NUT PRE-TACK WELDED UNDER THE TOP FLANGE OF THE STEEL BEAM 35
FIG. 3.7 NUT FASTENED ONTO THE PROFILED DECKING WITH WASHER IN BETWEEN 36
FIG. 3.8 REMOVE NUT FROM BEAM FLANGE SIDE 36
FIG. 3.9 DISASSEMBLE THE STEEL BEAM FROM CONCRETE SLAB 37
FIG. 3.10 GEOMETRIC DIMENSIONS OF PUSH-OFF TEST SPECIMENS 40
FIG. 3.11 DETAILS OF PROFILED STEEL DECKING – 1 MM-THICK LYSAGHT® BONDEK® II (UNIT: MM) 40
FIG. 3.12 GEOMETRIC DIMENSIONS OF TYPICAL COMPOSITE BEAM SPECIMENS 42
FIG. 3.13 DETAILS OF STEEL BEAM – UB203×133×30 (UNIT: MM) 43
FIG. 3.14 REINFORCEMENT BAR AND DEMOUNTABLE CONNECTOR DETAILING OF COMPOSITE BEAM SPECIMENS (UNIT: MM) 43

FIG. 3.15 BOLTED CONNECTOR 45
FIG. 4.1 NAC 28 DAYS CUBE FAILURE MODE 52
FIG. 4.2 RAC 28 DAYS CUBE FAILURE MODE 52
FIG. 4.3 CONCRETE CYLINDER TEST 53
FIG. 4.4 TENSILE COUPON TEST SETUP 54
FIG. 4.5 STEEL MATERIAL STRESS-STRAIN CURVES 55
FIG. 4.6 PUSH-OFF TEST SETUP 56
FIG. 4.7 FAILURE MODES OF COMPOSITE BEAM SPECIMENS 65
FIG. 4.8 DEFORMED CONNECTORS 66
FIG. 4.9 LOAD–SLIP CURVES OF PUSH-OFF SPECIMENS 68
FIG. 4.10 FE MODEL 70
FIG. 4.11 CONCRETE MATERIAL STRESS-STRAIN CURVES 73
FIG. 4.12 COUPLING CONSTRAINT ASSIGNED 74
FIG. 4.13 MESH SUMMARY 76
FIG. 4.14 MESH SENSITIVITY ANALYSIS 76
FIG. 4.15 TEST AND FE FAILURE MODES 79
FIG. 4.16 TEST AND FE LOAD–SLIP CURVES 80
FIG. 5.1 COMPOSITE BEAM FOUR-POINT BENDING TEST SETUP 90
FIG. 5.2 LOCATIONS OF STRAIN GAUGES ACROSS THE MID-SPAN BEAM SECTION 91
FIG. 5.3 FAILURE MODES OF COMPOSITE BEAM SPECIMENS 95
FIG. 5.4 LOAD–MID-SPAN DEFLECTION CURVES OF COMPOSITE BEAM SPECIMENS 96
FIG. 5.5 LOAD–SLIP CURVES OF COMPOSITE BEAM SPECIMENS 100
FIG. 5.6 MID-SPAN DEFLECTION–SLIP CURVES OF COMPOSITE BEAM SPECIMENS 101
FIG. 5.7 LOAD-STRAIN CURVES OF COMPOSITE BEAM SPECIMENS 105

Preface

In recent years, industries worldwide have been increasingly focused on environmental protection, energy conservation, and recycling, and the construction industry is no exception. Living in Singapore, a city-state with a thriving construction sector yet severely limited resources, I have witnessed firsthand the challenges posed by our reliance on imported building materials. The construction workforce primarily consists of foreign labour, and essential materials for concrete production, such as sand, aggregate, and steel, must be imported. Political factors in neighbouring countries can sometimes restrict the export of sand and gravel to Singapore, prompting the government to advocate for substituting and reusing building materials.

Among these alternatives, recycled aggregate has been recognised as a valuable resource. The rapid development of real estate in Singapore, coupled with its limited land area, has led to the premature demolition of many buildings that do not reach their design lifespan, providing a substantial source to produce recycled aggregate.

With a decade of experience in structural design and seven years in technical management within the construction sector, I have observed contractors' reluctance to use shear studs in steel structures, particularly for temporary constructions. Despite being a common and effective connection method, shear studs create a strong bond between the concrete slab and the steel beam. This can lead to challenges when it becomes necessary to dismantle these temporary structures within a few years, as the shear studs inhibit the reuse of the steel beams. This situation often results in increased overall costs.

This observation sparked my interest in exploring demountable shear studs, which can reduce the required steel dimensions while ensuring the repeated reuse of materials. My research has shown that I am not alone in this pursuit; many researchers have investigated similar concepts. However, there is a notable gap in studies addressing using RAC in demountable composite beams. This gap highlighted the need for further exploration.

Fortunately, I received funding support from the Singapore Economic Development Board and an opportunity to conduct my research at the University of Glasgow's Singapore campus, allowing me to turn my ideas into reality. Unlike those who began their PhD studies immediately after graduation, my extensive practical experience has influenced my research approach, prioritizing engineering applications. This background has led me to explore unique aspects that diverge from previous studies, resulting in findings not previously addressed in the literature. While others may have reached similar conclusions, they might not have recognised their significance, whereas I have come to appreciate their practical implications. I hope the conclusions drawn from this research will provide a solid foundation for applying the structural forms mentioned earlier.

Acknowledgement

First and foremost, I would like to express my sincere gratitude to the Singapore Economic Development Board for their funding and to the University of Glasgow for offering me this invaluable opportunity to pursue a PhD after over a decade of work experience. I also sincerely appreciate my company, China Jingye Engineering Corporation Limited (Singapore Branch), for allowing me to pursue PhD studies while maintaining my full-time job.

I extend my heartfelt thanks to my two supervisors, Professor Liang Yating and Professor Peter Grassl, who have provided unwavering guidance and support over the past four years. Their mentorship has taught me to approach problems with a research-oriented and exploratory mindset, enabling me to analyse issues, devise solutions, and draw insightful conclusions.

Additionally, I would like to express my gratitude to Professor Zhao Ou, Doctor Jiang Ke, and Shi Yuxiao at Nanyang Technological University (NTU). As the University of Glasgow's Singapore campus lacked the necessary facilities for laboratory experiments and finite element analysis software, their generous assistance allowed me access to NTU's laboratories and analytical software. This great help enabled me to conduct experiments and numerical simulations during valuable time slots.

Finally, I would like to express my heartfelt appreciation to my wife. During my absences after work and over the weekends due to PhD study, she has taken care of our two children and guided their studies alone. Without the support and companionship of my family, I may not have been able to persevere to the end.

Author's Declaration

I declare that, except where explicit reference is made to the contribution of others, that this dissertation is the result of my own work and has not been submitted for any other degree at the University of Glasgow or any other institution.

Printed Name: WANG MINGDA

Signature:

Definitions/Abbreviations

CFST	Concrete-Filled Steel Tube
C-H	Calcium Hydroxide
C-S-H	Calcium Silicate Hydrate
COV	Coefficient of Variation
FEM	Finite Element Method
ITZ	Interfacial Transition Zone
LVDT	Linear Variable Displacement Transducer
NAC	Natural Aggregate Concrete
RAC	Recycled Aggregate Concrete
RACFST	RAC-filled steel tube
RACFSST	RAC-filled stainless-steel tube
SSD	Saturated Surface Dry condition for aggregates
SG	Strain Gauge

Symbols

f_{cu}	concrete compressive cube strength
f_c	concrete compressive cylinder strength
E_{cm}	secant modulus
E	elastic modulus / Young's modulus
$\sigma_{0.2}$	0.2% proof strength
$E_{0.2}$	0.2% elastic modulus
σ_u	ultimate strength
ε_u	corresponding ultimate strain
ε_f	fracture strain
P_u	ultimate load per connector in push-off test
δ_u	corresponding ultimate slip in push-off test
σ_{nom}	engineering stress
ε_{nom}	engineering strain
σ_{ub}	ultimate strength of bolt
ε_{ub}	ultimate strain of bolt
σ_{true}	true stress
ε_{ln}^{pl}	true plastic strain
$P_{Rd,S}$	steel shear resistance per connector
$P_{Rd,C}$	concrete shear resistance per connector
k_t	reduction factor on connector design shear resistance due to profiled steel decking
n_r	number of connectors
b_0	minimum pan width
h_p	rib height
h_{sc}	connector height
V_b	basic concrete breakout strength
c_{a1}	concrete edge distance
A_{vc}	projected area for the anchor
$\psi_{ed,V}$	breakout edge effect factor
$\psi_{c,V}$	breakout cracking factor
$\psi_{h,V}$	breakout thickness factor
N_y	yield loads in bending test
δ_y	corresponding mid-span deflections under yield loads

N_u	ultimate loads in bending test
δ_u	corresponding ultimate mid-span deflections in bending test
M_u	ultimate moment in bending test
η_{pred}	degree of shear connection
$V_{b,pred}$	shear resistance of an individual bolted shear connector
V_s	minimum of the maximum possible tensile resistance of the steel beam and the maximum possible compression resistance of concrete slab
A_s	gross cross-sectional area of the steel beam
b_{eff}	effective width of the concrete slab
h_c	thickness of the composite slab
M_{pred}	plastic moment resistance of a composite beam
T_s	tensile resistance of the steel beam
h	depth of the steel beam
x_c	depth of the plastic neutral axis (PNA) to the most compressed fibre of the concrete slab
C_c	compressive resistance of the concrete slab
T_s	tensile resistance of the steel beam
x_c	depth of the concrete compressive stress block
C_s	resistance of the steel beam top flange in compression
x_s	corresponding depth of the PNA to the top of the flange
y_s	distance from the bottom of the steel section to the centroid of the steel section in tension
$M_{pred,S}$	flexural resistance of a composite beam predicted by simplified method

1 INTRODUCTION

1.1 Background

As the focus on the implementation of the 3Rs (Reduce, Reuse, Recycle) in building and demolition waste intensifies, the construction sector adopts waste recycling to enhance environmental stewardship and resource efficiency. Concrete is the most utilised man-made construction material worldwide, often consisting of 40 to 50% coarse aggregate by total weight. Coarse aggregate is obtained from natural resources by rock mining or riverbed dredging. Each year, the construction sector consumes significant quantities of natural aggregates, leading to the exhaustion of raw materials and the degradation of ecosystems. The limitation of land and resources is a reality, particularly in a small nation like Singapore. It is imperative for industry to optimise limited resources. Therefore, Singapore's construction sector is advocating for the reduction of natural aggregate usage and the promotion of material circularity, such as recycled concrete aggregates, by stipulating the pertinent conditions in the green building certification scheme. Recycled concrete aggregates, a type of sustainable construction material, are produced from crushed concrete sourced from demolition waste. Recycled aggregate concrete is characterised by the partial or complete replacement of natural coarse aggregates with recycled coarse aggregates (Brito & Saikia, 2013; Tam et al., 2021; Neves & Brito, 2022). Nevertheless, recycled aggregate concrete (RAC) exhibits diminished strength, stiffness, and ductility compared to natural aggregate concrete (NAC), attributable to the significantly inferior mechanical properties of recycled aggregates resulting from physical and chemical degradation during the recycling process (Xiao et al., 2005; Tam et al., 2018; Guo et al., 2018), thereby limiting the application of RAC in structural (load bearing) elements of buildings and bridges. Fig. 1.1 (Betonwerk Büscher 2023) shows typical applications of RAC in non-structural elements.

Fig. 1.1 Interior walls with RAC

Although RAC's mechanical limitations restrict its widespread use in load-bearing structures, RAC may find its application in temporary building structures (<3 years) and short-lease building structures (<30 years), which typically call for lower design loads and lower durability requirements than permanent structures with longer lease. The floor system commonly used in these temporary and short-lease structures is the concrete-steel composite beam with a reinforced concrete slab and a series of shear connectors. This composite floor system features a reinforced concrete slab positioned atop a steel beam, laterally restrained by shear connectors to avert lateral-torsional buckling of the steel beams and facilitate composite action between the reinforced concrete slab and the steel beam. For a composite beam with a moderate-to-thick slab thickness under sagging bending, the neutral axis typically resides within the reinforced concrete slab due to the substantial cross-sectional compressive resistance of the slab in comparison to the tensile strength of the steel beam. Accordingly, only the top layer of the slab may experience a relatively high stress level, with the remaining layers lightly loaded. Therefore, the RC slab in temporary and short lease building structures is an ideal structural component for promoting the application of RAC.

Typically, the implementation of the composite floor system in building construction requires the satisfaction of the following criteria:

- Strength Requirements: The flooring system must withstand dead loads (self-weight, finishes, etc.) and live loads (occupants, furniture,

equipment, etc.) without failure. In steel-concrete composite systems, shear connections must ensure sufficient composite action.

- Deflection Limits Serviceability Criteria: Deflection limits are established to avert excessive sagging or discomfort. L/360 for live loads (e.g., flooring in residential structures). L/240 for total loads (including both dead and live loads).
- Vibration Performance: Floors must exhibit low detectable vibrations, especially in workplace and home environments. The fundamental frequency of the floor should generally exceed 4 Hz to ensure human comfort.
- Fire Resistance: Floors must comply with fire resistance ratings as stipulated by applicable codes. This can be achieved through minimal slab thickness, concrete cover and fire-resistant materials (e.g., vermiculite or intumescent coatings).
- Durability: The steel components must be safeguarded against corrosion using methods such as galvanisation or coatings.

The technical challenges of using RAC in structural applications stem from the varying sources and quality of the recycled aggregate produced. Therefore, in a local context, to promote recycled aggregate, SS EN 12620 and BS 8500 encompass a broad spectrum of aggregates, including recycled aggregates, with stipulations for both utilisation and testing requirements. The properties of concrete materials often diminish due to the residual mortar attached to recycled aggregates; thus, it is crucial to modify the design mix by employing a lower water-to-cement ratio to preserve the intended concrete strength.

In order to effectively use concrete-steel composite beams in temporary and short-lease structures, the design of the composite beam should allow for easy assembly and disassembly on site. In conventional composite steel floor construction, welded shear studs are commonly adopted to provide lateral constraints between the concrete slab and the steel beam. However, during the demolition process, it is difficult to remove the RC slab from the steel beam whilst maintaining the intactness of the steel beam, hence hindering the re-utilisation of steel beams.

To facilitate the reuse of the steel beam, demountable shear connectors may be used to replace the conventional welded shear studs in the composite floor system. At the assembling stage, the shear connector needs to be installed onto the steel beam with ease to provide horizontal shear resistance. While at the disassembling stage, the shear connector will be demounted with little effort, allowing the entire slab to be uplifted and removed from the steel beam without damage.

This study proposes a novel sustainable and demountable concrete-steel composite floor system—RAC–steel composite beams utilising demountable shear connectors. The proposed sustainable and demountable concrete-steel composite floor system will significantly save resources and reduce carbon emissions.

1.2 Research objectives

This study aims at exploring the structural behaviour of composite beams that combine RAC with demountable shear connectors, offering a more sustainable and flexible solution for temporary and short-lease structures.

The primary aims of the research are:

- To examine the shear resistance, stiffness, and failure mechanisms of demountable shear connections in RAC by push-off tests.
- To assess the ultimate bending resistance and deflection performance of these composite beams by full-scale bending tests.
- To evaluate the influence of different ratios of recycled aggregate in a uniform-grade concrete on mechanical properties and overall structural performance, in comparison to NAC.
- To validate experimental results by finite element numerical modelling, analyse correlations with real performance and compare findings against current design codes (EC3, EC4, AISC and ACI) to assess compliance with structural standards.
- To assess the sustainability benefits, life cycle effectiveness, and reusability potential of RAC-steel composite beams including demountable

shear connectors, hence promoting circular economy activities in construction.

This research presents three unique innovations and significant contributions:

- This study differs from most researchers who analyse recycled RAC by keeping a constant design mix while altering the recycled aggregate replacement ratio, which leads to variable concrete design strength; instead, it focusses on more practical situations found in real engineering applications. It determines a constant concrete design strength by modifying the water-to-cement ratio in the concrete mix, facilitating a more accurate assessment of resistance fluctuations concerning the recycled aggregate replacement ratio.
- The push-off tests are adapted from EC4, which used a solid slab, and may not accurately forecast concrete failure due to the restricted edge distance resulting from the utilised profiled steel decking. Thus, the same profiled decking used in the composite beam bending test has been applied, facilitating a more accurate evaluation of push-off results alongside bending data that maintain similar concrete boundary conditions.
- Both full and partial degrees of connection are analysed to efficiently address potential occurrences in engineering applications, particularly as fewer shear connectors are preferred for simplicity of demountability.

The outcome of this research will enhance understanding of how RAC, combined with demountable shear connectors, can be effectively used in structural applications without compromising mechanical performance. Furthermore, this study will help fill the existing knowledge gap regarding the application of RAC with designed compression strength rather than fixed water-to-cement ratio with designed recycled aggregate replacement percentages.

1.3 Thesis outline

Chapter 1 presents the context and justification for this research, focusing on the potential applications of recycled aggregate concrete (RAC) and demountable

shear connectors in composite beams. The research aims, scope and structure of the thesis are delineated.

Chapter 2 provides a comprehensive literature review, covering prior studies on RAC, various types of demountable shear connectors, and their respective applications. The chapter identifies key research gaps in the integration of RAC and demountable shear connectors, highlighting the need for further investigation.

Chapter 3 outlines the experimental testing plan for push-off tests and four-point bending tests. It includes details on the proposed material parameters, specimen sizes and the specimen preparation process.

Chapter 4 presents the experimental and numerical investigations on push-off tests, conducted on symmetric RAC slabs connected to central steel beams using demountable shear connectors. The study explores the cross-sectional resistance and structural behaviour of the connectors in RAC. The accuracy of codified design rules is also assessed using both experimental and numerical results.

Chapter 5 details the experimental investigation on the four-point bending behaviour of full-scale composite beams utilising RAC and demountable shear connectors. The study evaluates the bending resistance and overall structural performance of the composite system. The validity of design codes in predicting the ultimate bending resistance is critically examined.

Chapter 6 summarises the key findings and contributions in this research. Recommendations for future work on RAC-composite beams with demountable shear connectors are also provided, emphasizing areas where further research could be conducted to enhance understanding and application.

2 LITERATURE REVIEW

2.1 Introduction

This chapter provides an extensive review of prior studies on recycled aggregate concrete (RAC), demountable shear connectors and their structural applications. The review commences with an examination of the microstructural characteristics and mechanical properties of RAC, followed by an overview of structural components utilising RAC. Subsequently, different types of demountable shear connectors and their effectiveness in composite beams are reviewed, and various shapes of profiled steel decking and its application in composite floor systems are summarised. Finally, the review culminates synthesising findings, highlighting key observations and identifying existing research gaps.

2.2 Recycled aggregate concrete (RAC)

2.2.1 Microstructure

Before reviewing the microstructure of RAC, it is essential to understand the microstructure of NAC. NAC is the conventional concrete produced using crushed stone, sand and gravel from nature. The composition consists of three primary phases: cement paste, aggregate, and the interfacial transition zone (ITZ), as shown in Fig. 2.1 (Mehta & Monteiro, 2006).

The ITZ is typically a 10-50 micrometre thick zone surrounding aggregate particles. In this region, the structure of the cement paste differs significantly from the one of the bulk paste, particularly exhibiting low density, high porosity, and reduced stiffness and strength， as summarised by Chen et al. (2024). This variation arises from the inadequate packing of cement particles around the aggregates, commonly referred to as the "wall effect." Consequently, the ITZ exhibits a higher local water-to-cement ratio, which can be further exacerbated by localised bleeding during hydration.

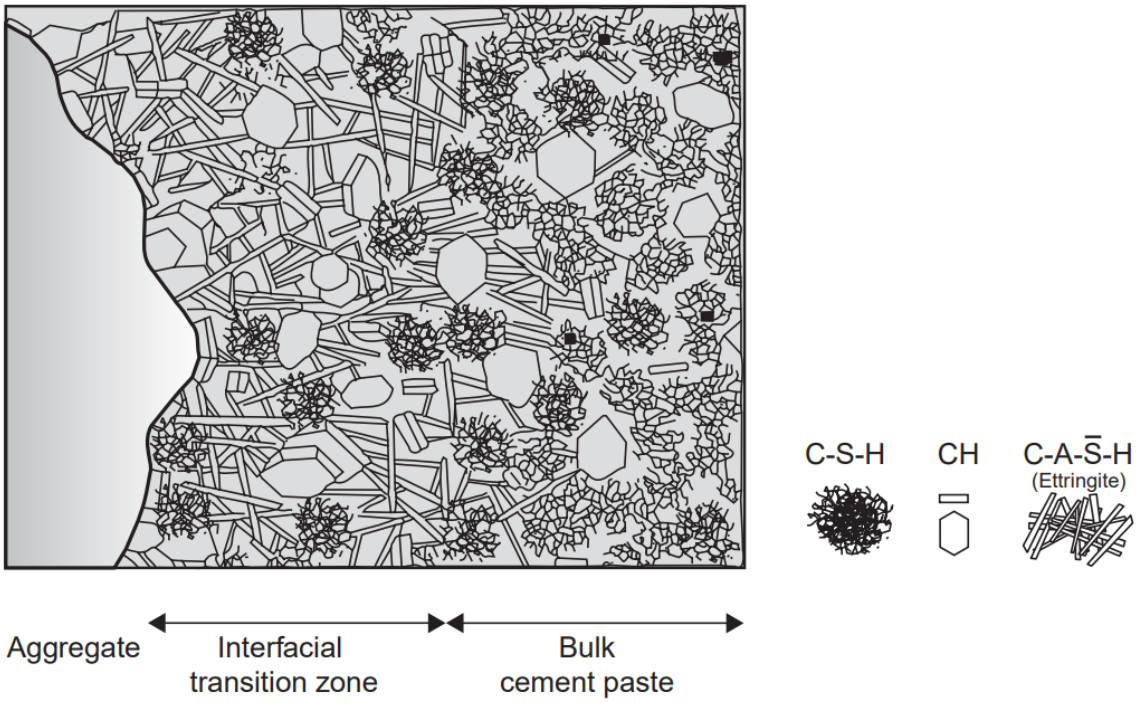

Fig. 2.1 Interfacial Transition Zone

The characteristics of the ITZ include:

- Less un-hydrated cement: The ITZ has a lower quantity of unreacted cement particles compared to the bulk paste.
- Higher porosity: The ITZ is more porous, potentially impacting the overall durability of the concrete.
- Lower density: This phase is less dense than both the bulk paste and the aggregate.
- Reduced calcium silicate hydrate (C-S-H): There is a decrease in the quantity of C-S-H, which is critical for strength development in concrete.
- Increased concentration of oriented crystals: The ITZ contains a greater concentration of oriented calcium hydroxide (CH) and ettringite crystals.

The interfacial porosity in the ITZ creates interconnected microporosity, which will significantly influence the permeability of concrete. The elevated porosity enhances water movement and stress concentration, hence expediting creep and shrinkage. In NAC, the ITZ typically exhibits lower crack resistance compared to the other phases, making it more prone to fracture. This weak link within the concrete matrix often results in lower overall strength and enhanced transport properties, leading to diminished durability.

RAC is made of recycled coarse aggregate and cement paste. In contrast to the natural aggregate, the recycled aggregate contains traces of past cement mortar, as the recycling process is unable to completely eliminate the cement mortar from the recycled aggregate's surface. Xiao et al. (2012a) summarised that the microstructure of RAC typically shows two layers of ITZ: an older ITZ resulting from the adhered previous cement mortar and a newer ITZ established between the recycled aggregate and the fresh cement paste, as illustrated in Fig. 2.2. The study by Etxeberria et al. (2006) showed that more than 50% of recycled aggregate retained residual cement mortar, resulting in the formation of the new ITZ between the fresh cement paste and aggregate, as well as between the fresh cement paste and the residual cement mortar. At locations where the new cement paste bound onto the past cement mortar, there were two layers of ITZ: the original ITZ between the aggregate and the residual cement mortar and the new ITZ between the residual cement mortar and fresh cement paste.

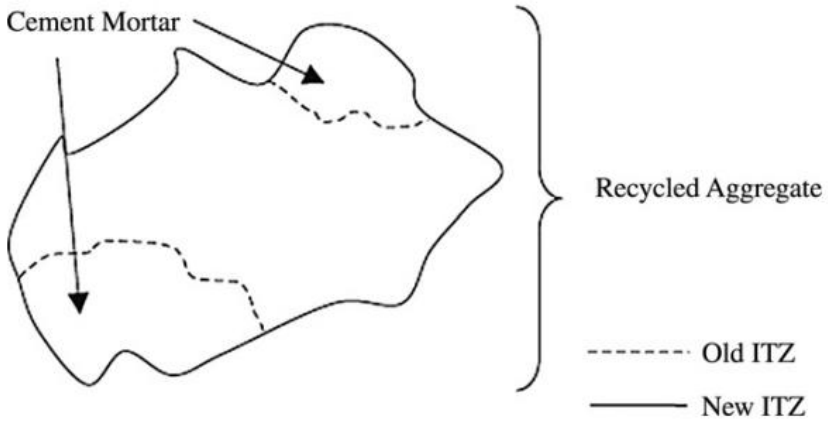

Fig. 2.2 Microstructure of RAC prepared with recycled aggregate

The key feature differentiating RAC from NAC at the microstructural level is the two-layered ITZ. This two-layered ITZ influences the overall mechanical resistance and durability of the structure. The mechanical properties of the newly developed ITZ between the residual cement mortar and new cement paste are greatly influenced by those of the residual cement mortar and the previous ITZ. According to Chen et al. (2024), the ITZ is frequently regarded as the most vulnerable area in concrete, acting as the principal region for crack initiation and propagation, and is susceptible to stress concentrations. In contrast to NAC, RAC has two layers of ITZ, leading to a higher prevalence of ITZ inside a specific volume of concrete, which results in an increased number of weak zones. The characteristics of residual cement mortar are not influenced by the new concrete mix design but are significantly affected by the parent concrete mix design. Etxeberria et al.

(2006) discovered that, in most cases, the aged mortar has weaker mechanical properties than the new paste. In the conclusion of this research, the weakest part in the RAC is either along the recycled aggregate's old ITZ or at the portion cutting through the attached old mortar. In another research, Du et al. (2010) found that the weakest part is between the recycled aggregate and new cement paste instead, i.e. the new ITZ. The different conclusions drawn in the above-mentioned studies could be attributed to recycled aggregate's parent concrete quality. In Etxeberria et al.'s (2016) study, the grade of the parent concrete used for the recycling process was unknown. In Du et al.'s (2010) study, the parent concrete has an original concrete strength grade of C50, taken from the airport runway. Moreover, the experimental findings from Liu et al. (2011) indicate that the new cement mortar significantly influences the strength and elastic modulus of RAC more than the aged mortar attached to the recycled aggregate.

2.2.2 Compressive strength

Recycled aggregate obtained from lower-quality parent concrete can produce higher-grade concrete. The compressive strength of RAC is primarily determined by the water-to-cement ratio of the new design mix. In contrast, the strength of the parent concrete from which the recycled aggregate was produced has only a minor influence (Sri Ravindrarajah and Tam, 1985). Xiao et al. (2012a) reviewed the experimental studies on RAC in China from 1996 to 2011. It was found that for a given water-to-cement ratio, the compressive strength of RAC generally diminishes as the proportion of the recycled aggregate increases. The loss in compressive strength is negligible when the recycled aggregate replacement ratio is below 30% of the total coarse aggregate. The utilisation of 100% recycled aggregate may results in a reduction in the compressive strength of RAC by up to 20% compared to the control mix, as illustrated in Fig. 2.3. Exteberria et al. (2007) conducted an experimental analysis of the mechanical properties of concrete mixtures with 0%, 25%, 50%, and 100% recycled aggregate replacement and drew similar conclusions. In their study, the compressive strength showed negligible variation from 0% to 25% recycled aggregate for a specific water-to-cement ratio of 0.55. However, to maintain an equivalent compressive strength of 38MPa for mixes with 50–100% recycled aggregate, the water-to-cement ratio needed to be reduced by 4–10% (to 0.52 and 0.50, respectively). In the absence of this

correction, the compressive strength of the 100% recycled aggregate mixture was noted to diminish by 20–25%. Similarly, the research by Padmini et al. (2009) revealed that to attain equivalent compressive strength ranging from 21 MPa to 45 MPa, RAC requires a reduced water-to-cement ratio, and an increased cement content compared to NAC.

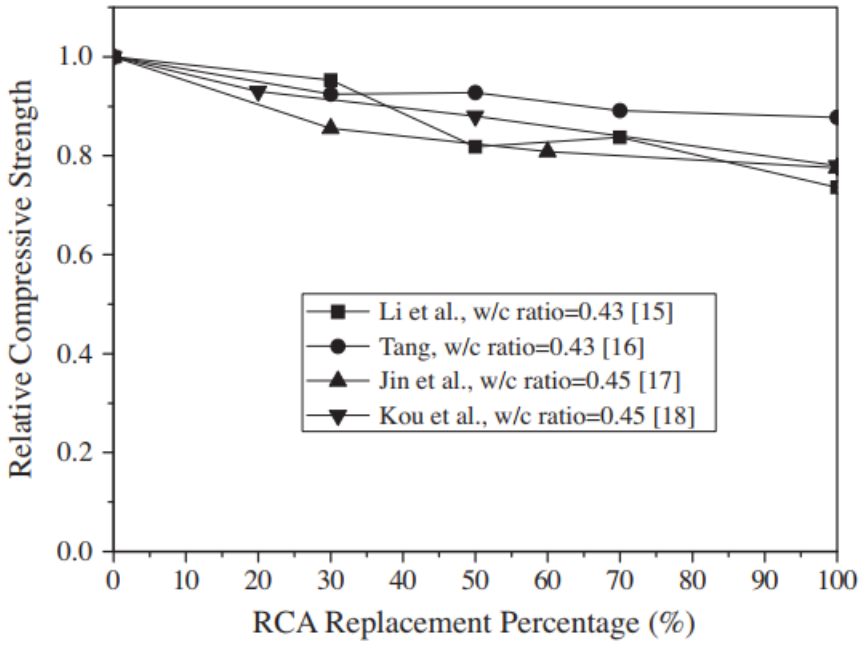

Fig. 2.3 Recycled aggregate content vs compressive strength

In the experimental study conducted by Yong and Teo (2009), they compared the compressive strengths of three concrete mixes, all with a water-to-cement ratio of 0.41: i) 100% natural aggregate, ii) 50% natural aggregate and 50% recycled aggregate, and iii) 100% recycled aggregate. Their test results indicated that compared with NAC, the mix with 50% recycled aggregate replacement exhibits a lower 3-day strength but a comparable strength afterwards. The mix with 100% recycled aggregate replacement achieved a higher early-stage compressive strength (40.24 MPa at 3 days and 57.99 MPa at 28 days) until 42 days, after which the compressive strength became slightly lower than the NAC. Topcu & Sengel (2004) found that the cylinder strength for RAC with 100% recycled aggregate substitution is 23.5% and 33% lower than NAC in the grade of C16 (water-to-cement ratio 0.64) and C20 (water-to-cement ratio 0.57), respectively.

2.2.3 Tensile, splitting tensile and flexural tensile strength

Only a few research investigations have concentrated on examining the uniaxial tensile strength of RAC. Xiao et al. (2012a) noted that the tensile strength of RAC parallels its compressive strength; as the proportion of recycled aggregate rises, the tensile strength diminishes. At a 100% recycled aggregate replacement, the tensile strength is roughly 30% inferior to that of NAC. Liu et al. (2011) found that the uniaxial tensile strength of RAC was similar to that of NAC, as illustrated in Fig. 2.4.

Xiao et al. (2012a) concluded that the trend of splitting tensile strength in RAC parallels that of its compressive strength: an increased replacement ratio of recycled aggregate correlates with a decrease in splitting tensile strength. Fig. 2.5 illustrates that a 100% replacement results in approximately a 30% reduction in splitting tensile strength. The test results of Yong and Teo (2009) indicated that the effect of recycled aggregate content on splitting tensile strength follows a similar trend to that on compressive strength; specifically, the split tensile strength of RAC with a 50% recycled aggregate replacement is equivalent to that of natural NAC at 4.5 MPa. The split tensile strength of RAC with a 100% recycled aggregate replacement is 5 MPa at 28 days, going above that of NAC. Padmini et al. (2009) stated that, for any specified compressive strength of concrete, the splitting tensile strength of RAC is inferior to that of the original concrete.

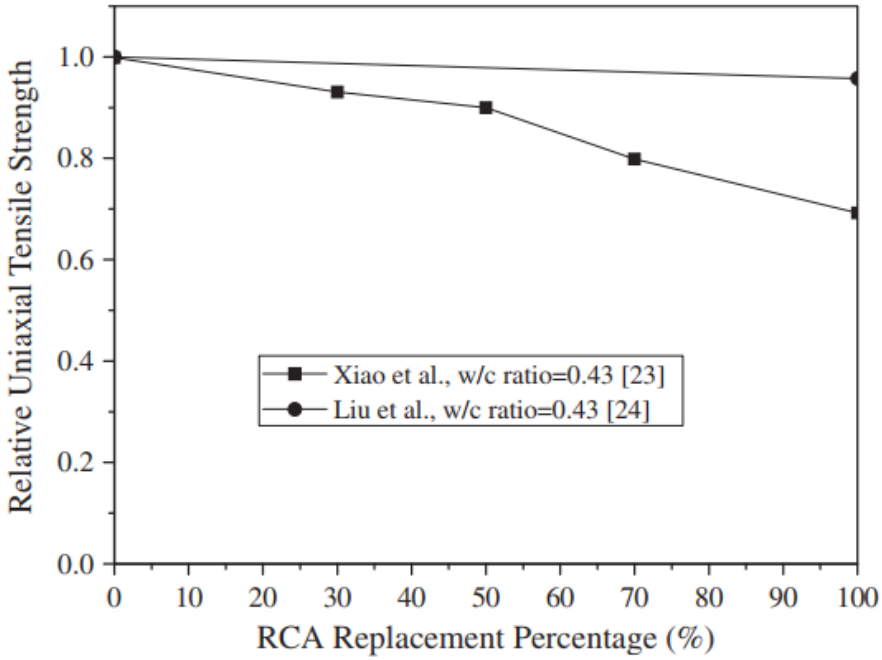

Fig. 2.4 Recycled aggregate content vs uniaxial tensile strength

In some instances, RAC demonstrated superior performance to NAC in terms of tensile strength. Exteberria et al. (2007) ascribed this enhancement to the superior absorption capacity of the residual mortar bonded to the recycled aggregate, which signifies a strong connection between the aggregate and mortar matrix. While this leftover mortar may be vulnerable to compressive failure, small amount improve tensile strength by promoting a more seamless interface between the mortar and the aggregate.

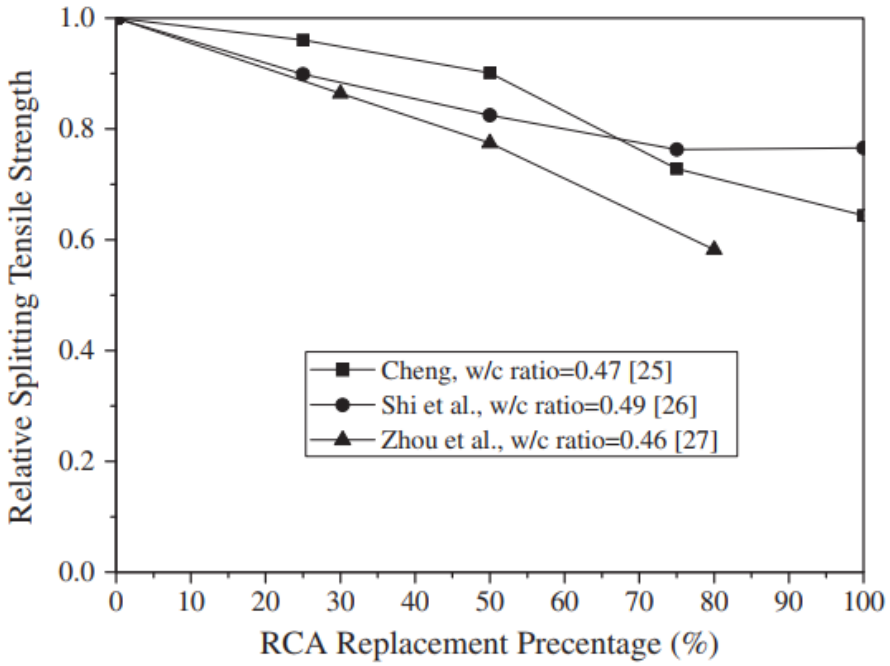

Fig. 2.5 Recycled aggregate content vs splitting tensile strength

RAC's splitting tensile strength and flexural strength did not display a consistent pattern compared to original concretes of similar composition. The tensile strength of RAC can be comparable to that of NAC, primarily because of the increased cement paste concentration in RAC (Sri Ravindrarajah and Tam, 1985). Xiao et al. (2012a) summarised that recycled aggregate exerts a negligible effect on the flexural tensile strength attribute, as illustrated in Fig. 2.6. Yong and Teo (2009) showed that NAC has higher flexural tensile strength of 6.8 MPa at 28 days compared to 50% and 100% recycled aggregate replacement, which achieved 5.8 MPa and 6.2 MPa, respectively. Padmini et al. (2009) assessed that, for any specified compressive strength of concrete, the flexural tensile strength of RAC is inferior to that of the source concrete from which the recycled aggregate is produced.

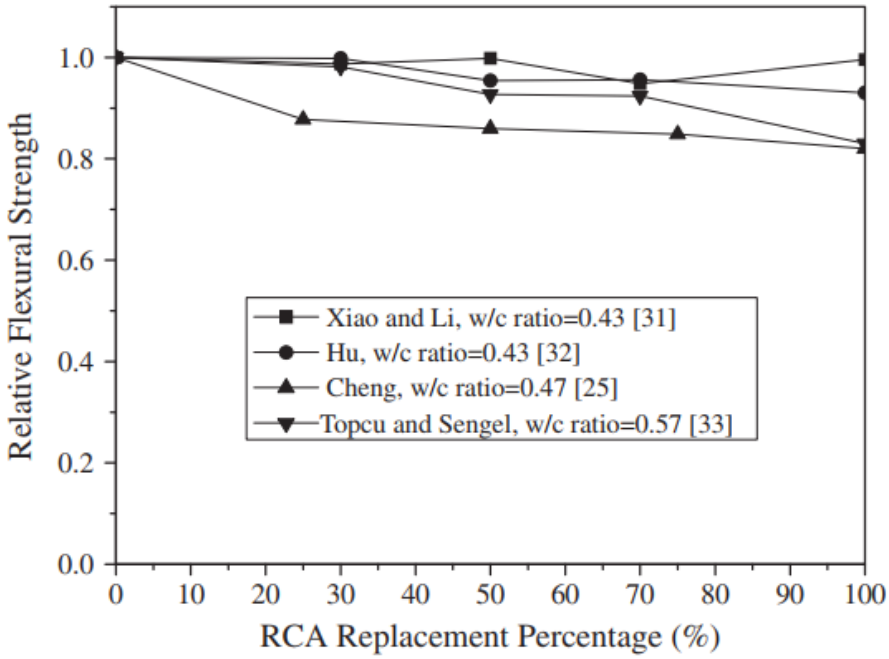

Fig. 2.6 Recycled aggregate content vs flexural tensile strength

2.2.4 Shear strength

A few researchers have conducted studies on the shear strength of RAC. Xiao et al. (2012a) concluded that the shear strength of RAC exhibits a pattern analogous to its compressive strength; specifically, an increase in the proportion of recycled aggregate correlates with a decrease in shear strength, as illustrated in Fig. 2.7. When the replacement reaches 100%, the shear strength decreases by approximately 30%. Rahal (2007) discovered that the shear strength of RAC was 87.7% of that of NAC with the identical design mix.

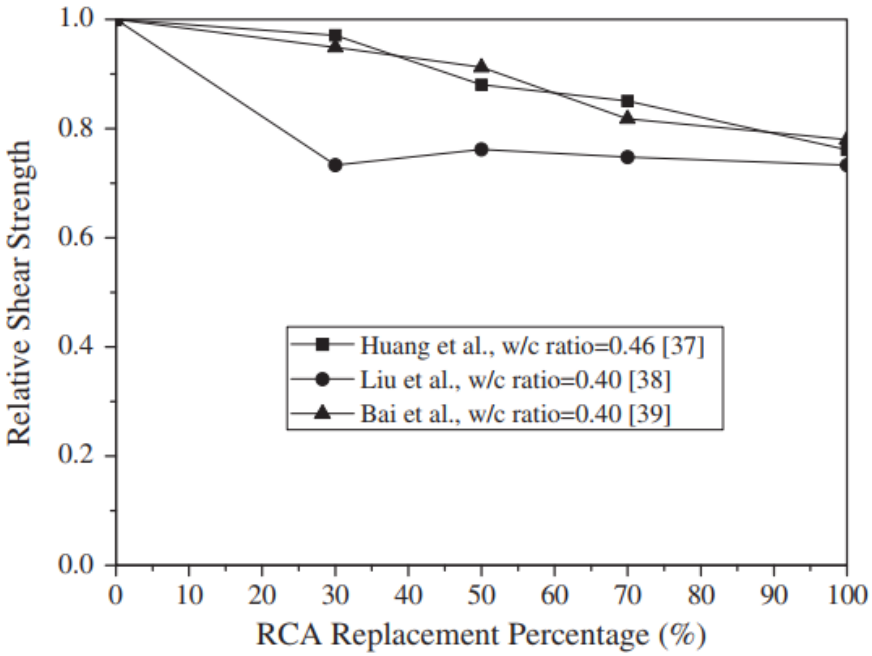

Fig. 2.7 Recycled aggregate content vs shear strength

2.2.5 Elastic modulus

Sri Ravindrarajah & Tam (1985) concluded that, based on the same cube strength, the elastic modulus of RAC is, on average, approximately 70% of that of NAC. When the comparison is made using cylinder strength, this factor increases to about 85%. Xiao et al. (2012a) summarised that the elastic modulus of RAC is about 45% lower compared with NAC, as illustrated in Fig. 2.8. McNeil & Kang (2013) stated that, generally, the elastic modulus of RAC is inferior to that of NAC, although considerable variability exists among research concerning the extent of this reduction. The elastic modulus is primarily influenced by the aggregate characteristics rather than the concrete's overall properties. Rahal (2007) found that the elastic modulus for RAC was merely 3% inferior to that of NAC. Padmini et al. (2009) concluded that the elastic modulus of RAC is inferior to that of its original concrete. A smaller aggregate size results in a more significant drop in its elastic modulus.

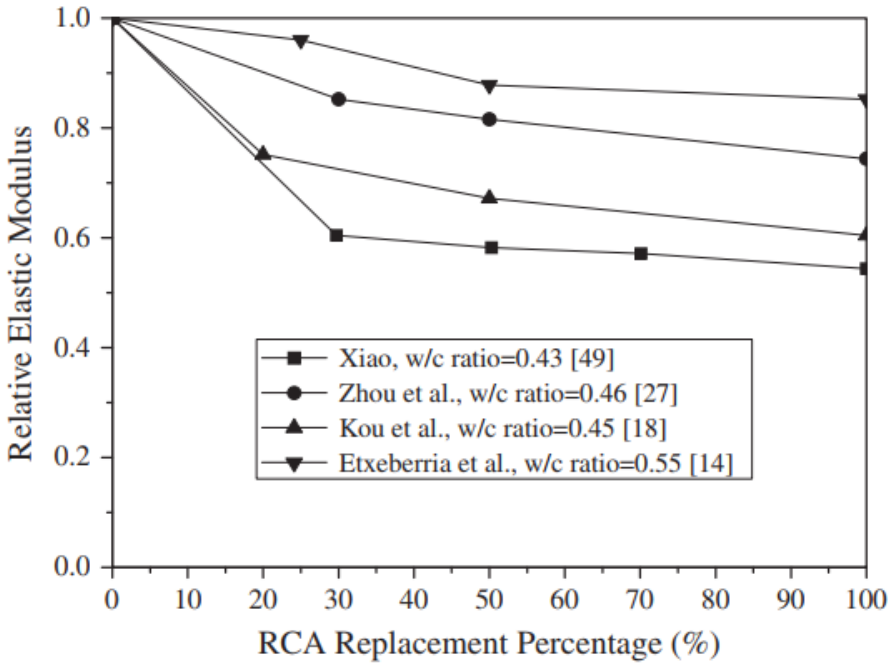

Fig. 2.8 Recycled aggregate content vs elastic modulus

2.2.6 Shrinkage and Creep

Sri Ravindrarajah & Tam (1985) discovered that substituting recycled aggregate for natural aggregate results in an increase in the drying shrinkage of concrete. The disparity in shrinkage between RAC and NAC was more pronounced in higher-grade concrete compared to lower-grade concrete. The increased drying shrinkage observed in RAC may result from a combination of factors, including a lower elasticity modulus of the aggregate, a higher proportion of shrinking mortar content, and a more significant amount of free water used. Additionally, RAC with aggregate sourced from higher-grade original concrete exhibited more significant shrinkage than those with lower-grade concrete. The higher cement content in the recycled aggregate mortar component may be the contributing factor. Xiao et al. (2012a) summarised that the shrinkage deformation escalates with a higher content of recycled aggregate, as illustrated in Fig. 2.9. Domingo-Cabo et al. (2009) observed that the RAC with a 20% recycled aggregate replacement exhibited comparable shrinkage to the NAC during the initial stages, and the shrinkage in RAC was 4% more than in NAC only after 6 months. The shrinkage observed at 50% and 100% recycled aggregate replacement was 12% and 70% higher, respectively, as illustrated in Fig. 2.10. Sagoe-Crentsil et al. (2001) found RAC appears similar trends with NAC on the rate of shrinkage. Moreover, strains

of RAC are 35% higher than NAC at 365 days. Cement content shows an insignificant effect on drying shrinkage.

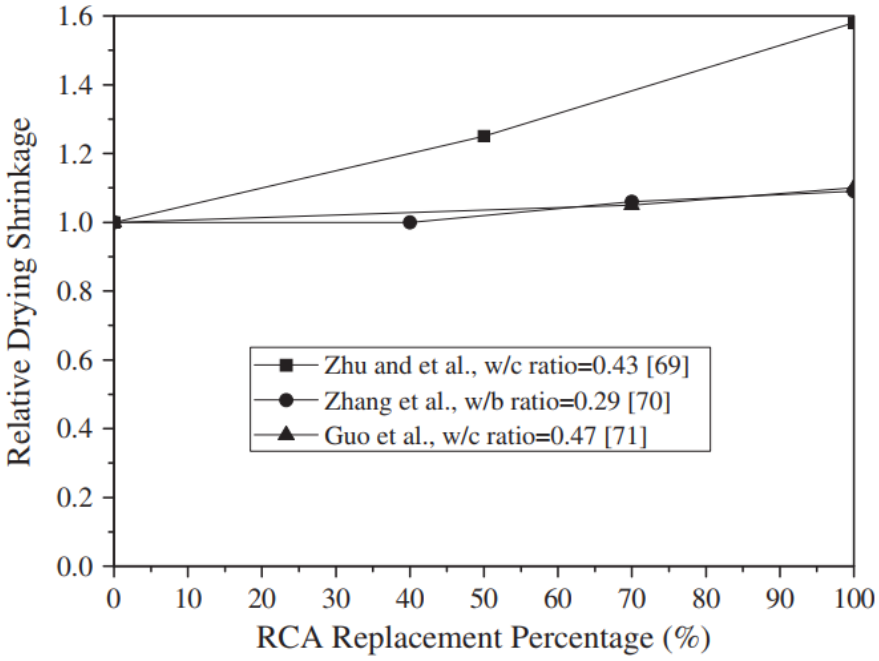

Fig. 2.9 Recycled aggregate content vs drying shrinkage

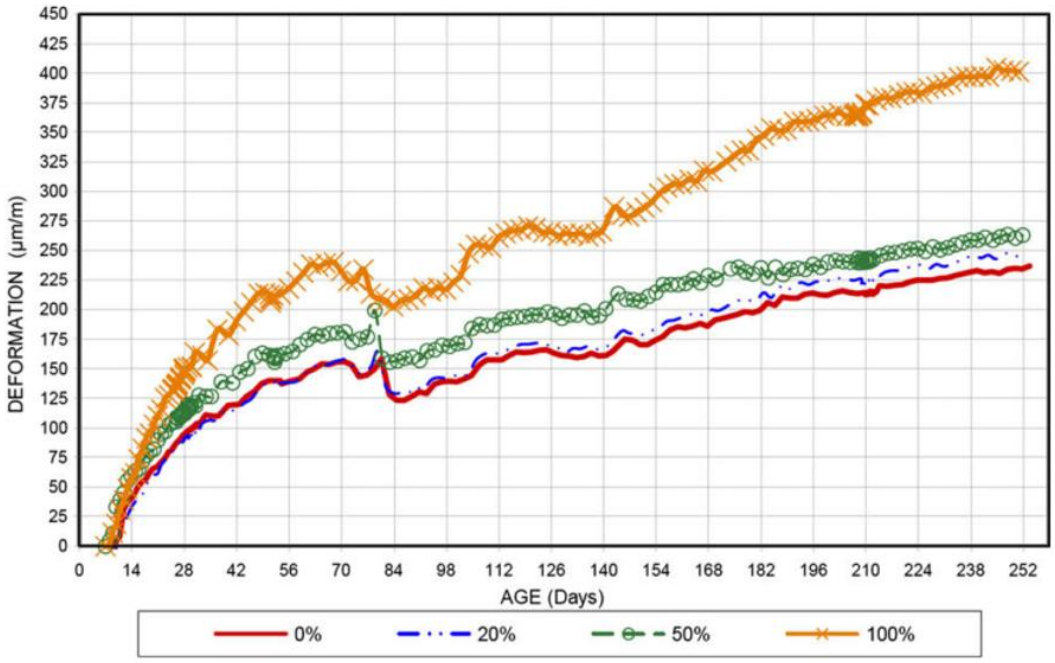

Fig. 2.10 Recycled aggregate content vs shrinkage deformation relative to concrete age

Sri Ravindrarajah & Tam (1985) discovered that RAC exhibited higher creep strain than NAC. The observed increase in creep strain can be attributed to the diminished restraint against volume changes in the cement mortar. This is a consequence of utilising weaker concrete aggregates and the inclusion of a creeping mortar component within the concrete aggregates. Furthermore, the

cement content in the mortar component of the recycled aggregate may influence the creep behaviour of RAC. The specific creep values for NAC and RAC exhibited an increase as the concrete strength diminished. Xiao et al. (2012a) summarised that the creep deformation rises with an increase in recycled aggregate content, as illustrated in Fig. 2.11. Domingo-Cabo et al. (2009) observed that the creep deformation of RAC with 20% recycled aggregate is 35% higher than that of the NAC after a period of 6 months. The creep deformation increased by 40% and 50%, with 50% and 100% recycled aggregate, respectively, as illustrated in Fig. 2.12.

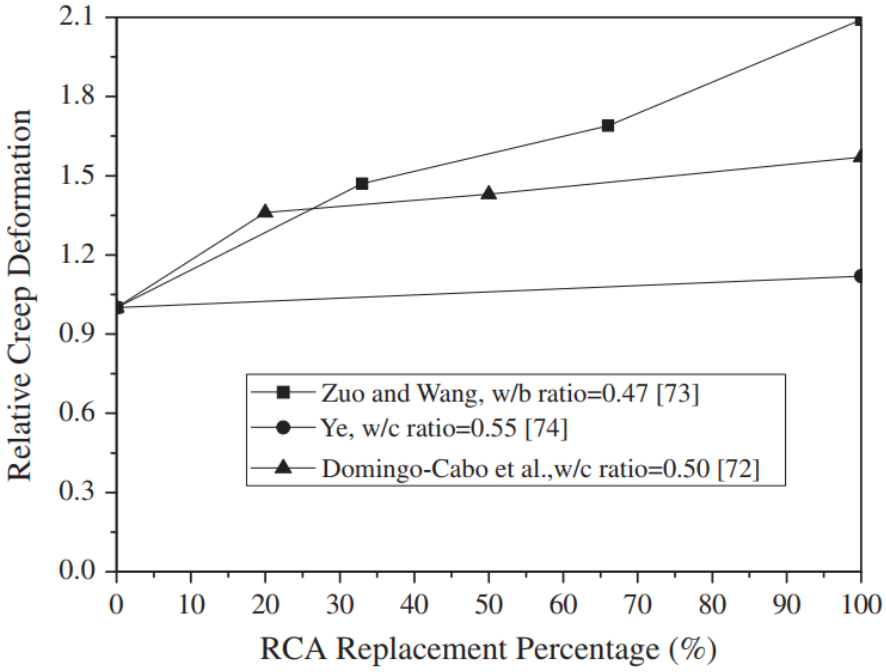

Fig. 2.11 Recycled aggregate content vs creep deformation

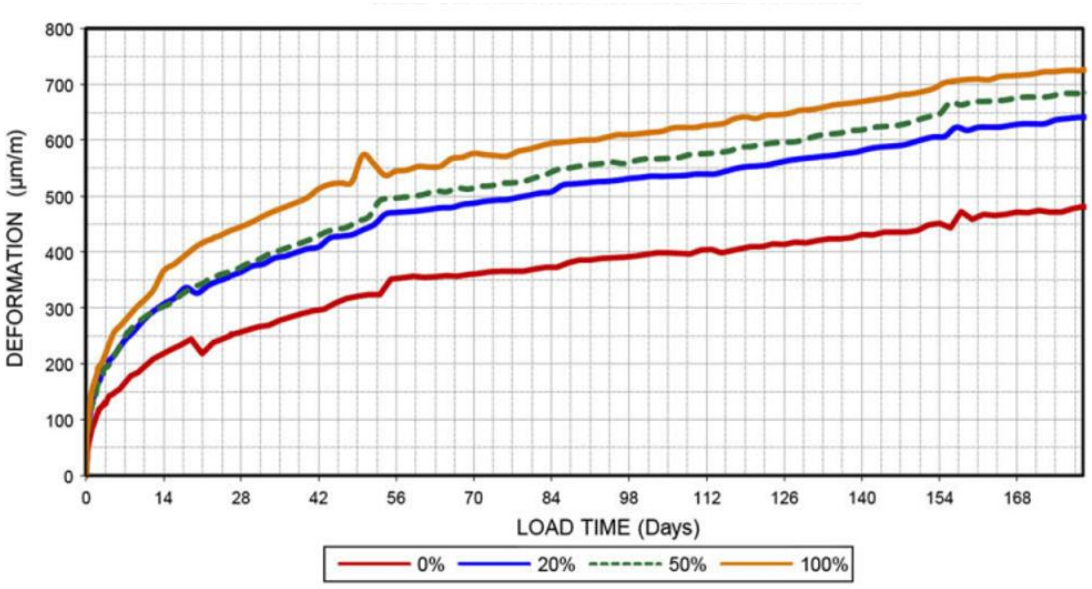

Fig. 2.12 Recycled aggregate content vs creep deformation relative to concrete age

2.2.7 Structural application

A notable research trend in the structural application of RAC is its integration with steel or stainless-steel tubes. The confinement effect offered by the tubes helps to compensate for the limitations of RAC's material properties. This area of research has garnered significant attention, with a considerable number of studies conducted on RAC-filled steel or stainless-steel tubes. Consequently, a review of existing studies on this application has been undertaken to draw insights and inform future research directions.

A summary of prior research on RACFST members has been presented. Numerous experimental and numerical investigations have been undertaken to examine the cross-sectional compressive behaviour of RACFST stub columns with various profiles, including square (Yang et al., 2021; Yang et al., 2023; Yang and Han, 2006; Lyu et al., 2021), rectangular (Yang et al., 2021; Yang et al., 2023), circular (Yang and Han, 2006; Lyu et al., 2021; Xiao et al., 2012; Xiamuxi et al., 2023; Wang et al., 2015; de Azevedo et al., 2021), and round-ended (Zhao et al., 2023). The studies investigated the impact of recycled aggregate replacement ratios, evaluated the relevance of existing design guidelines, and suggested more precise design methodologies. Chen et al. (2017) investigated the structural behaviour of circular RACFST beams and beam-columns, revealing that the CFST composite system markedly enhanced the ductility and load-bearing capacity of RAC. Yang and Han (2006a) conducted an experimental investigation on the global buckling behaviour of circular and square RACFST columns and beam-columns, assessing the precision of established design standards. Xiamuxi et al. (2024) performed research on the flexural behaviour of square reinforced RACFST beams, demonstrating that reinforcement improved the flexural capacity of these beams. Investigations conducted by Li et al. (2017), Yang and Hou (2012), and Zhao et al. (2024) about RACFST stub columns exposed to fire revealed the adverse effects of high temperatures on ultimate strength and elastic modulus and proposed new design equations.

The research on RACFSST components is summarised as follows. Experimental investigations assessed the cross-sectional behaviour and capacities of RACFSST stub columns subjected to axial compression (Yang and Ma, 2013; Tam et al., 2014; Zhang et al., 2022b) and combined bending and compression (Zhong et al.,

2022; Zhong and Zhao, 2022), evaluating the confinement effect, proposing analytical models for axial responses, and enhancing existing design approaches. He et al. (2021) examined the flexural buckling behaviour and resistance of circular RACFSST columns, analysing the impacts of member dimensions and recycled aggregate replacement percentage through experimental and numerical methods. Compression tests conducted by Wang et al. (2024; 2024a; 2024b; 2025) on RACFSST stub and long columns exposed to post-fire conditions quantified the reductions in structural capacity and stiffness, discussed the impacts of recycled aggregate replacement ratios and heating durations, and evaluated the applicability of current design standards.

Over the past ten years, certain academics have empirically examined the structural behaviour of composite slabs utilising RAC. Wang et al. (2016) carried out a 268 days long-term test on a single span composite slab using RAC. The findings indicated that deflection resulting from non-uniform shrinkage is considerable. The long-term deflection resulting from persistent loading and shrinkage is approximately four times greater than the short-term deflection, with shrinkage contributing roughly 50% to the total deflection. Zhang et al. (2020) conducted a 500-day long-term evaluation of a two-span continuous composite slab utilising concrete made from 100% recycled fine and coarse aggregates. The long-term deflection is 1.4 to 2.5 times of the short-term results. In the hogging moment region, the long-term crack width is 2.2 to 4.2 times larger than the short-term measurements. The utilisation of 100% recycled aggregate led to a 16% augmentation in mid-span deflection and a 58% escalation in crack width in the hogging moment zone adjacent to the intermediate support.

2.3 Demountable shear connector

Steel-concrete composite beams are commonly utilised in construction of buildings and bridges owing to their superior load-carrying capacities, ductility and seismic performance (Liu, Bradford and Abdolreza, 2017; Faella et al., 2010; Ban et al., 2015; Li et al., 2011). The prevailing technique for attaining composite action in steel–concrete composite slabs employ welded shear studs, which are affixed to the steel beam flange and implanted into the concrete slab, leading to

difficulties for composite slab prefabrication and demolition at the expiration of their operational lifespan. To further improve the construction efficiency and reusability of the composite slabs, the bolted shear connector has been proposed and investigated, with a brief review of previous relevant studies summarised herein.

Apparently, in the composite beam, shear connectors play an important role in enabling the composite slab and steel beam to function together as one structural member to resist design actions. Generally, there are two main sorts of demountable shear connectors. The first type is as shown in Fig. 2.13(a), which consists of a bolt and two sets of nuts and washers on both faces of the flange as shear connector; by fastening tight the two sets of nuts and washers onto the top flange of the steel beam, the shear connector could provide necessary strength and stiffness to facilitate the transfer of the longitudinal shear force between the concrete and the steel sections. The other type is Nelson demountable shear connectors, seen in Fig. 2.13(b), which is machined from the welded shear stud, characterised by a reduced collar, threads at bottom of shank, and one set of nut and washer. Owing to the recess of the shank, this shear connector can be fastened with only one set of nut and washer beneath the steel flange. (Rehman et al. 2016)

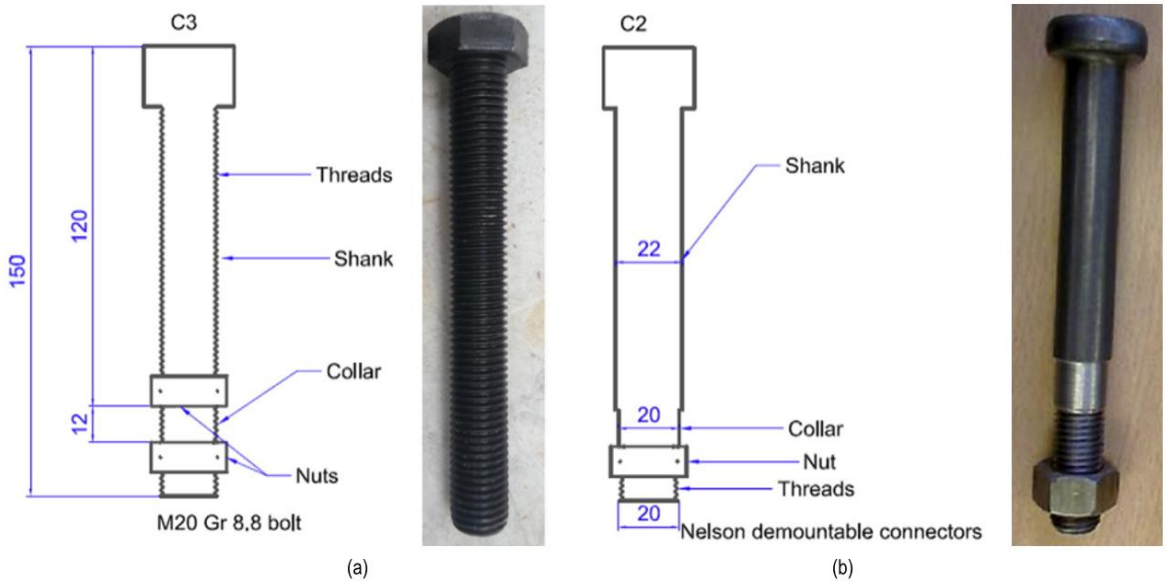

Fig. 2.13 Different type of demountable connectors

Rehman et al. (2016) performed push-off tests on composite beams using bolted shear connectors. The findings showed that the bolted shear connectors have comparable shear capacity and even higher ductility than welded shear studs.

Experimental results showed that a combination of EC3 and EC4 could accurately predict the shear capacity of demountable shear connectors. Pavlović et al. (2013) found in their experimental tests that shear resistance of bolted connectors is 95% of that of welded studs, though their stiffness was only 50% due to pre-drilled holes being larger than the bolt diameter. The study highlighted that the bolted connector's shear resistance was 20% higher than EC3 predictions due to nut-flange friction and the catenary effect. In the study carried out by Dai et al. (2015), the shear resistance of demountable connectors could be accurately modelled using FEM and predicted by EC4 calculations. The results demonstrated that the failure manner of the bolted shear connector is contingent upon the concrete strength. The failure mechanism occurs in the concrete if the concrete grade is below C30. The failure mode occurs in the steel connector when the concrete grade is C30 or above. Similar push-off tests were also carried out by Chen et al. (2014) and Ataei & Zeynalian (2021) to investigate the shear behaviour and capacity of friction-grip bolted shear connectors, while Henderson et al. (2017) conducted experimental investigations on the shear behaviour and capacity of blind bolted shear connectors.

To further study the influence of the fabrication method, push-off tests and numerical simulations were also conducted by Liu et al. (2023) to investigate the shear resistance and behaviour of steel–concrete composite flooring systems with bolted shear connectors and cast in-situ or precast concrete slab. Suwaed & Karavasilis (2020) examined the efficiency of friction-based shear connectors (FBSCs) and revealed that they contributed to beam stiffness even with a shear connection degree as low as 32%, below the minimal threshold stipulated by EC4. Their results showed full composite action between the concrete and the steel section up to 36% of the maximum moment, with minimal slip and no measurable uplift.

Pathirana et al. (2015) conducted four-point bending tests and numerical simulations on the retrofitted steel-concrete composite beams with both welded and bolted shear connectors and concluded that bolted connectors provided comparable shear resistance and ductility compared with the welded shear connectors. Lam et al. (2017; 2021) and Rehman et al. (2016; 2018) conducted experimental and numerical evaluations on the structural response and capacity

of demountable bolted shear connectors using push-off tests and four-point bending beam tests, demonstrating the demountability, reusability, and recyclability of the composite beams following testing under service loading conditions. Moynihan & Allwood (2014) confirmed similar performance between bolted and welded connectors through beam tests across different spans. All maximum moment resistances are above the predicated value by EC4.

Kwon et al. (2010) performed a fatigue loading test on a 22 mm diameter bolted shear connector subjected to a 310 MPa stress range, and the double-nut bolt connector exhibited no failure after 5 million loading cycles. Subsequently, it experienced static loading, and the residual strength reached 224 kN. This exhibits markedly superior fatigue strength compared to conventional welded shear studs.

2.4 Profiled steel decking

Profiled steel decking in the composite slab plays many roles, including serving as a working platform with minimal propping, working as a concrete form during the concrete casting stage, and providing additional bending resistance due to excellent tensile capacity. There are many different steel decking types with various geometries available in the market, as shown in Fig. 2.14 (Burnet & Oehlers, 2001). The standard varieties of profiled decking utilised in engineering applications include re-entrant or dove-tailed ribs, trapezoidal forms, and L-shaped or re-entrant L profiles. Concrete is poured against these ribs to create a connection that transfers the shear at the interface. The shear resistance arises from chemical bonding, which is the first to be lost following contact slide, followed by mechanical bonding, which is determined by the protrusion and indentation of the rib. Embossments significantly enhance this bonding (Burnet & Oehlers, 2001). However, the selection of the rib profile is not solely driven by structural resistance; concrete material savings and the resultant reduced structural self-weight is one of the key considerations, followed by the workability of shear stud installation inside the pan and lastly, the installation method available for the secondary support required beneath the composite slab.

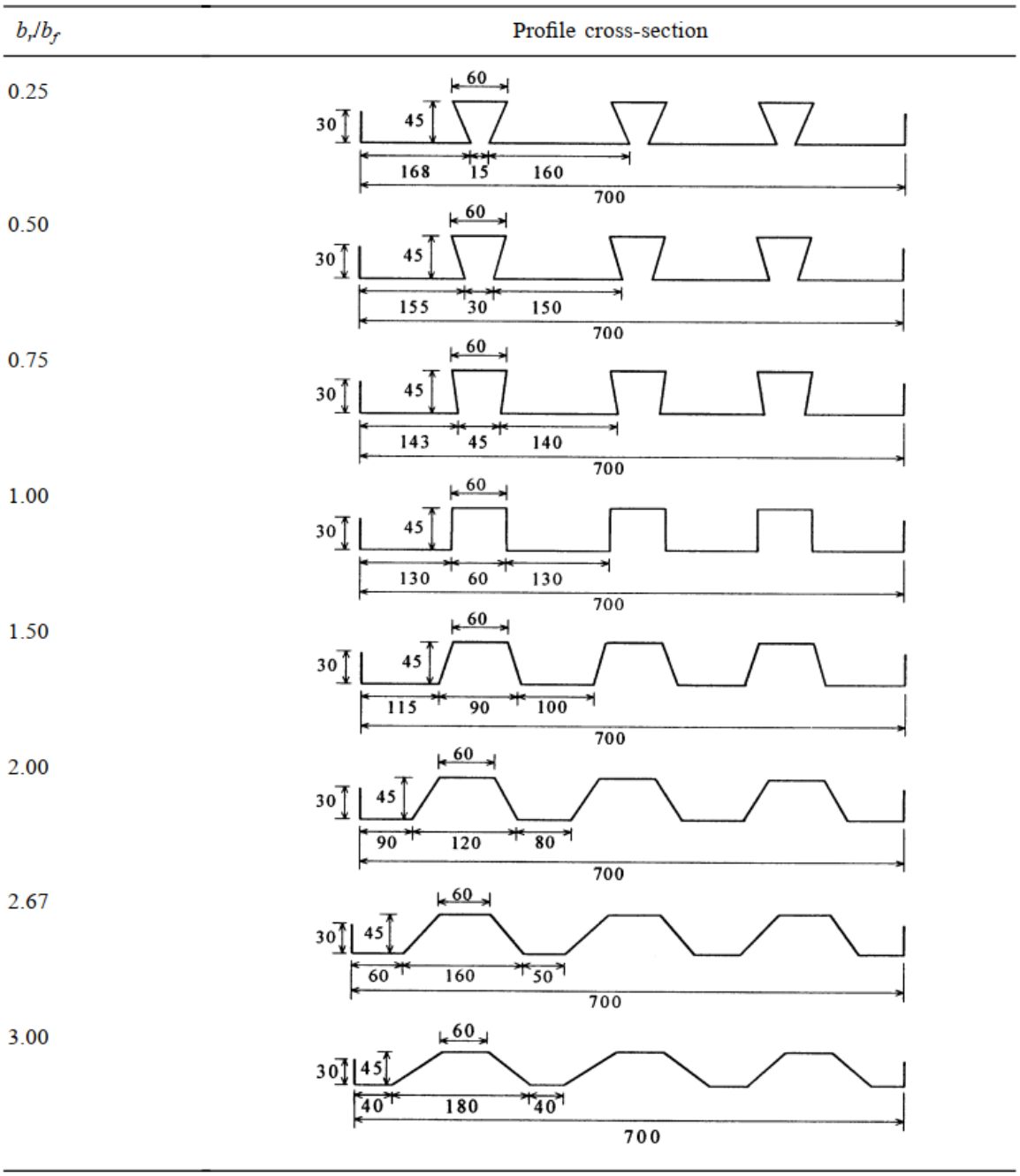

Fig. 2.14 Different geometric variations of profiled steel decking

In Southeast Asia, the local market commonly offers three types of profiled steel decking: Lysaght® Bondek® II, LCP Lycordeck®, and TATA ComFlor®. Bondek is one of the most popular commercial products adopted in various building projects, including Marina Bay Sands in Singapore and the KLCC Petronas Towers in Malaysia. The typical profiles are shown in Fig. 2.15(a). The recess in the rib features many interlocking accessories for ceiling-mounted services without requiring drilling through the steel deck into the concrete slab. This characteristic contributes to its popularity and acceptance. LCP Lycordeck is a competitor to Bondek and other types of profiled steel decking. It features a unique closed rib profile and large

pan, allowing for flexible placement of shear studs at spacings of 100 mm, 200 mm, or 300 mm, as shown in Fig. 2.15(b). This product has been used in One Raffles Place and Ion Orchard in Singapore and the International Finance Centre in Hong Kong. Compared to the two above, the distinguishing feature of TATA ComFlor® is its deep pan, which can be up to 225 mm as shown in Fig. 2.15(c), compared to the typical pan depth of around 55 mm. The larger recess creates a greater sectional modulus, enabling it to be used in long-span composite concrete/steel floor systems, such as 6 m unpropped spans, compared to the typical 3 m unpropped spans for the earlier two products mentioned. However, the downside is that such deep recess compromises the composite action of the concrete slab with the steel beam underneath.

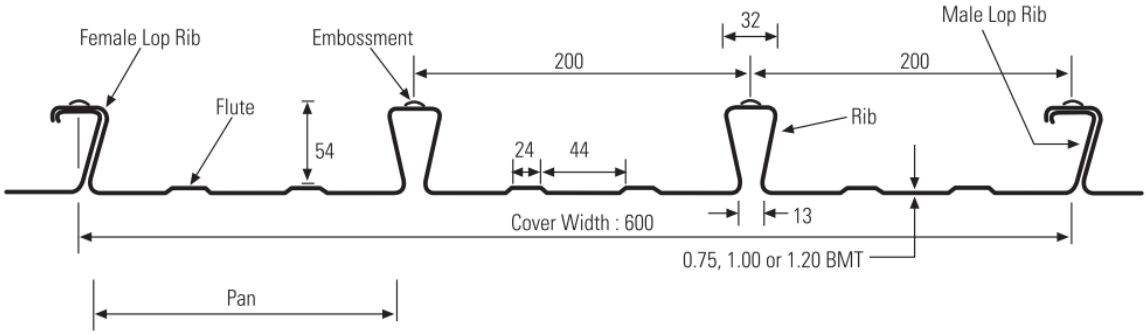

(a) LYSAGHT® BONDEK® II profile

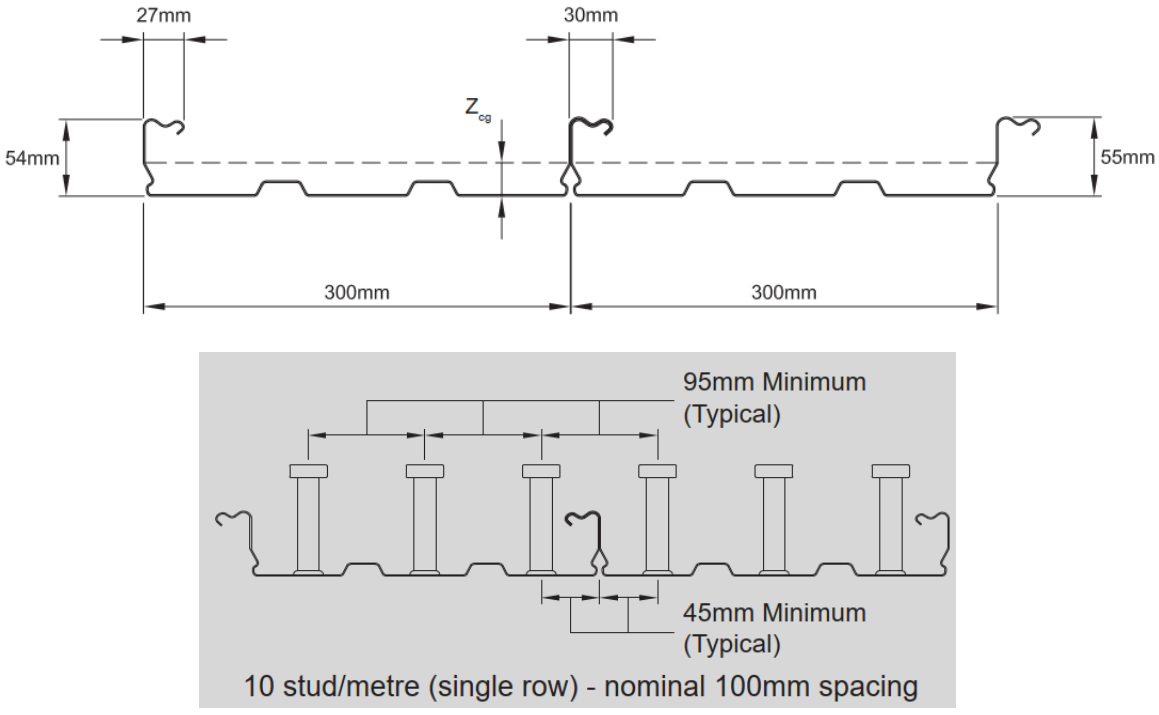

(b) LCP LYCORDECK® profile and possible shear stud arrangement

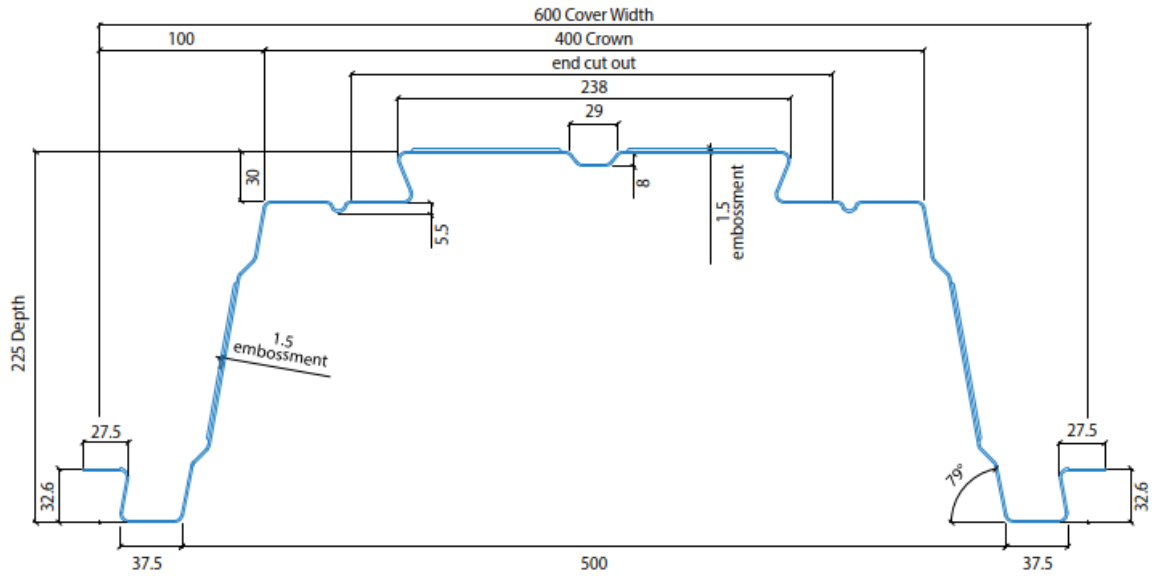

(c) ComFlor® 225 profile

Fig. 2.15 Three common types of profiled steel decking

2.5 Summary

This chapter presents a thorough literature review on recycled aggregate concrete (RAC), demountable shear connectors, profiled steel decking and their structural applications.

At the microstructural level, RAC is characterised by a two-layered ITZ: an existing ITZ resulting from the residual cement mortar attached to the recycled aggregate and a newly produced ITZ between the recycled aggregate and the fresh cement paste. This microstructural difference leads to degraded mechanical properties and shrinkage and creep performance of RAC compared to its NAC counterpart.
In spite of its inferior mechanical behaviour and long-term performance, RAC could utilise demolition and construction wastes, save natural resources and reduce carbon emissions, which makes it still be of research significance. There is a research trend of using RAC in structural members, mainly for CFST and CFSST components. However, there are not many studies on composite beams or slabs using RAC, and the focus of these studies was more on long-term behaviour than structural ultimate capacity.

Different demountable shear connectors and their structural performance in composite beams/slabs have been reviewed. These demountable shear connectors were shown to have comparable shear strength and stiffness with welded shear studs, along with superior fatigue strength compared to conventional welded shear studs. However, no study has been undertaken to examine the shear performance of demountable shear connectors in the composite beam using RAC. The shear-slip response is expected to be different due to the reduced material properties of RAC.

Furthermore, the majority of prior research on RAC has been on the alteration of mechanical properties of the concrete mix with various replacement percentages of recycled aggregate while keeping the water-to-cement ratio unchanged. This approach has led to variability in the compressive strength of concrete, making it difficult to determine whether differences in structural performance are due to the recycled aggregate itself or the inherently lower compressive strength of RAC. In typical design circumstances, the design is based on concrete with a specific strength grade, which is essential for determining the sizing of structural members and ensuring that the minimum concrete grade requirements dictated by exposure classes are met. If RAC is to be incorporated into the design, it must also achieve a specified compressive strength. When using RAC to maintain equivalent strength levels, adjusting the water-to-cement ratio is necessary. This adjustment is particularly crucial in the design of composite beams and slabs, as the concrete's strength directly influences the final sizing of these structural members. Therefore, a significant research gap exists that underscores the need to examine the behaviour of composite beams utilising RAC with a fixed design strength in conjunction with demountable shear connectors. The insights gained from this research could lead to developing guidelines for future applications.

3 PROPOSED SUSTAINABLE AND DEMOUNTABLE COMPOSITE FLOOR SYSTEM AND TESTING PLAN

3.1 Introduction

In order to offer a more sustainable and reusable solution to the floor system in temporary and short-lease structures, an RAC composite floor system using demountable shear connectors is proposed in this work. This chapter begins with an introduction to the novel composite slab system using RAC and demountable shear connectors, followed by the testing programme designed to investigate the shear-slip behaviour of the demountable connectors and the overall structural performance of this novel composite floor system under four-point bending.

3.2 Proposed sustainable and demountable floor system

In this work, a sustainable and reusable floor system is proposed to be used in temporary and short lease building structures. The composite floor system is formed up of a RAC slab, profiled steel decking, and a series of demountable shear connectors, as seen in Fig. 3.1.

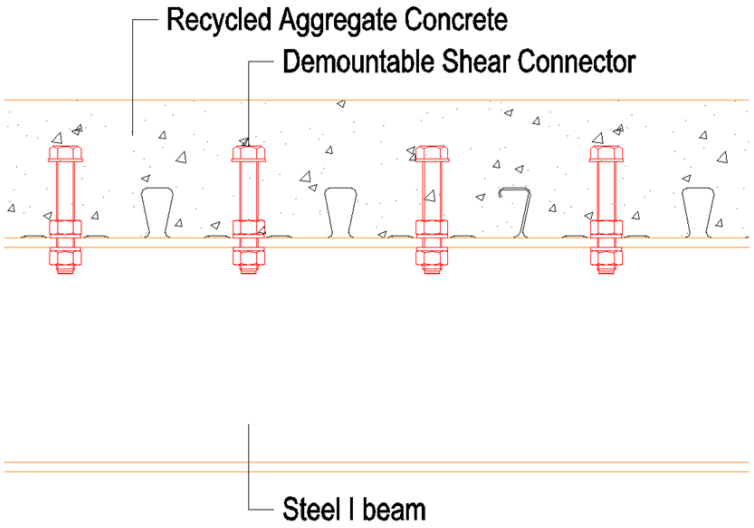

Fig. 3.1 Proposed floor system

3.2.1 RAC

In an engineering context, in order to use RAC in structural members, the concrete matrix is required to satisfy a specific strength. Therefore, in this experimental programme, concrete mixes with varying percentages of recycled aggregate replacement are designed to achieve the same target strength by adjusting the water-to-cement ratio whilst keeping a constant free water content. In this way, the same cross-section dimensions can be adopted for specimens with different RAC mixes, which allows a straightforward comparison on the results.

Moreover, within a local framework, the processing and testing criteria for recycled concrete aggregate are delineated in SS EN 12620 and BS 8500. Therefore, foreign sources lacking obvious compliance with SS EN 12620 and BS 8500 were excluded from the proposed concrete mix. This research will not verify the variance in the sourcing and quality of recycled aggregate, which may influence the material qualities of concrete design.

The cost of concrete is affected by its workability and grade. Local providers provide RAC and NAC at equal unit prices for ordinary concrete without particular workability specifications, such as self-compacting characteristics or prolonged setting time retardants. The availability of RAC is contingent upon the supply of recycled aggregate, which is directly associated with the extent of demolition projects in the local market.

3.2.2 Shear connectors

As mentioned in Section 2.5, there are two commonly used types of demountable shear connectors. The first type is the bolted connector, consisting of a bolt with two pairs of nuts and washers. The second type is the Nelson demountable shear connector, produced from a welded shear stud with a reduced collar and threads at the bottom of the shank, featuring only one set of nuts and washers. (Rehman et al. 2016)

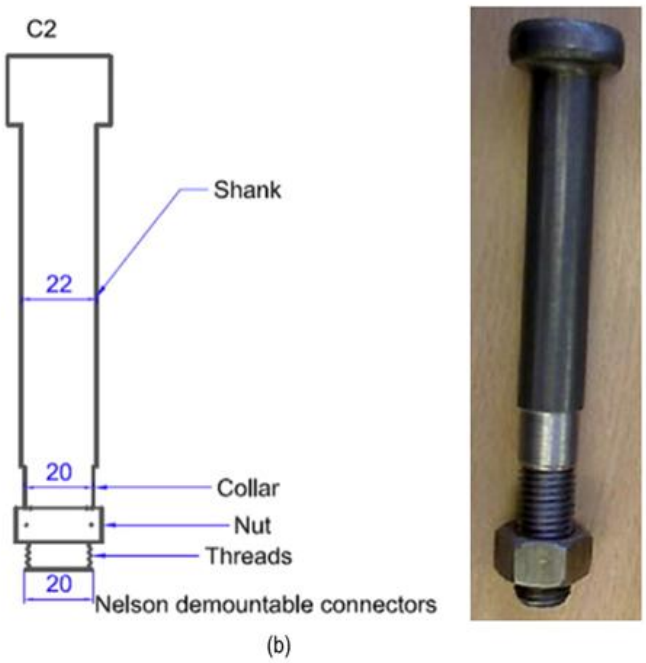

Fig. 3.2 Nelson demountable shear connector

Although the Nelson demountable connector requires less screwing work, its round head makes it more difficult to be fastened compared to the conventional bolt with a hexagonal bolt head. Furthermore, the reduced collar in the Nelson connector is only 2 mm smaller in diameter than the shank above it. Predrilled holes with tolerances exceeding 1 mm can lead to an insufficient contact area between the recess of the shank and the flange around the bolt hole. Additionally, the Nelson demountable connector requires customization, complicating its widespread adoption in the industry. While the diameter of the predrilled hole may potentially be minimised to enhance contact between the shank and the steel surface, this modification would compromise essential construction tolerances, rendering it impracticable in actual building contexts. Conversely, diminishing the collar size to increase the recess between the shank and the collar may undermine the steel's shear resistance, so considerably impairing the shear connector. Consequently, this method is likewise not advisable. Therefore, in this study, aiming at more practical engineering applications, the first form of demountable shear connectors—i.e., bolts with two sets of nuts—is adopted.

Before specimen preparation, the possibility of using regular bolts with a single nut (Fig. 3.3a) was explored. The nut was pre-tack welded under the top flange of the Steel beam to facilitate fixing the bolt onto the Steel beam through the predrilled holes on the decking and Steel beam top flange. The results showed

that the decking could not be fully attached to the I beam due to the clearance bolt holes, resulting in concrete leakage at the gap between the bolt and decking during casting. Subsequently, regular bolts with double nuts and a single washer (Fig. 3.3b) were tested. The bottom nut was pre-tack welded beneath the top flange of the Steel beam. The washer was placed atop the decking and restrained by the top nut. However, the regular bolt had an insufficient thread length to fit in two nuts and a Steel beam flange, so full thread bolts were used at the end (Fig. 3.3c).

In contrast to traditional welded shear studs, priced at roughly $1 per unit, an M20 bolt is estimated to cost around $1.50 each pair. Nonetheless, the installation of welded shear studs necessitates a welding device and supplementary labour, elevating the overall supply and installation cost to approximately $3.50 per unit. Conversely, the M20 bolt necessitates only normal tightening, rendering fastened shear connectors more economically advantageous overall.

Bolted shear connectors provide an advantage for on-site installation as they do not necessitate a stud welding gun or electricity, in contrast to welded shear studs. Nonetheless, accuracy is essential for the installation of bolted shear connectors. The decking including predrilled holes must be positioned meticulously to guarantee accurate alignment with predrilled holes on the I-beam top flange. Welded shear studs permit more versatile placement since they do not necessitate predrilled holes, facilitating installation in diverse configurations.

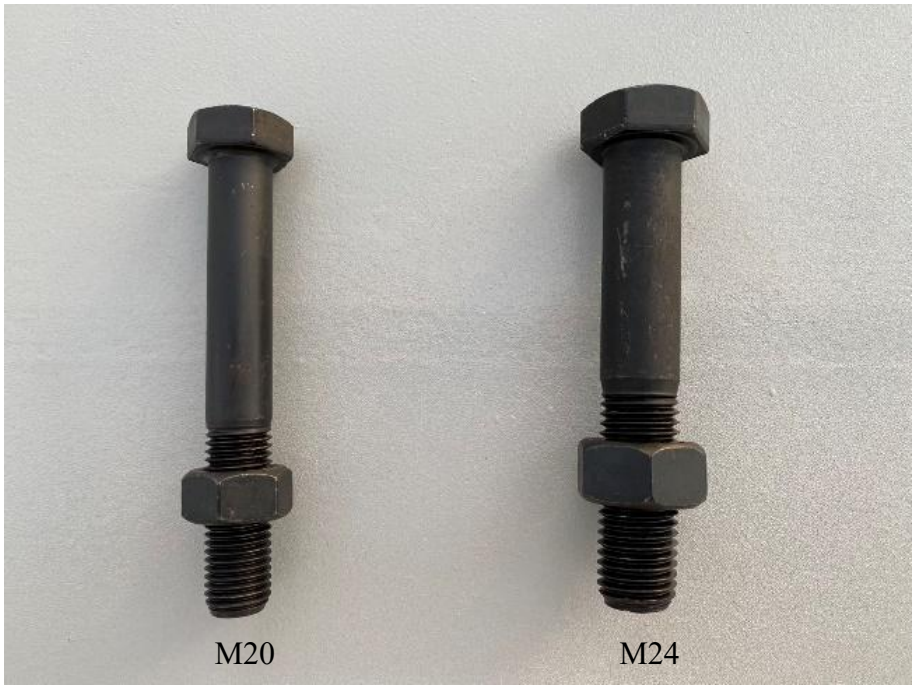

(a) regular bolts with single nut

(b) regular bolts with double nuts

(c) full thread bolt with double nuts

Fig. 3.3 Bolted shear connector

3.2.3 Arrangement of shear connectors

For this research, Lysaght® Bondek® II (Bondek) has been selected as the profiled steel decking. This product is the most commonly used in the local market, and its re-entrant rib design provides flexibility when aligning pre-drilled holes on the deck with those on the beam flange. The re-entrant rib profile also features interlocking accessories that enable ceiling-mounted services without the need to drill into the concrete slab, enhancing its popularity.

This steel decking is characterised by 54 mm high recess ribs in inverted trapezoid shapes, with the pans arranged at a spacing of 200 mm. Consequently, the arrangement of shear connectors must comply with the geometry of the profiled decking; specifically, the spacing of the shear connectors must be a multiple of 200 mm. Before installation, holes with an additional 2 mm diameter clearance are pre-drilled to allow for the fixing of demountable shear connectors, as shown in Fig. 3.4.

Fig. 3.4 Decking with predrilled holes

3.2.4 Assembling and disassembling

Prior to assembling of the composite slab and the underlying steel beam, bolt holes are drilled into both the profiled decking and the top flange of the Steel beam (see Fig. 3.5) in accordance with the shear connector arrangement plan. Then, the proposed demountable bolted shear connectors can be inserted into the pre-drilled bolt holes on the profiled steel decking and the steel beam. Fig. 3.3(c) illustrates that each demountable bolted shear connector contains one full thread bolt, one washer and two nuts. One of the nuts is pre-tack welded beneath the top flange of the Steel beam (See Fig. 3.6), while the other fastened onto the profiled decking, with the washer placed in between (See Fig. 3.7), After the decking and the Steel beam are assembled, the RAC slab can be casted on top of the decking.

Fig. 3.5 Steel beam with predrilled holes on top flange

Fig. 3.6 Nut pre-tack welded under the top flange of the Steel beam

Fig. 3.7 Nut fastened onto the profiled decking with washer in between

After testing, the composite system will be flipped over so the steel beam faces upwards. The bolt, which was tack-welded to the top flange, have shifted from its initial position due to slippage between the concrete and steel sections. This bolt will then be untightened, as shown in Fig. 3.8. Once untightened, the entire beam can be elevated and detached from the composite slab, as illustrated in Fig. 3.9. In actual engineering applications, disassembling will occur in the normal orientation since the steel beam is connected to supporting elements at both ends. The floor slab will need to be cut into sections and lifted off the steel beam by loosening the bolts from below. The concrete can then be processed to produce recycled aggregate, while the steel beam can be reused.

Fig. 3.8 Remove nut from beam flange side

Fig. 3.9 Disassemble the steel beam from concrete slab

3.2.5 Sustainability and circular economy

Regarding sustainability, Xiao et al. (2018) state that while the production of RAC exhibits a greater global warming potential (GWP, kg) than NAC — 11% higher for aggregate production and 2% higher for cement production (attributable to the extra cement needed to attain equivalent characteristic compressive strength as NAC)—the comprehensive embodied carbon footprint of RAC is reduced when evaluating the entire lifecycle. A lifecycle assessment (LCA) revealed that included the end-of-life phase (such as landfill and transportation of demolition trash) resulted in the overall embodied carbon footprint of a RAC structure being 7.93% lower than that of a NAC structure. This is especially important in local contexts when natural aggregates depend on foreign imports. Conversely, recycled aggregates can be generated locally from building debris, hence diminishing the embodied carbon footprint of RAC.

The implementation of demountable shear connectors in a flooring system presents considerable benefits in accordance with circular economy concepts. These connections facilitate the separation of steel beams from the concrete section without compromising their integrity or operation, permitting reuse without the necessity for complete reprocessing into raw material. This method

minimises waste and enhances resource efficiency, consistent with circular economy objectives.

For temporary constructions and short-term lease buildings with a normal lifespan of 3 to 15 years, the embodied carbon linked to the demolition phase can be 5 to 10 times greater than that of normal structures planned for 50 to 70 years of use. This results from the continual disassembly and reassembly necessary for such edifices. The proposed floor solution, utilising recycled aggregate concrete (RAC) and reusable steel structure, presents considerable benefits in this context. The utilisation of RAC diminishes the requirement for virgin materials and reduces the carbon footprint linked to concrete production. Moreover, the steel parts can be reused again, so diminishing the demand for new materials and lessening waste. The advantages of the suggested system—namely reduced embodied carbon, improved sustainability, and resource efficiency—are markedly enhanced in temporary and short-term building applications.

3.3 Testing plan and specimen preparation

In this sub-section, specimens were designed to test the proposed sustainable and demountable composite floor system, mainly through push-off tests and full-scale four-point bending tests.

3.3.1 Push-off tests

A total of six steel–RAC composite slabs and two steel–NAC composite slabs were designed in this testing plan. As shown in Fig. 3.10, each specimen consisted of a grade S355 steel UB203×133×30 I-section member, two reinforced composite slabs, and demountable bolted shear connectors with staggered arrangement. In NAC, certain researchers have noted a modest decrease (about 5%) in the shear resistance of bolted connectors relative to welded studs. Nevertheless, the majority of research suggest that bolted connectors offer similar shear resistance and ductility in comparison to welded shear connectors. The structural behaviour of welded studs is clearly delineated in design codes including Eurocode, AISC, and ACI. Due to limited funding and the comprehensive validation of welded studs

in prior research, welded studs in NAC are excluded from the specimens in this investigation. The comparison may instead rely on anticipated outcomes drawn from known code standards for welded studs in NAC.

All the composite slabs were designed with a fixed width *B* of 600 mm and a uniform overall thickness h_c of 130 mm. The length *L* of the slab was 600 mm for M20-200 specimens and 800 mm for M24-400 specimens. The slabs are made of four concrete types, with recycled aggregate replacement ratios *r* of 0%, 30%, 70% and 100%, namely NA, RA30, RA70 and RA100, respectively. Three degrees of recycled aggregate replacement ratio were chosen for a thorough comparison. Initially, 0% replacement (i.e., NAC) was established as the reference point for comparison. The 30% replacement ratio was used, as it constitutes the highest limit permitted by municipal authorities for the utilisation of recycled aggregate in the concrete mix. Third, a 100% replacement, denoting the total substitution of coarse aggregate with recycled aggregate, was established as the maximum limit to examine the system's performance under complete replacement. An intermediate replacement ratio of 70% was incorporated to guarantee a consistent and seamless distribution of outcomes, derived as the average of 30% and 100%. This method facilitates a more comprehensive examination of the system's behaviour across various replacement ratios. All concrete mixtures were designed with a target cylinder strength of 40 N/mm^2, a common concrete grade chosen to address exposure circumstances, ensure durability, and deliver adequate compressive resistance to properly exploit the composite action in a composite floor system. The Lysaght® bondek® II profiled decking with grade G550 cold-formed steel and a nominal thickness t_d of 1 mm was used, the details of which are given in Fig. 3.11. The composite slab was reinforced with grade 500 N/mm^2 reinforcing bars with a nominal diameter of 10 mm and a bar spacing of 200 mm in both the transverse and the longitudinal orientations.

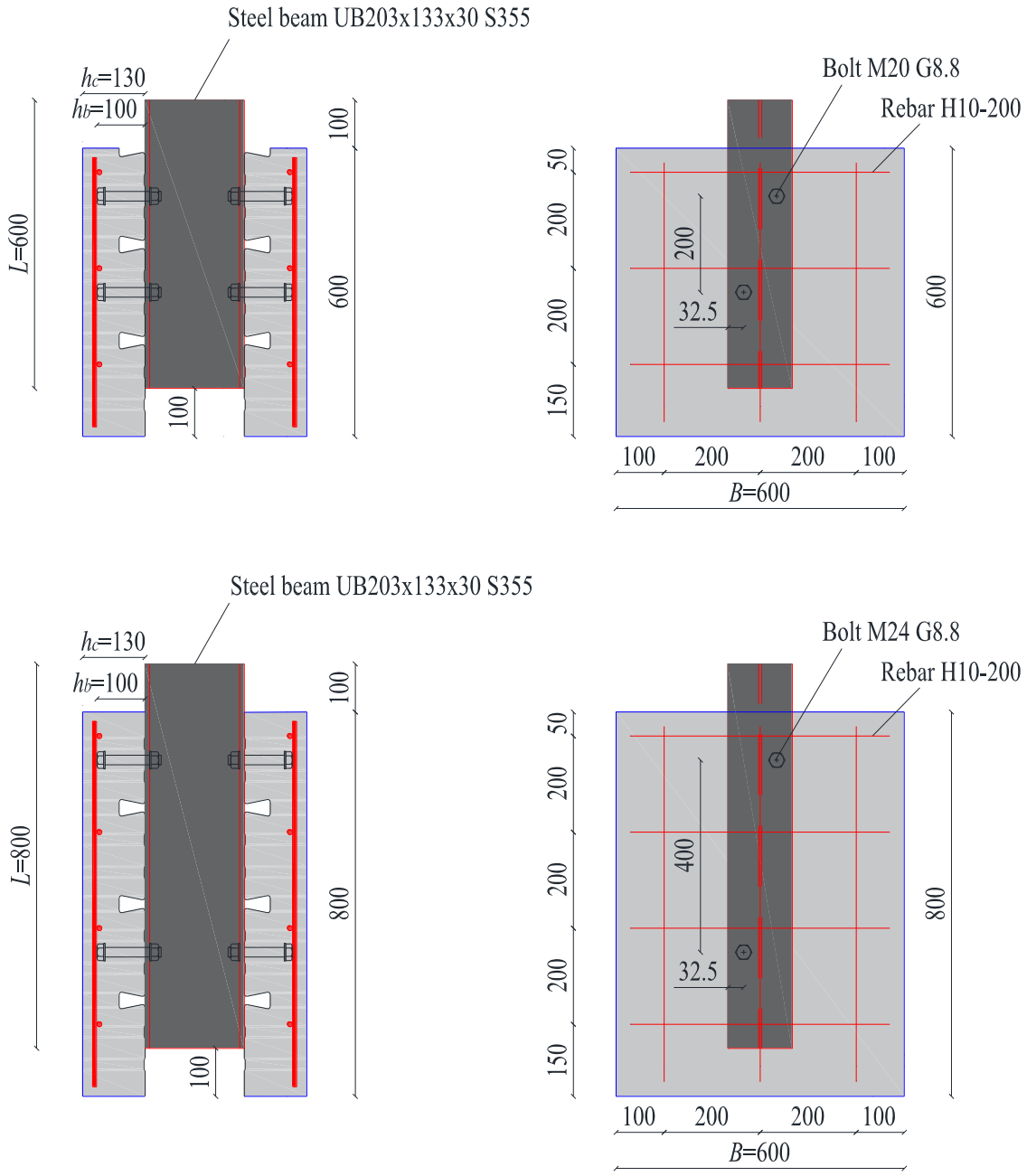

Fig. 3.10 Geometric dimensions of push-off test specimens

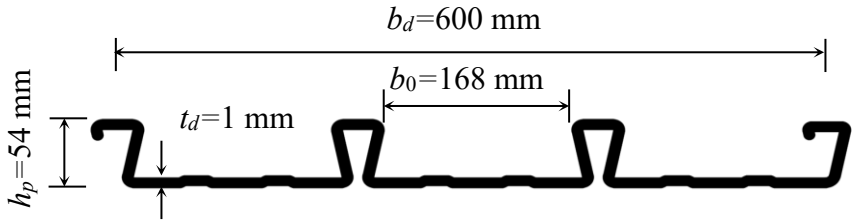

Fig. 3.11 Details of profiled steel decking – 1 mm-thick Lysaght® bondek® II (unit: mm)

For each type of concrete adopted to cast composite slab, two sizes of class 8.8 bolted shear connectors – M20 and M24 (i.e. the nominal diameters *d* of 20 mm and 24 mm, respectively) were used, leading to eight push-off specimens in total.

Bolted shear connectors were arranged in a staggered pattern with two different spacings - 200 mm and 400 mm, as seen in Fig. 3.10, respectively. All bolted shear connectors have an identical bolt length h_b of 100 mm. The nominal pre-drilled bolt hole diameters d_0 were 2 mm larger than the bolt diameters. Table 3.1 tabulates the key design details of all the push-off specimens. The specimen ID consisted of the bolted shear connector identifier (M20 and M24), the longitudinal spacing between two connectors (200 mm and 400 mm) and the concrete material identifier (NA, RA30, RA70 and RA100).

Table 3.1 Specifications of push-off test specimens and test results

Specimen ID	Concrete	Connector	
	r (%)	d (mm)	s (mm)
M20-200-NA	0	20	200
M20-200-RA30	30	20	200
M20-200-RA70	70	20	200
M20-200-RA100	100	20	200
M24-400-NA	0	24	400
M24-400-RA30	30	24	400
M24-400-RA70	70	24	400
M24-400-RA100	100	24	400

3.3.2 Four-point bending tests

In total, four steel–RAC composite beams and one steel–NAC composite beam, with an identical total length L of 6000 mm but different bolted shear connectors and concrete types, were designed for full-scale four-point bending tests. As shown in Fig. 3.12, each composite beam specimen consisted of a grade S355 steel I-section beam, Lysaght® bondek® II profiled steel decking and a concrete slab. All specimens used the same UB203×133×30 I-section steel beam, as shown in Fig. 3.13, where h is the outer section depth, b_f is the flange width, t_f and t_w are the flange and web thicknesses, respectively, and r is the corner radius. The profiled steel decking was made of grade G550 cold-formed steel with a nominal thickness t_d of 1 mm. The geometric parameters of a profiled steel decking unit are previously shown in Fig. 3.11, where b_d is the width of the unit profiled steel decking and h_p is the depth of the high recess rib. The concrete slab of all

specimens had the identical overall width B of 1000 mm and overall thickness h_c of 130 mm. Three types of concrete were adopted, namely NA, RA30 and RA100, which denote the concrete with the recycled aggregate replacement ratios r of 0%, 30% and 100%, respectively. The concrete slab was fortified with reinforcement bars having a nominal diameter of 10 mm and a nominal yield strength of 500 N/mm^2. The spacing of reinforcement bars along both transverse and longitudinal directions was 200 mm, resulting in the meshing details shown in Fig. 3.14.

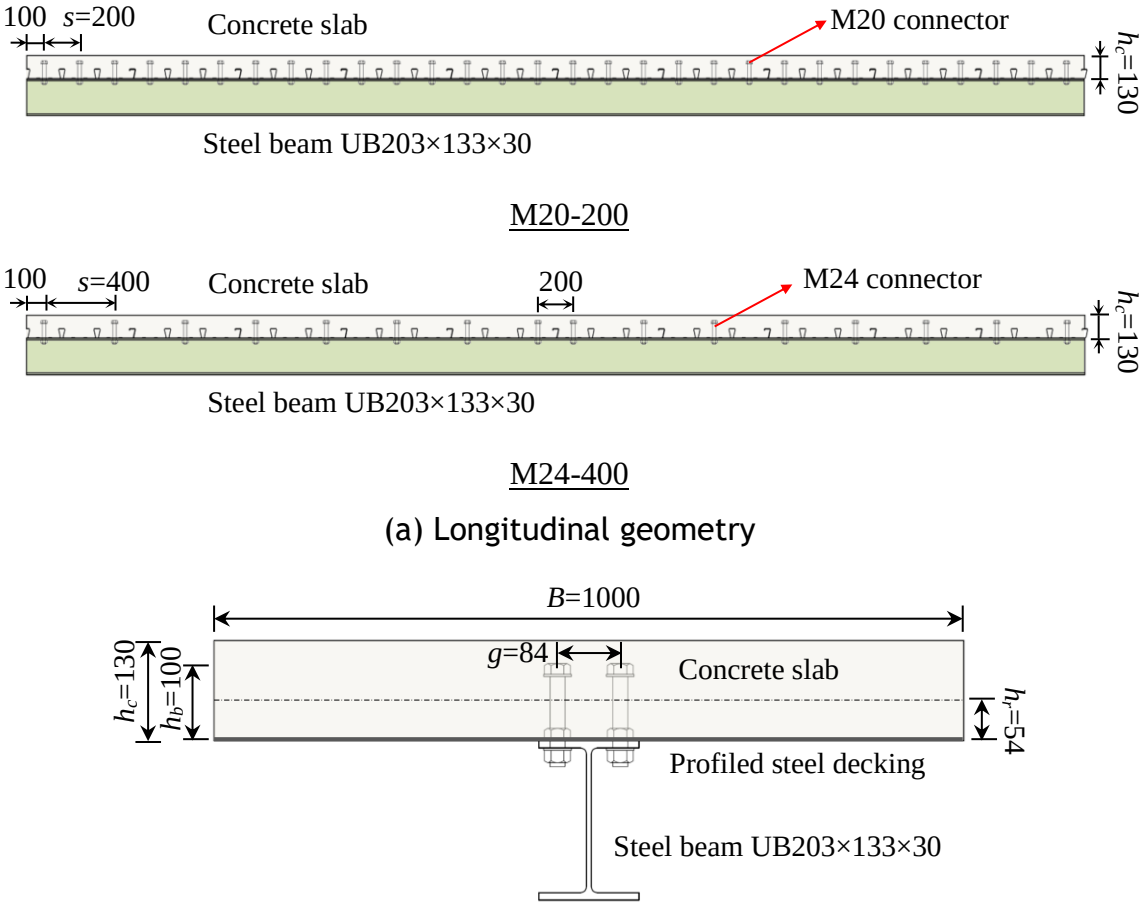

Fig. 3.12 Geometric dimensions of typical composite beam specimens

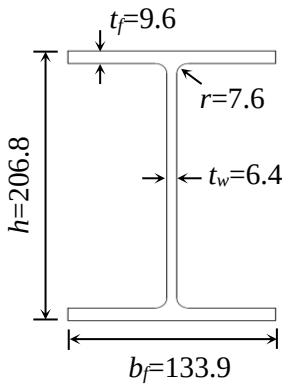

Fig. 3.13 Details of steel beam – UB203×133×30 (unit: mm)

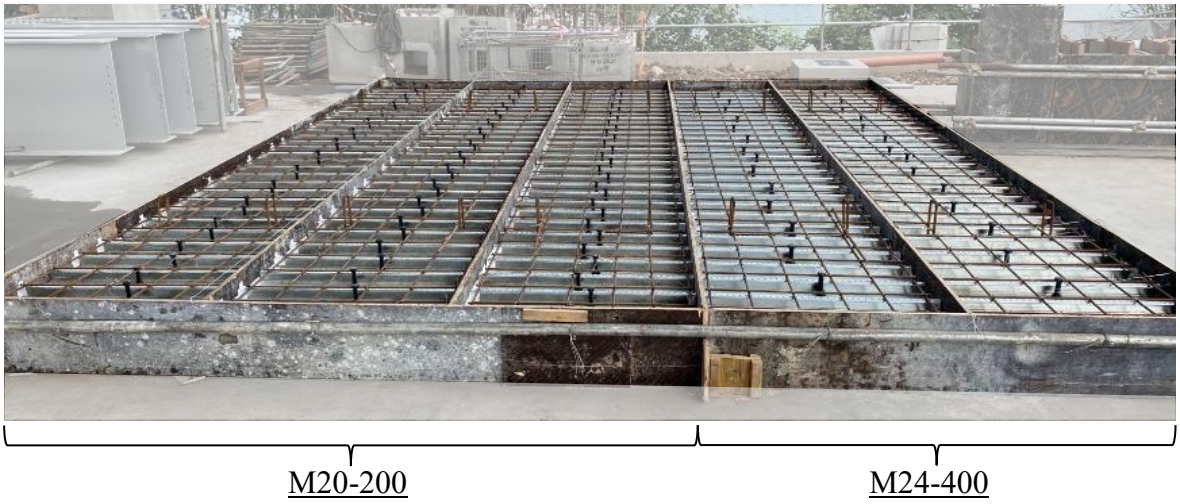

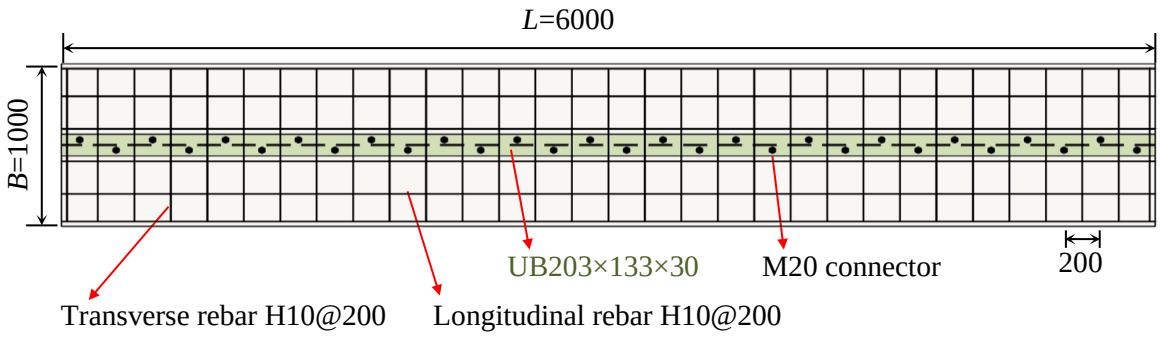

M20-200

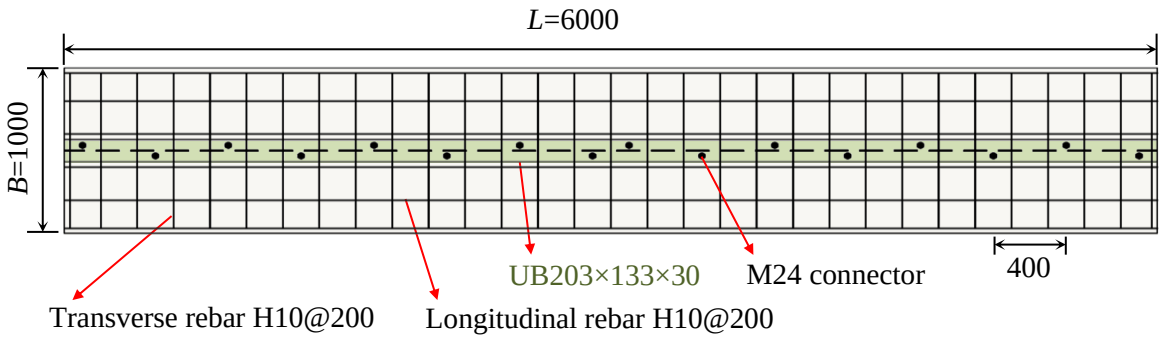

M24-400

Fig. 3.14 Reinforcement bar and demountable connector detailing of composite beam specimens (unit: mm)

In order to assemble the composite slab and steel I-beam and provide an appropriate degree of connection for each composite beam specimen, two sizes of bolted connectors were installed through the pre-drilled bolt holes in the top flange of the steel I-beam and the profiled steel decking. Similar to the push-off tests, each bolted connector contained one full thread bolt, one washer positioned atop the profiled steel decking, and two nuts, which were pre-tack welded beneath the top flange of the steel I-beam – see Fig. 3.15(a) and above the profiled steel decking to restrain the washer – see Fig. 3.15(b). Two sizes of full thread class 8.8 bolts – M24 and M20, with an identical bolt length h_b of 100 mm and the nominal diameters d of 24 mm and 20 mm, respectively, were utilised in the present study. The nominal diameters of the pre-drilled bolt holes d_0, exceeded the bolt diameters by 2 mm. The bolted shear connectors were evenly distributed with a staggered pattern along the composite beam specimens. The quantity of bolted shear connectors was carefully designed to investigate the effect of the degree of shear connection on the steel–RAC composite beam specimens. Specifically, the degree of shear connection was designed to be 1.0 (i.e. full shear connection) for the specimens utilising M20 bolted shear connectors, leading to a total of 30 M20 bolted shear connectors for each specimen. Conversely, for test specimens employing M24 bolted shear connectors, the shear connection degree was set below 1.0 (partial shear connection), resulting in 16 M24 bolted shear connectors per specimen.

(a) Bolted connector connected to top flange of steel I-beam

(b) Bolted connector connected to profiled steel decking

Fig. 3.15 Bolted connector

Figs 3.12(a) and 3.12(b) illustrate the locations and spacings of bolted connectors along the longitudinal and transverse directions, respectively. The transverse spacing *g*, defined as the distance between two consecutive bolt hole centres along the transverse direction, was designed to be 84 mm for all the test specimens. For the composite beam specimens with M20 bolted shear connectors, the internal longitudinal spacing *s* was 200 mm and the end distance between the centre of the outermost bolted connector and the end of the composite beam was 100 mm, while for the composite beam specimens with M24 bolted shear connectors, the internal longitudinal spacing *s* was 400 mm and the end distance remained 100 mm. Table 3.2 summarises the key design details for each specimen. The labelling system starts with the bolted connector type (M20 or M24) and is followed by the internal longitudinal spacing of the connectors (200 mm or 400 mm) and the concrete type (NA, RA30 or RA100).

Table 3.2 Design details of composite beam specimens

Specimen ID	Steel beam	Concrete Slab				Shear Connector		
		r (%)	B (mm)	L (mm)	h_c (mm)	d (mm)	h_b(mm)	s (mm)
M20-200-NA	UB203×133×30	0	1000	6000	130	20	100	200
M20-200-RA30	UB203×133×30	30	1000	6000	130	20	100	200
M20-200-RA100	UB203×133×30	100	1000	6000	130	20	100	200
M24-400-RA30	UB203×133×30	30	1000	6000	130	24	100	400
M24-400-RA100	UB203×133×30	100	1000	6000	130	24	100	400

3.4 Summary

This chapter presents the development of a sustainable and demountable composite floor system incorporating RAC and demountable shear connectors designed for temporary and short-lease structures. The chapter introduces the novel composite floor system, consisting of profiled steel decking, an RAC slab, and demountable shear connectors. This system aims to deliver a reusable floor solution with minimal environmental impact.

The chapter details the materials and components used in the system. Various RAC mixes with different replacement ratios for the concrete were designed to meet target strength requirements through adjustments to the water-to-cement ratio. This approach allowed direct comparisons across different RAC compositions while maintaining consistent specimen dimensions. Two main types of demountable shear connectors are discussed: bolted connectors (with two sets of nuts and washers) and Nelson demountable connectors. However, the bolted connector was chosen for this study due to its practicality and ease of application.

The chapter also addresses the arrangement of shear connectors within the floor system. Lysaght® Bondek® II, a commonly used steel decking with a re-entrant rib profile, was selected to facilitate the alignment of pre-drilled holes. The unique geometry of the decking influences the spacing of the connectors, with the deck's 200 mm pan spacing dictating the connector layout.

The process of assembling and disassembling the composite system is described, where bolts are inserted into pre-drilled holes on the profiled steel decking and the top flange of the steel I-beam. Following testing, the system is disassembled by untightening the bolts and separating the beam and concrete slab. When applied in realistic engineering settings, this process would require the floor slab to be cut and lifted for recycling while the steel I-beam remains reusable.

A comprehensive testing plan is outlined to assess the structural performance of the proposed system. The testing programme includes push-off tests and full-scale four-point bending tests. The push-off tests assess the shear-slip behaviour of the demountable connectors using various RAC mixes with different connector sizes

and spacings. Eight specimens featuring varying recycled aggregate replacement ratios and connector configurations were tested to evaluate the load-bearing capabilities of the connectors. For the full-scale bending tests, five specimens of composite beams with differing recycled aggregate replacement ratios and degrees of shear connection underwent four-point bending to study the overall structural behaviour.

Tables summarise the design details of each test specimen, including specifications for the steel I-beam, RAC slab, and arrangement of shear connectors. Specimens are labelled according to connector size, spacing, and recycled aggregate replacement ratio, providing a clear framework for interpreting test results.

In summary, this chapter outlines the design, material selection, assembly method, and testing plan for a sustainable composite floor system that can be disassembled and reused, highlighting its potential application in building structures.

4 PUSH-OFF EXPERIMENTS AND NUMERICAL MODELLING

4.1 Introduction

This chapter investigates the shear-slip behaviour of demountable shear connectors in RAC composite slabs through experimental and computational methods. The chapter starts with the presentation of material preparation and testing on concrete and steel, followed by the experimental testing on push-off specimens, in which two connector arrangements and four recycled aggregate replacement ratios were adopted, resulting in a total of eight specimens. The push-off test results, including failure modes and ultimate loads, as well as load – slip curves, are presented in detail. Alongside the testing programme, numerical simulations were conducted, during which finite element models were initially evaluated against the test results and subsequently offered additional insights into structural performance. Finally, the applicability of the pertinent codified design methodologies for steel–NAC composite slabs with welded shear connectors, as delineated in EN 1994-1-1 (2004) and ANSI/AISC 360-16 (2016), was assessed based on the test data.

4.2 Material tests

4.2.1 Concrete

Single-sized natural aggregate and recycled aggregate with a nominal size of 20 mm, together with natural sand and Ordinary Portland cement, were adopted to fabricate the NAC and RAC employed in this study. Both the coarse and fine aggregates were graded to BS EN 12620 (2008). To compensate for the water absorption during mixing, all fine and coarse aggregates were maintained in a saturated surface dry (SSD) condition, with the SSD specific gravity in a range between 2.60 and 2.65. To achieve the target design strength of 40 N/mm^2 for concrete mixes with varying recycled aggregate replacement ratios, modified water-to-cement ratios were adopted while keeping a constant added water. Admixtures were also adopted, including the retarding plasticiser for delaying the

concrete setting and hardening and the superplasticiser for reducing the required water and maintaining the workability of fresh concrete.

The mass contents of the mixtures for each of the four analysed concrete (i.e. NA, RA30, RA70 and RA100) are presented in Table 4.1. For each type of concrete, six 150x150x150mm concrete cube samples and three 150x300mm concrete cylinders were cast and cured alongside the corresponding push-off specimens under the identical condition. Three concrete cubes were tested on Day 7, and the other three on Day 28 to verify if the design mix achieved the intended design strength. Table 4.2 presents the 7-day and 28-day compressive strengths of different concrete mixes.

The results show that the different design mixes can achieve similar target mean strength. Different failure modes were observed on the cube test between NAC and RAC, as the crack line on RAC linked together and was split into pieces.

Table 4.1 Proportions of concrete mixtures (unit: kg/m^3)

Concrete type	Cement	Water	Water-to-cement Ratio	Sand	Natural aggregate	Recycled aggregate	Retarding plasticiser	Super-plasticiser
NA	385	164	0.43	786	1010	0	1.50	4.54
RA30	405	164	0.40	757	707	303	1.57	5.02
RA70	425	164	0.39	739	303	707	1.65	5.53
RA100	445	164	0.37	721	0	1010	1.73	6.06

Table 4.2 Summary of 7 days and 28 days concrete compressive strength

DESIGN	7 DAYS f_{cu} (N/mm^2)				28 DAYS f_{cu} (N/mm^2)			
MIX	C1	C2	C3	Mean	C4	C5	C6	Mean
40NA	42.6	43.9	43.9	43.5	50.4	50.9	48.7	50.0
40RA30	36	36.6	36.6	36.4	52.3	50.7	51.4	51.5
40RA70	44.1	43.1	41.9	43.0	55.4	57.8	59.8	57.7
40RA100	40.1	42	40.8	41.0	51.6	52.1	57.6	53.8

Fig. 4.1 NAC 28 days cube failure mode

Fig. 4.2 RAC 28 days cube failure mode

Moreover, concrete cylinder tests were performed in parallel with the push-off tests to assess the concrete properties, as illustrated in Fig. 4.3. Two strain gauges were affixed at the midpoint of the concrete cylinder to quantify compressive strains during these experiments. Table 4.3 presents the average material properties of each type of concrete, encompassing the concrete compressive strength f_c from three concrete cylinder tests conducted on the testing day, as

well as the secant modulus E_{cm}. The values were juxtaposed with the theoretical computations derived from BS EN 12390-13 (2013).

Fig. 4.3 Concrete cylinder test

Table 4.3 Key material properties of concrete

Concrete type	f_c (N/mm^2)	E_{cm} (N/mm^2)
NA	38.2	36890
RA30	36.5	32932
RA70	38.3	34600
RA100	39.3	38400

4.2.2 Steel

The essential material parameters and stress-strain curves of the adopted grade S355 steel I-section member and grade G550 steel profiled decking was acquired using tensile coupon tests. According to the dimension requirements prescribed in EN ISO 6892-1 (2016) and ASTM E8/E8M-15a (2015), three flat coupons were extracted from the flange and web of the steel I-section member and the profiled decking. Fig. 4.4 depicts the experimental setup, wherein a coupon specimen was placed in an ATM 50 kN universal machine. Two strain gauges were affixed at the midpoint of the coupon to measure the longitudinal strains, and a calibrated

extensometer with a 50 mm gauge length was attached to capture the elongations in the necking region of the specimen. Tensile loads were exerted by the universal machine under displacement control, with an initial loading speed of 0.05 mm/min prior to attaining 0.2% proof strength and an increased speed of 0.8 mm/min until fracture occurred.

Fig. 4.4 Tensile coupon test setup

The resulting strain rates conformed to the specifications specified in EN ISO 6892-1 (2016) and ASTM E8/E8M-15a (2015). The complete spectrum of recorded stress-strain curves is exhibited in Fig. 4.5. On the basis of the stress-strain histories, the essential measured values of material parameters are presented in Table 4.4, where E donates the Young's modulus, $\sigma_{0.2}$ represents the 0.2% proof strength, σ_u and ε_u are the ultimate strength and the corresponding strain, and ε_f is the fracture strain.

Table 4.4 Material properties measured from tensile coupon tests

Coupon ID	E (GPa)	$\sigma_{0.2}$ (MPa)	σ_u (MPa)	e_u (%)	e_f (%)
S355-F	209.2	363.8	528.8	11.5	16.8
S355-W	204.6	413.5	541.1	12.8	19.1
G550	187.3	645.5	658.1	1.4	2.7

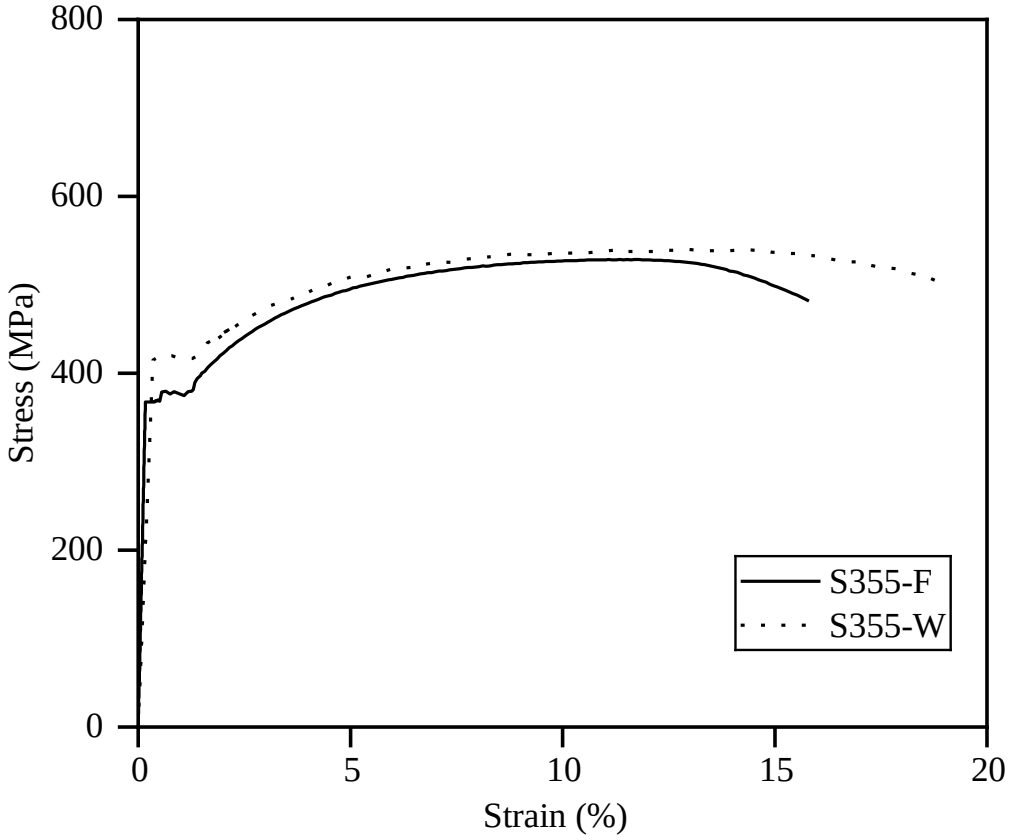

(a) Steel I-beam

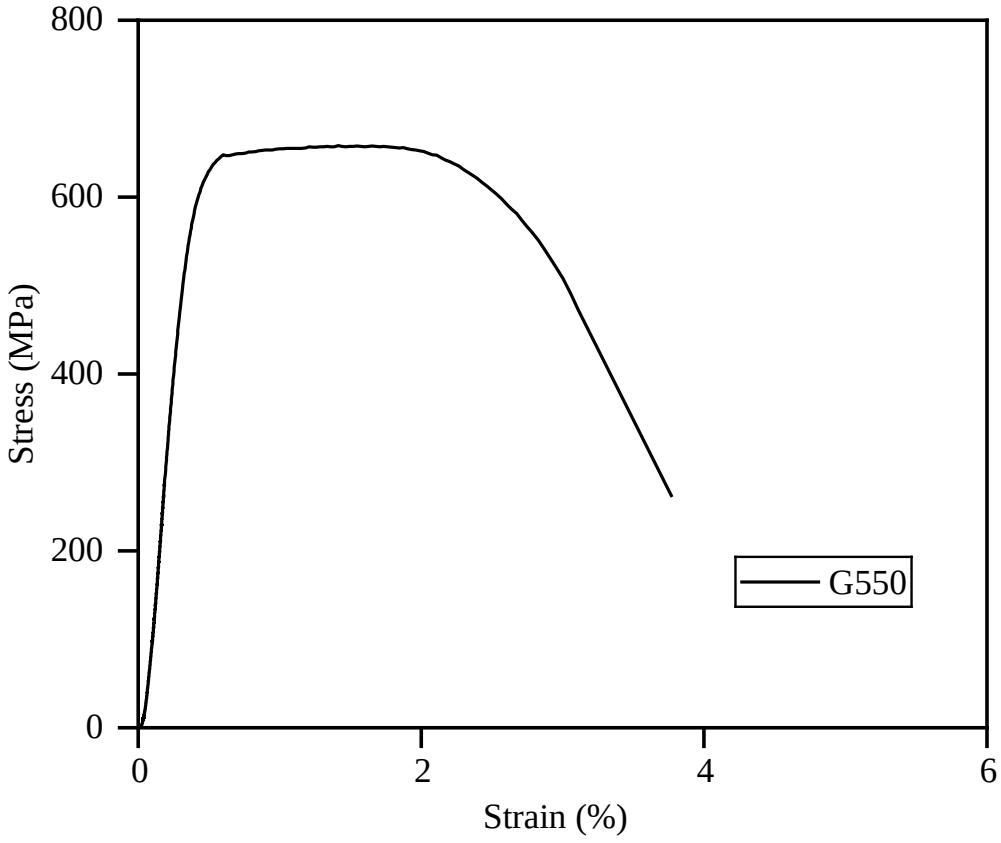

(b) Decking

Fig. 4.5 Steel material stress-strain curves

4.3 Push-off tests

To examine the load-carrying capacity, stiffness and ductility of demountable bolted shear connectors, push-off tests were carried out on eight full-scale composite slab specimens. As detailed in Section 3.3.1, each push-off specimen consisted of two composite slabs connected to a steel I-section member using bolted connectors. Fig. 4.6 illustrates the test setup of the push-off test. A displacement-controlled Instron 1000 kN hydraulic testing equipment with fixed end platens was used to exert the axial compression load onto the steel member at a constant loading rate of 0.5 mm/min. To acquire the relative slips between the steel member and composite slab resulting from the axial load, four linear variable displacement transducers (LVDTs) were vertically installed, two at the top of the steel member (LVDT-V1 and LVDT-V2, one on each side of the steel section) and two at the top of the concrete sections (LVDT-V3 and LVDT-V4, one on each slab). These LVDTs measured the vertical displacements in the steel member and the slab, which were subsequently used to derive the relative slips between them. In addition to the vertical LVDTs, another two horizontal LVDTs (LVDT-H1 and LVDT-H2) were installed at the quarter-length locations on the web of the steel member to monitor the out-of-plane displacements of the steel member.

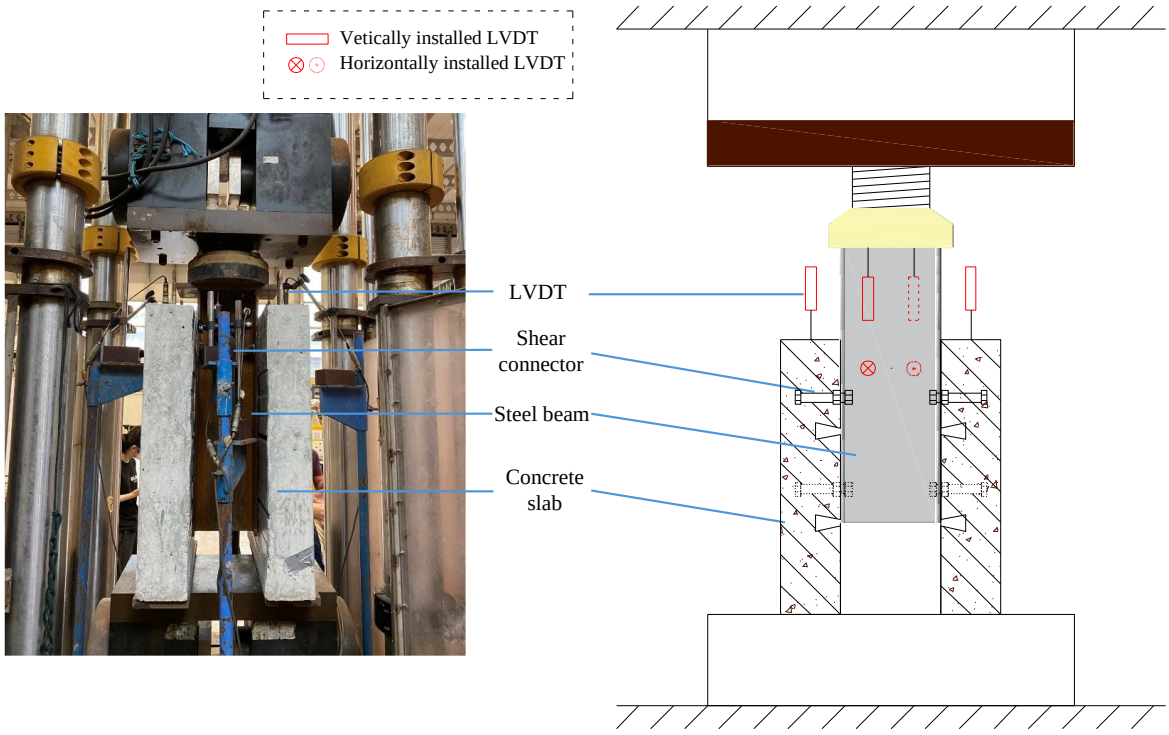

Fig. 4.6 Push-off test setup

4.4 Discussion on test results

4.4.1 Failure modes

The failed push-off specimens are shown in Fig. 4.7, which sheds light on the general failure modes of the specimens. In addition, to observe the shear fractures surrounding the bolted connectors, the composite slabs were demounted from the steel member and the profile decking was cut off, revealing the crack pattern at the connector. Finally, shear connectors were taken out of the slab and their deformed shapes were examined. Both the crack pattern and the deformed configuration of shear connectors for each specimen are also displayed in Fig. 4.7.

Front

Back

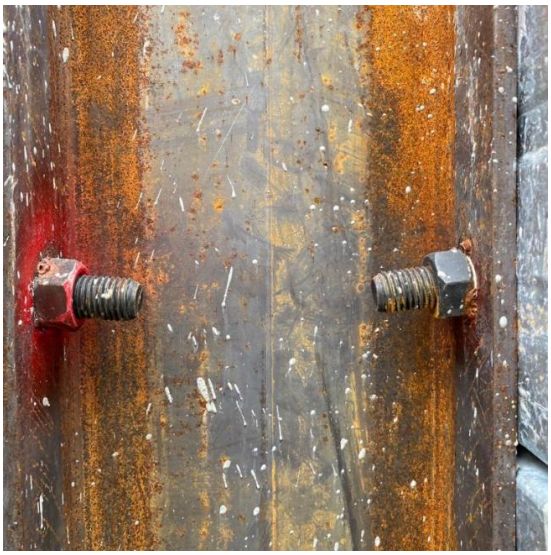

1st Row Connector

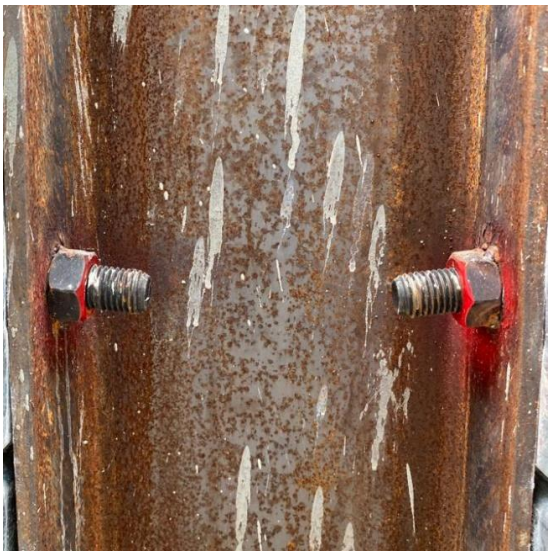

2nd Row Connector

Slab Inner Face

Slab Outer Face

(a) Failure mode of specimen M20-200-NA

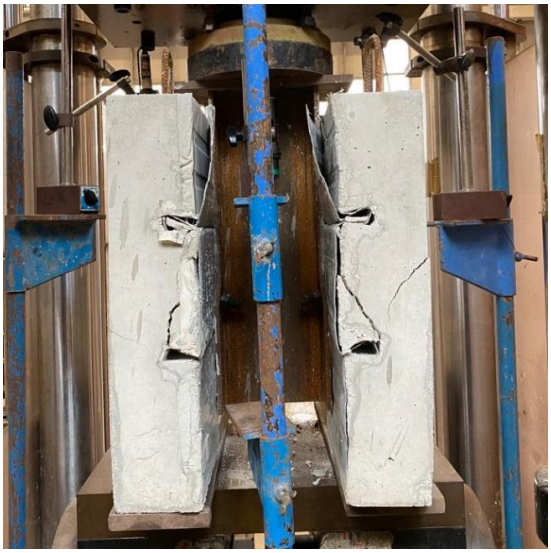

Front

Back

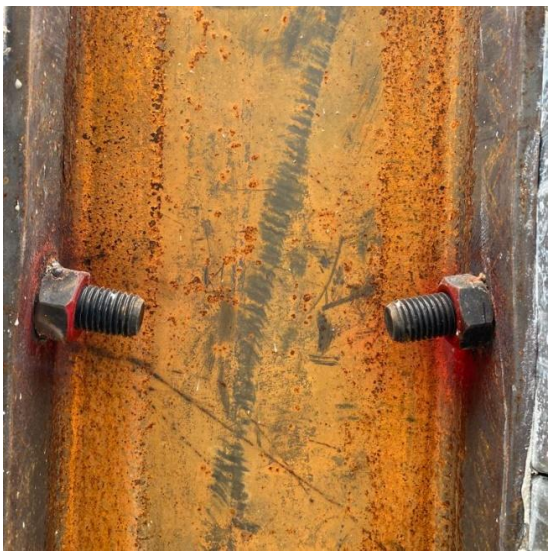

1st Row Connector

2nd Row Connector

Slab Inner Face

Slab Outer Face

(b) Failure mode of specimen M20-200-RA30

Front

Back

1st Row Connector

2nd Row Connector

Slab Inner Face

Slab Outer Face

(c) Failure mode of specimen M20-200-RA70

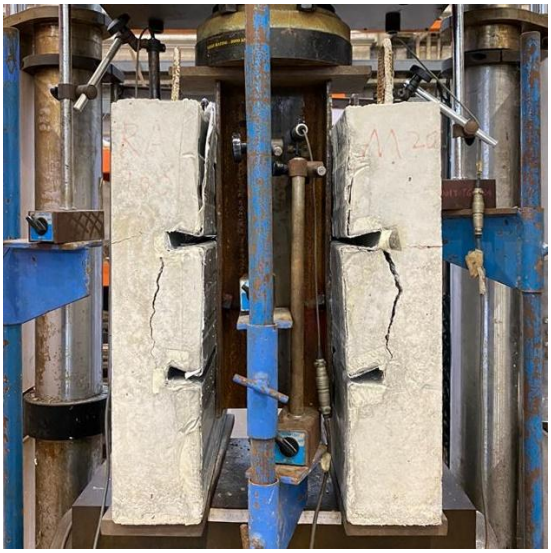

Front

Back

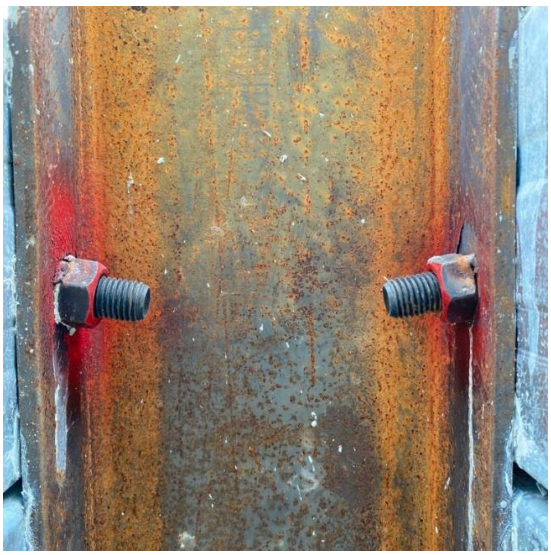

1st Row Connector

2nd Row Connector

Slab Inner Face

Slab Outer Face

(d) Failure mode of specimen M20-200-RA100

Front

Back

1st Row Connector

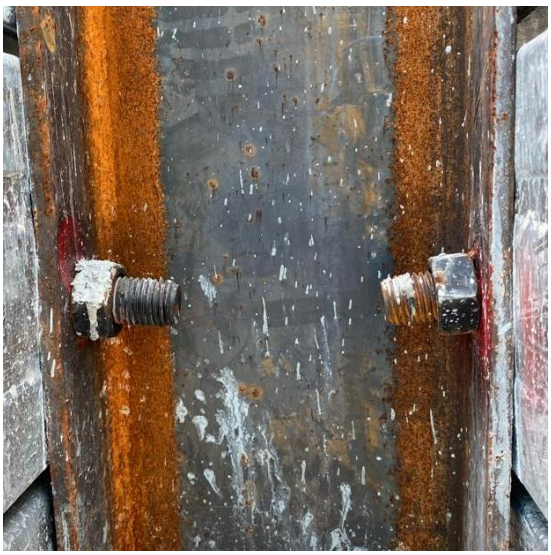

2nd Row Connector

Slab Inner Face

Slab Outer Face

(e) Failure mode of specimen M24-400-NA

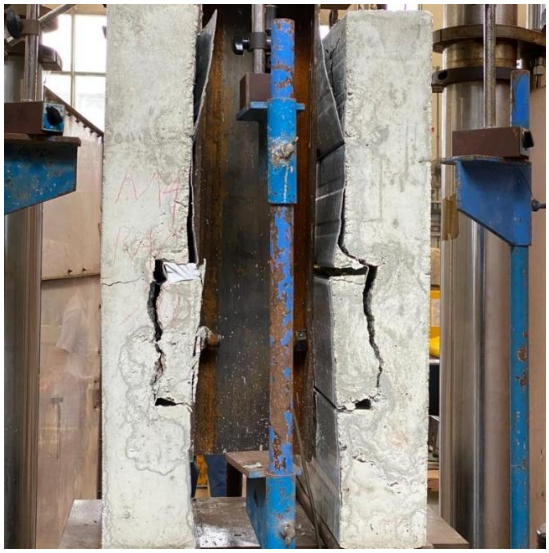

Front

Back

1st Row Connector

2nd Row Connector

Slab Inner Face

Slab Outer Face

(f) Failure mode of specimen M24-400-RA30

Front

Back

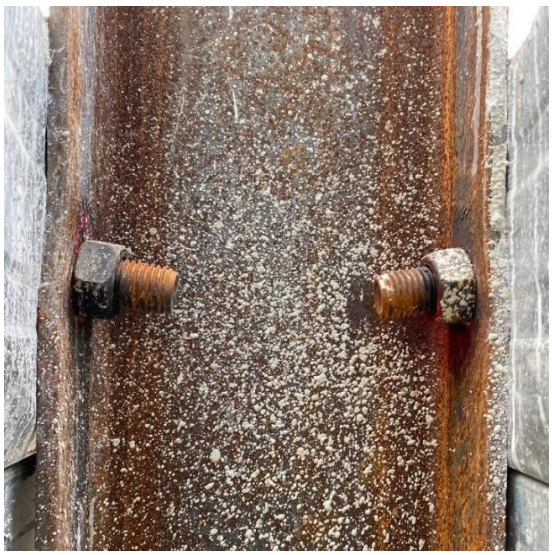

1st Row Connector

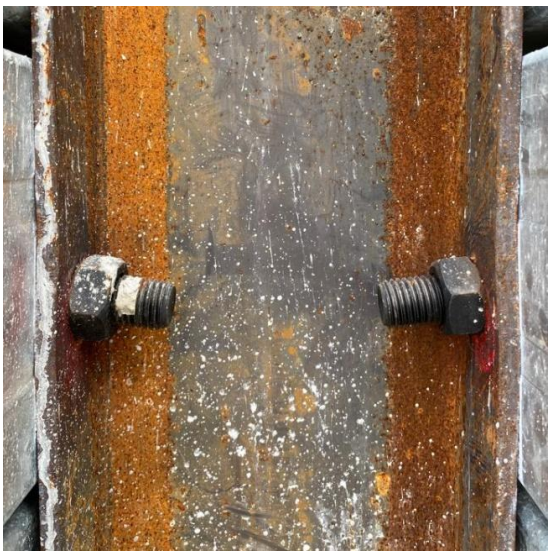

2nd Row Connector

Slab Inner Face

Slab Outer Face

(g) Failure mode of specimen M24-400-RA70

Front

Back

1st Row Connector

2nd Row Connector

Slab Inner Face Slab Outer Face

(h) Failure mode of specimen M24-400-RA100

Fig. 4.7 Failure modes of composite beam specimens

The concrete shear failure mode was observed upon testing for each composite slab specimen, with failed push-out specimens shown in Fig. 4.7. Besides the general failure modes, Fig. 4.7 also displays the demounted specimen after testing, where the shear cracks were observed on concrete in compression, while the bolted shear connectors were bent. Specifically, the shear cracks initiated at the vicinity of the connectors and propagated through the concrete slab, forming a cone shape with the base width approximately equal to about 3 to 4 times of the distance from the centre of the shear connector to the edge of the concrete block along the loading direction. Fig. 4.8 shows the deformed demounted bolted shear connectors after testing, where M20 connectors exhibited more significant deformations than M24 connectors but no connector fracture observed for all specimens.

(a) M20

(b) M24

Fig. 4.8 Deformed connectors

4.4.2 Load–slip curves

Figs 4.9(a) and 4.9(b) depict the load–slip curves for two series of push-off specimens – M20-200 and M24-400 (with M20 and M24 connectors, respectively), where the applied compressive loads, as measured by the testing machine's integrated sensor, are laid out against the relative slips between the steel member and the composite slab. All load–slip curves show prominent elastic and plastic regions, transiting at a small drop of load when the concrete shear cracks were initiated. In the elastic region, all the load–slip curves show a linear trend with

similar stiffnesses. Upon the formation of shear cracks surrounding the shear connectors, the slip increases rapidly, reflected by a flatter slope on the load-slip curve, which indicates a decrease in the shear stiffness of the specimen. Table 4.5 tabulates the ultimate load per connector P_u and the corresponding ultimate slip δ_u for all the push-off specimens. Table 4.5 illustrates that the ultimate load generally increases with the recycled aggregate replacement ratio for specimens with the same connector size and spacing. Moreover, the M24-400 push-off specimens have generally higher shear capacities but slightly lower ductility than their M20-200 counterparts.

Table 4.5 Design details of push-off test specimens and test results

Specimen ID	Concrete	Connector		Ultimate load per connector (kN)	Ultimate slip (mm)
	r (%)	*d* (mm)	*s* (mm)		
M20-200-NA	0	20	200	110.1	10.6
M20-200-RA30	30	20	200	133.3	11.6
M20-200-RA70	70	20	200	150.9	12.8
M20-200-RA100	100	20	200	157.6	14.4
M24-400-NA	0	24	400	147.0	9.9
M24-400-RA30	30	24	400	176.5	11.8
M24-400-RA70	70	24	400	167.6	10.6
M24-400-RA100	100	24	400	195.5	13.9

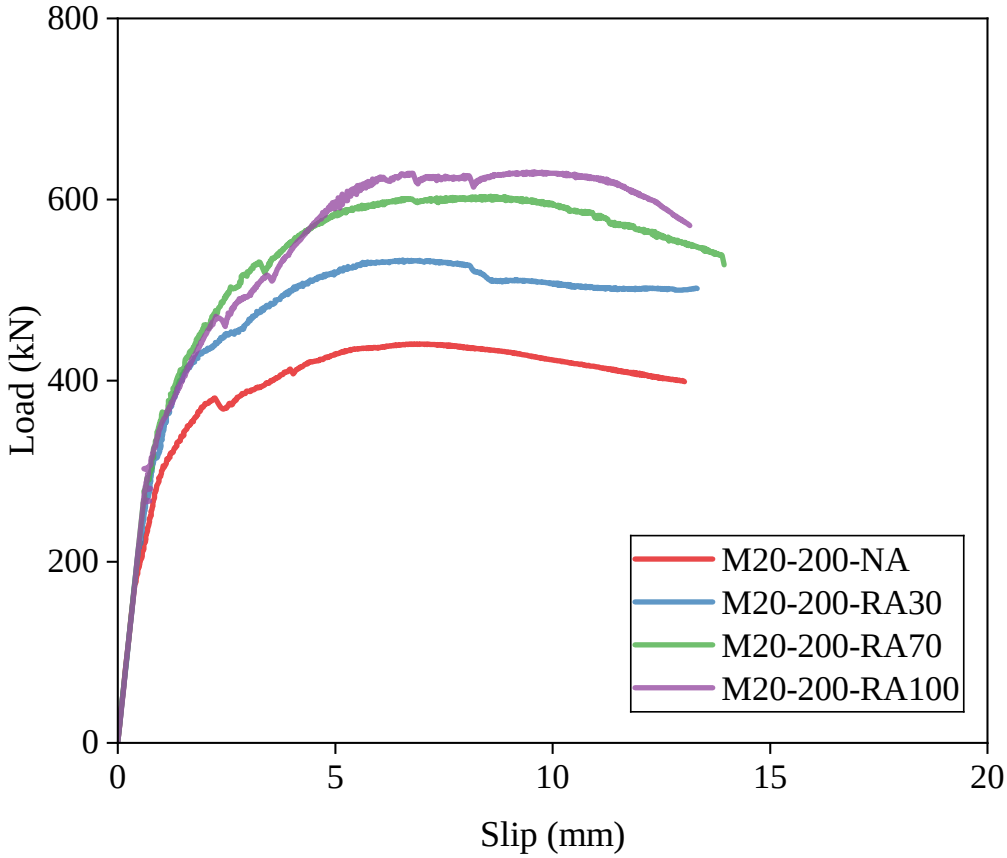

(a) M20 specimens

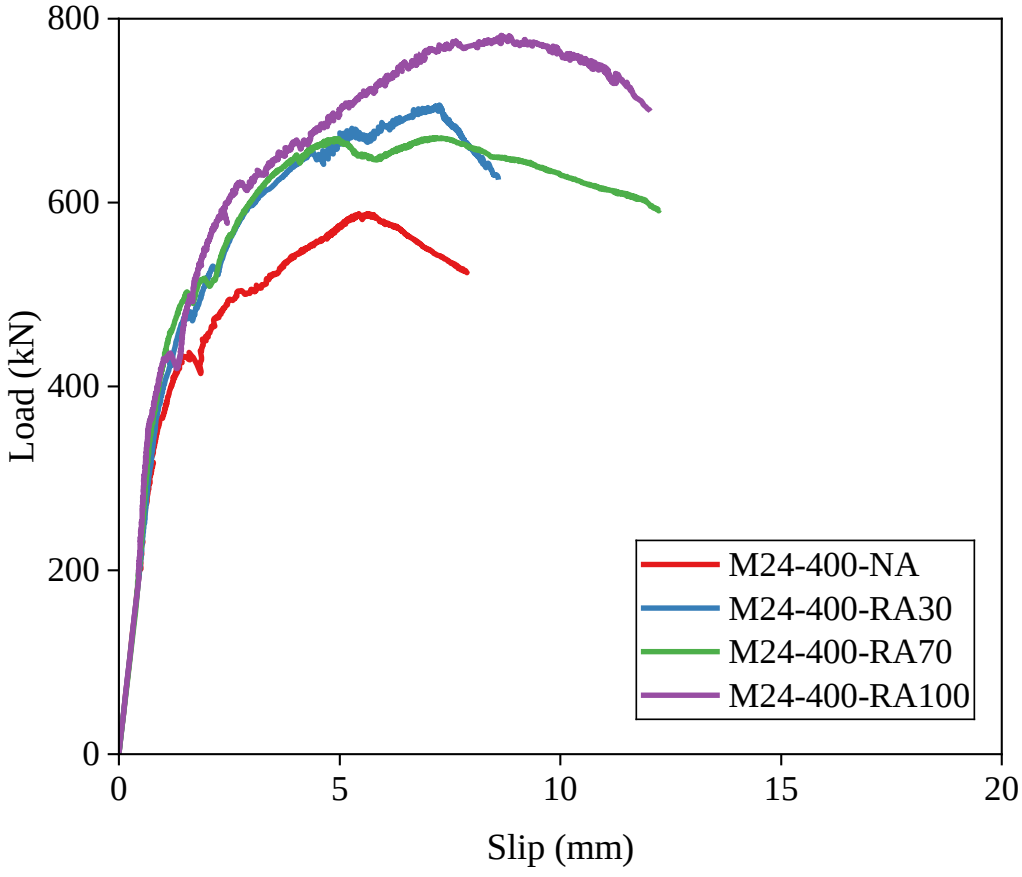

(b) M24 specimens

Fig. 4.9 Load–slip curves of push-off specimens

4.5 Numerical modelling programme

4.5.1 General

Alongside the experimental programme, numerical simulations were conducted utilising the nonlinear finite element (FE) software ABAQUS (2017) to enhance understanding of the failure mechanisms in steel–RAC composite slabs with demountable bolted shear connectors. The comprehensive modelling assumptions, methodologies, and protocols were initially outlined in Section 4.5.2. The produced finite element models were then validated against the experimental findings presented in Section 4.4.3.

4.5.2 Development of FE models

Each full-scale push-off composite slab specimen was modelled according to the designed geometric sizes and measured material properties. With the aim of improving the computational efficiency, only half of each specimen was modelled to decrease the number of finite elements. Fig. 4.10 presents the load and boundary conditions imposed on the half model. Full restraints on displacements and rotations were assigned to the reference point that coupled the entire concrete slab base and were also assigned to the decking base. Symmetry along the central line of the steel beam was defined as well, i.e., no horizontal movement was allowed. The eight-node brick element C3D8R (ABAQUS, 2017) was adopted herein to simulate the steel member, concrete slab and demountable bolted shear connectors of each specimen; the four-node shell element S4R (ABAQUS, 2017) was chosen to model the steel decking; and the two-node truss element T3D2 (ABAQUS, 2017) was applied to model the reinforcing bars within the concrete slab. All of these finite elements have been widely utilised in prior numerical analyses of steel–concrete composite slabs (Ciao et al., 2022; Kildashti et al., 2024; Li et al., 2024; Liu et al., 2023; Pavlović et al., 2013).

For the steel member and profiled decking, elastic-plastic material models were employed based on the associated stress-strain curves derived from the tensile coupon test, as shown in Fig. 4.5. A Poisson’s ratio of 0.3 was employed in the steel material models.

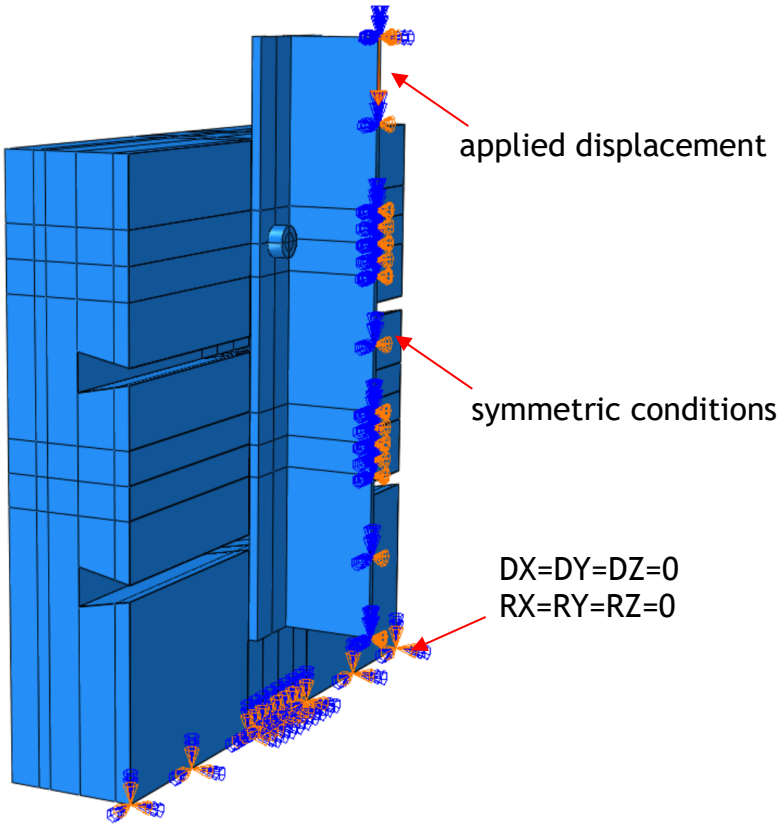

(a) boundary conditions, symmetric conditions and applied displacement

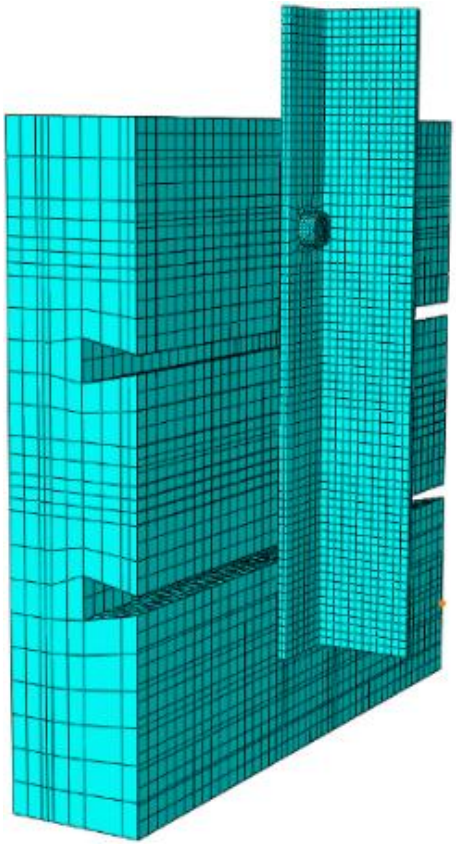

(b) mesh

Fig. 4.10 FE model

For bolted shear connectors, a Ramberg–Osgood material model (Ramberg & Osgood, 1943) was adopted up to the engineering ultimate stress, according to Eqs. (4.1) and (4.2). where: σ_{nom} and ε_{nom} are the engineering stress and strain, respectively; E_0 is the Young's modulus and taken as 200 GPa; $\sigma_{0.2}$ and σ_{ub} are the yield strength and the ultimate strength of bolt, which are respectively 640 MPa and 800 MPa for Grade 8.8 bolts; $\sigma_{0.2}$ is the strain at yielding; $E_{0.2}$ is the 0.2% elastic modulus and calculated from Eq. (4.3); ε_{ub} is the ultimate strain and taken as 0.055 (Li et al., 2020); n is a parameter and taken as 13.5 (Li et al., 2020); and m is another parameter calculated from Eq. (4.4).

$$\varepsilon_{nom} = \frac{\sigma_{nom}}{E_0} + 0.002\left(\frac{\sigma_{nom}}{\sigma_{0.2}}\right)^n, \text{when } \sigma_{nom} < \sigma_{0.2} \quad (4.1)$$

$$\varepsilon_{nom} = \frac{\sigma_{nom}-\sigma_{0.2}}{E_{0.2}} + \varepsilon_{ub}\left(\frac{\sigma_{nom}-\sigma_{0.2}}{\sigma_{ub}-\sigma_{0.2}}\right)^m + \varepsilon_{0.2}, \text{when } \sigma_{0.2} < \sigma_{nom} < \sigma_{ub} \quad (4.2)$$

$$E_{0.2} = \frac{E_0}{1+0.002nE_0/\sigma_{0.2}} \quad (4.3)$$

$$m = 1 + 3.5\sigma_{0.2}/\sigma_u \quad (4.4)$$

For all steel materials, the engineering stress-strain elastic-plastic curve up to the engineering ultimate stress was transformed into the true stress–plastic strain curve, following Eqs. (4.5) and (4.6), where σ_{true} represents the true stress and ε_{ln}^{pl} donates the true plastic strain. A linear true stress–plastic strain curve was assumed beyond the ultimate stress until fracture, with the fracture stress and strain set at $0.91\sigma_{ub}$ and 0.2 (Li et al., 2020), respectively.

$$\sigma_{true} = \sigma_{nom}(1 + \varepsilon_{nom}) \quad (4.5)$$

$$\varepsilon_{ln}^{pl} = ln(1 + \varepsilon_{nom}) - \frac{\sigma_{true}}{E} \quad (4.6)$$

The concrete damage plasticity model (ABAQUS, 2017) was employed for modelling the plastic behaviour of NAC and RAC. A typical Poisson's ratio of 0.20 was employed for concrete. The dilation angle, flowing potential eccentricity, ratio of the second stress invariant on the tensile meridian to that on the compressive meridian and viscosity parameter, which are used to describe the concrete's plastic behaviour, were taken as 40°, 0.1, 0.667 and 0.001,

respectively. The material compression behaviour was defined according to Eq. (4.7) by the constitutive model specified in EN 1992-1-1 (2004), while the material tension behaviour was defined according to Eq. (4.8) and (4.9) by the tension softening curve (Polus & Szumigała, 2019). The calculated stress-strain curves for the concrete material analysis are shown in Fig. 4.11.

$$\sigma_c = f_c \frac{k\eta - \eta^2}{1+(k-2)\eta} \tag{4.7}$$

Where $k = 1.05E_c \frac{\varepsilon_{c1}}{f_c}$ and $\eta = \frac{\varepsilon_c}{\varepsilon_{c1}}$

$$\sigma_t = E_c \varepsilon_t \text{ if } \varepsilon_t \leq \varepsilon_{cr} \tag{4.8}$$

$$\sigma_t = f_{ct}(\frac{\varepsilon_{cr}}{\varepsilon_t})^n \text{ if } \varepsilon_t \geq \varepsilon_{cr} \tag{4.9}$$

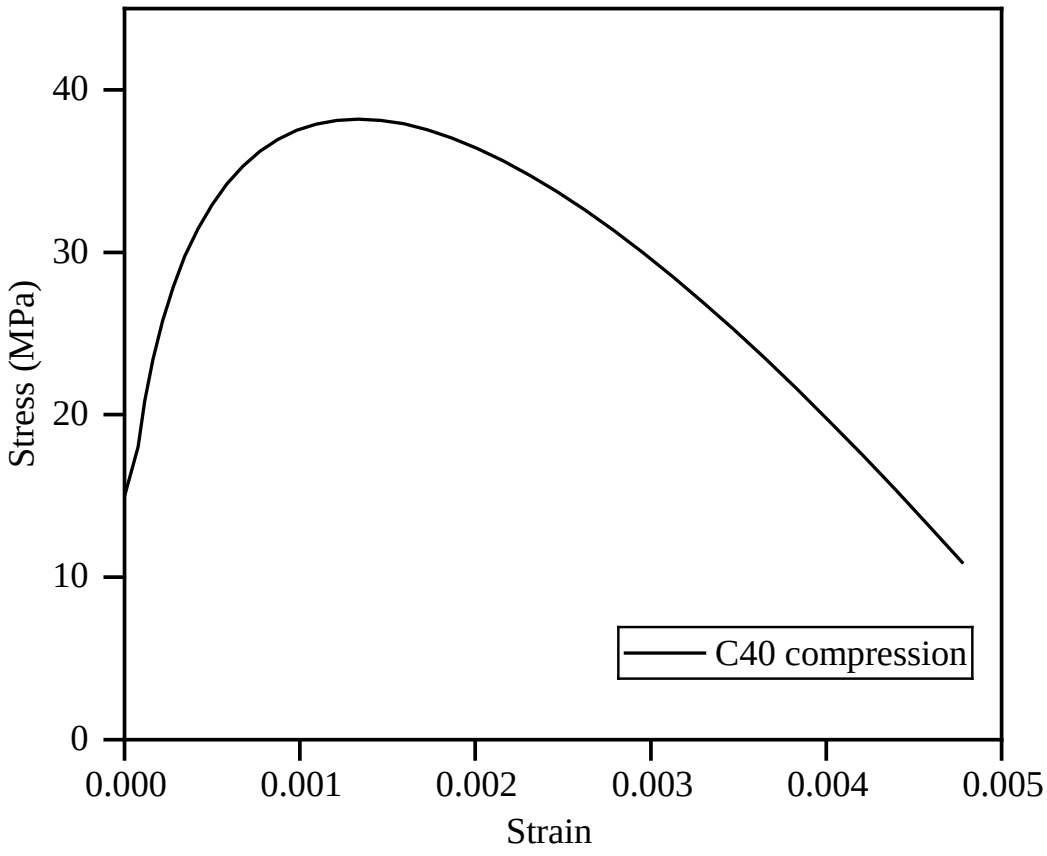

(a) compressive stress-strain curve

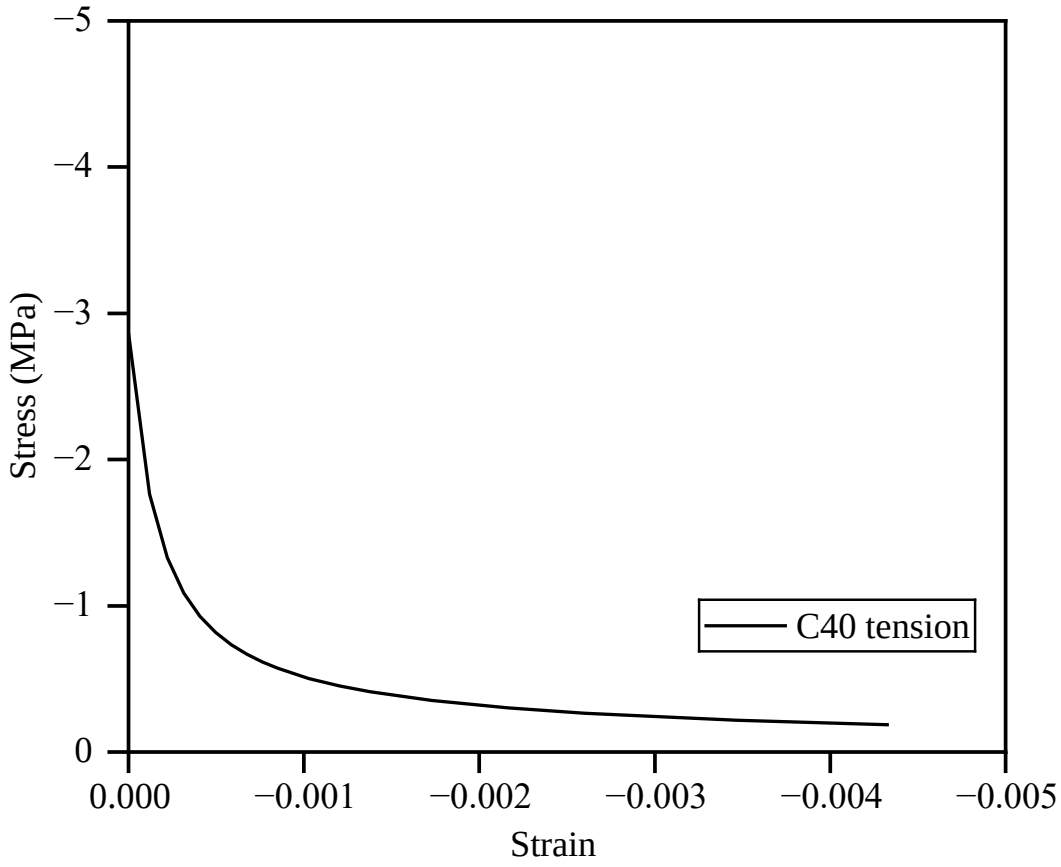

(b) tensile stress-strain curve

Fig. 4.11 Concrete material stress-strain curves

The interaction between the reinforcing bars and the concrete slab was simulated using an embedded region (ABAQUS, 2017). The interactions at concrete-to-connector, concrete-to-decking, decking-to-steel beam and connector-to-steel beam interfaces were modelled as surface-to-surface contact type. A hard contact was specified in the normal direction, facilitating the separation of contact faces while preventing penetration. A penalty approach was utilised in the tangential direction, with the friction coefficients taken as 0.4 for the contacts between the concrete slab and bolted shear connector, 0.6 for the contacts between the concrete slab and profiled decking and 0.2 for the contacts among the bolted shear connector, profiled decking and steel member. A preload of 1 kN was assigned to each bolted shear connector. The nodes of the bottom surface of the composite slab were coupled to a reference point (RP2) situated at the centre of the bottom surface, and the nodes of the top (loading) surface of the steel member were coupled to another reference point (RP1). The experimental boundary conditions were modelled by restraining all the nodes of RP1 and RP2 but permitting longitudinal translation of RP1 with a prespecified displacement.

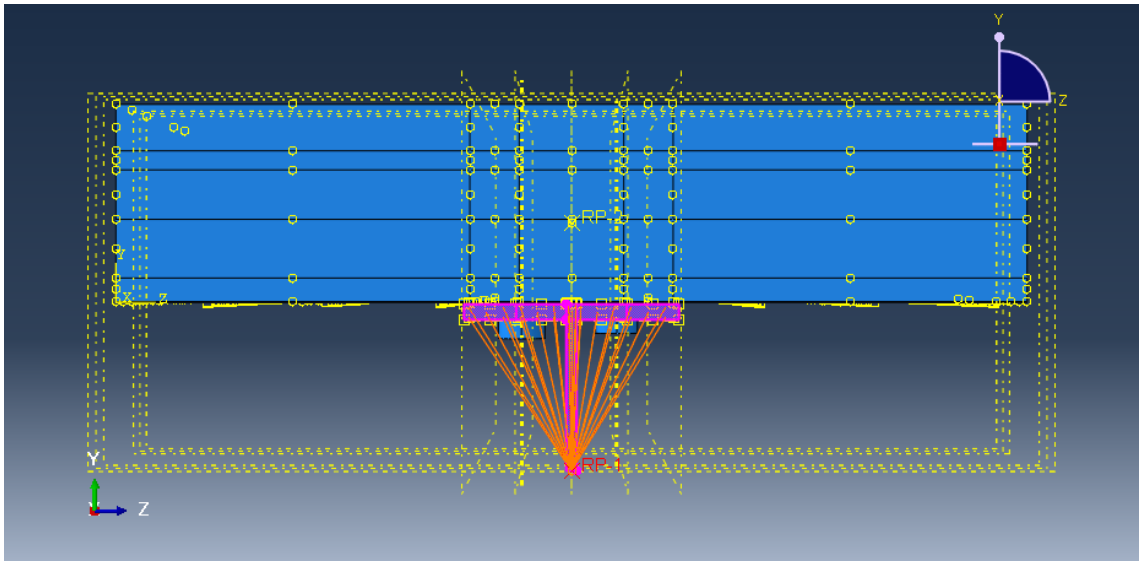

(a) View from top

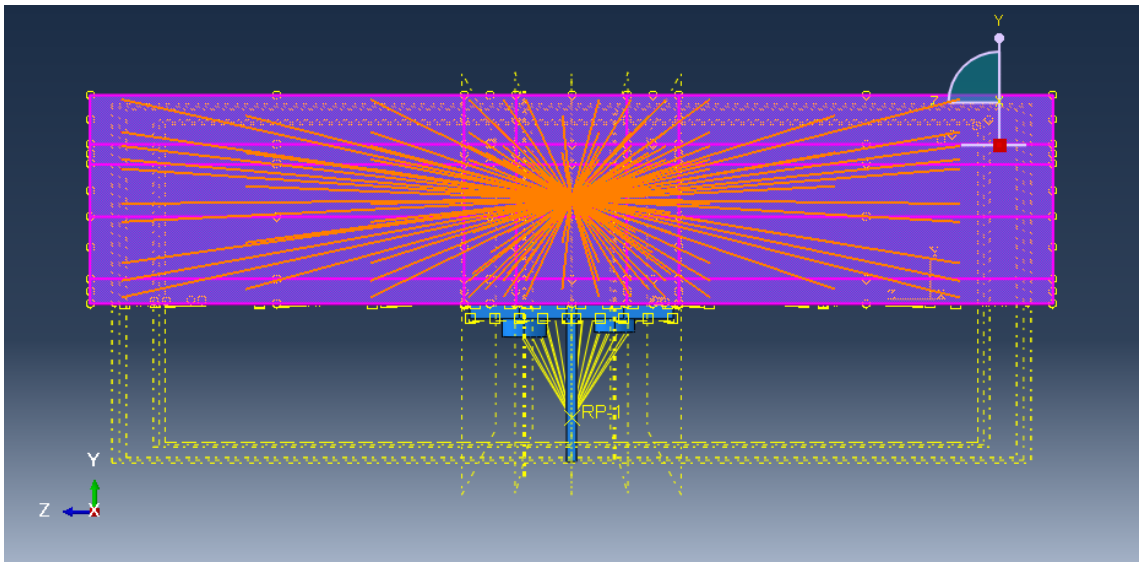

(b) View from bottom

Fig. 4.12 Coupling constraint assigned

Finally, the standard solver (ABAQUS, 2017), accounting for material nonlinearity and geometric nonlinearities, was applied to perform the numerical analysis on each developed FE model.

A mesh sensitivity study was conducted to optimise mesh sizes for balancing simulation accuracy and efficiency, with a coarser mesh (mesh0) and finer meshes (meshe1 and mesh2), as illustrated in Table 4.6 and Fig. 4.13. The load-slip curves were generated based on the analytical results, and the comparison is illustrated in Fig. 4.14 below, demonstrating that the mesh sizes utilised in mesh1 resulted in a converged solution. In conclusion, the proposed mesh configuration must adhere to the specifications outlined in mesh1, with mesh sizes established as

follows: 20 mm for the concrete slab, 15 mm for the steel member and decking, 10 mm for reinforcing bars, and 5 mm for shear connectors. Additionally, a finer in-plane mesh size of 10 mm is designated for discretising the areas surrounding bolt holes in the concrete slab and steel decking, while a 5 mm size is allocated for the stress concentration zones around bolt holes in the steel member, thereby ensuring an accurate representation of the curved geometries and the capture of failure patterns. Consequently, the mesh sizes utilised in mesh1 are employed in the numerical models for the subsequent study.

Table 4.6 Mesh size summary

	mesh0			mesh1			mesh2		
	global seed	local seed	nos. of elements	global seed	local seed	nos. of elements	global seed	local seed	nos. of elements
bolt	7		264	5		944	5		944
slab	30	10	10796	20	10	16715	15	10	25492
decking	30	10	1000	15	10	2720	15	10	2720
rebar	20		165	10		324	10		324
steel beam	30	10	857	15	5	1720	15	5	1720

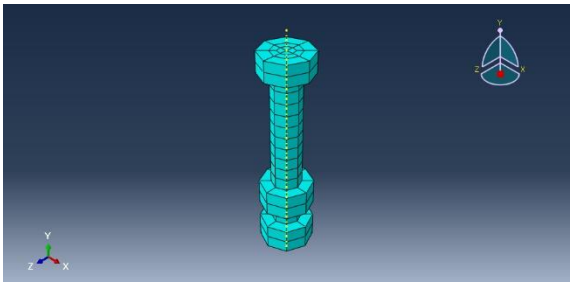

Global seed = 7

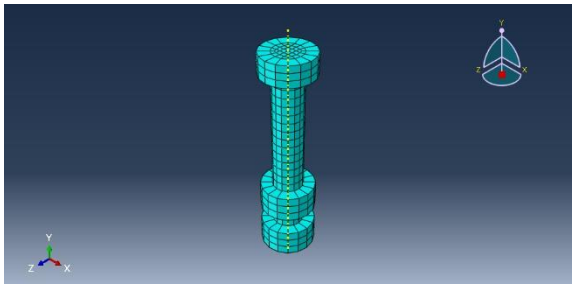

Global seed = 5

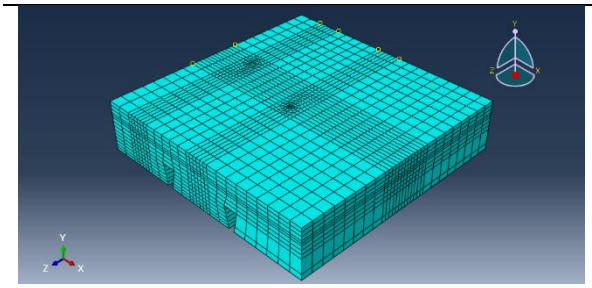

Global seed = 30, local seed = 10

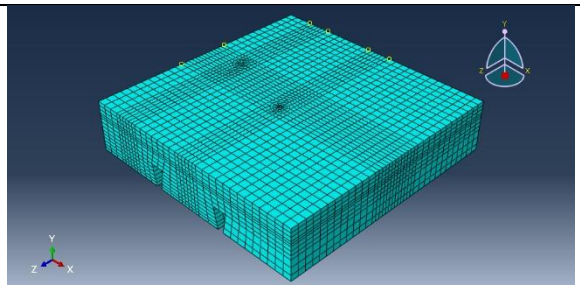

Global seed = 20, local seed = 10

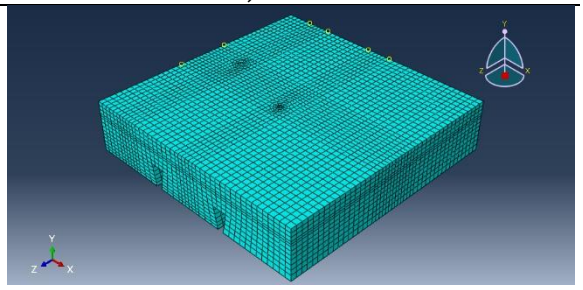

Global seed = 15, local seed = 10

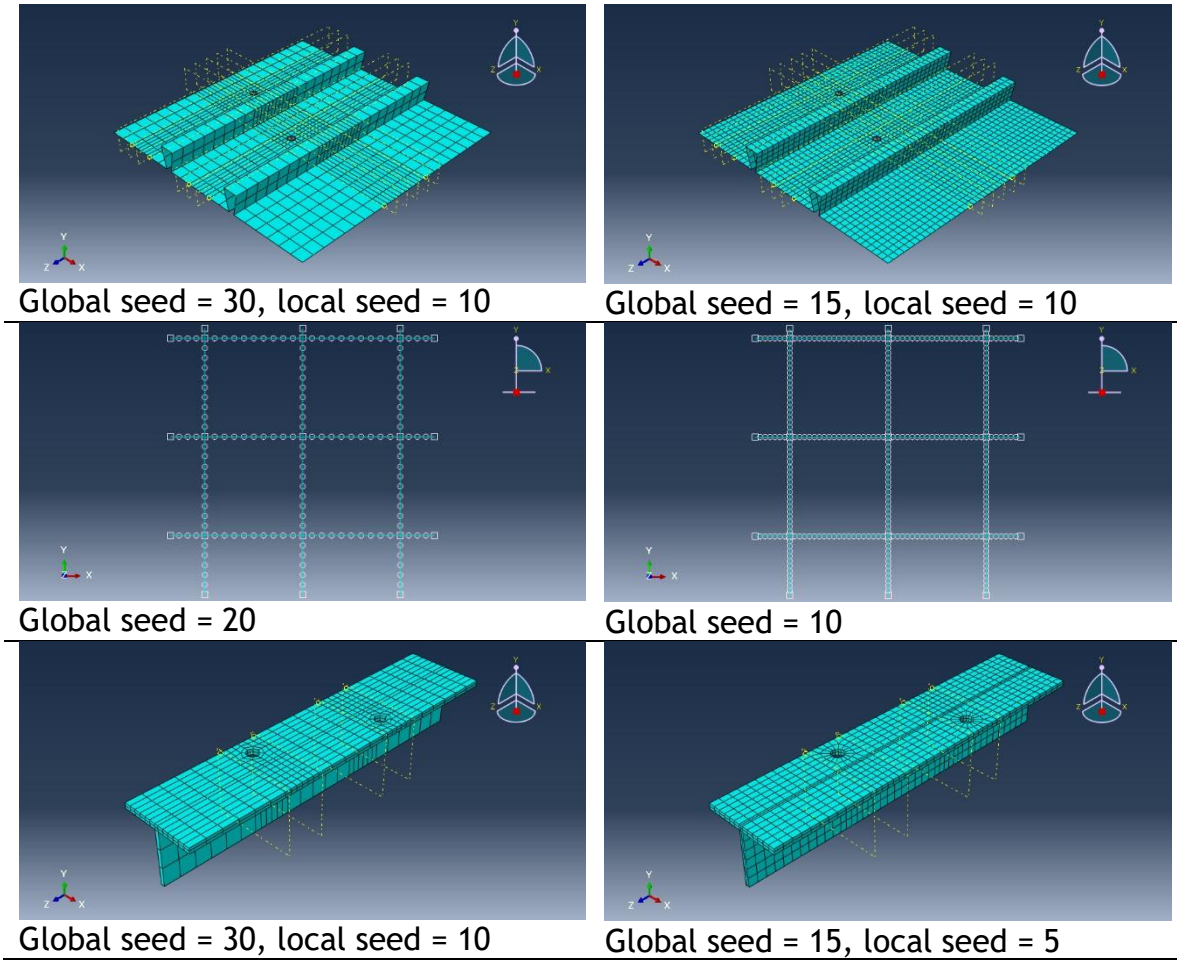

Fig. 4.13 Mesh summary

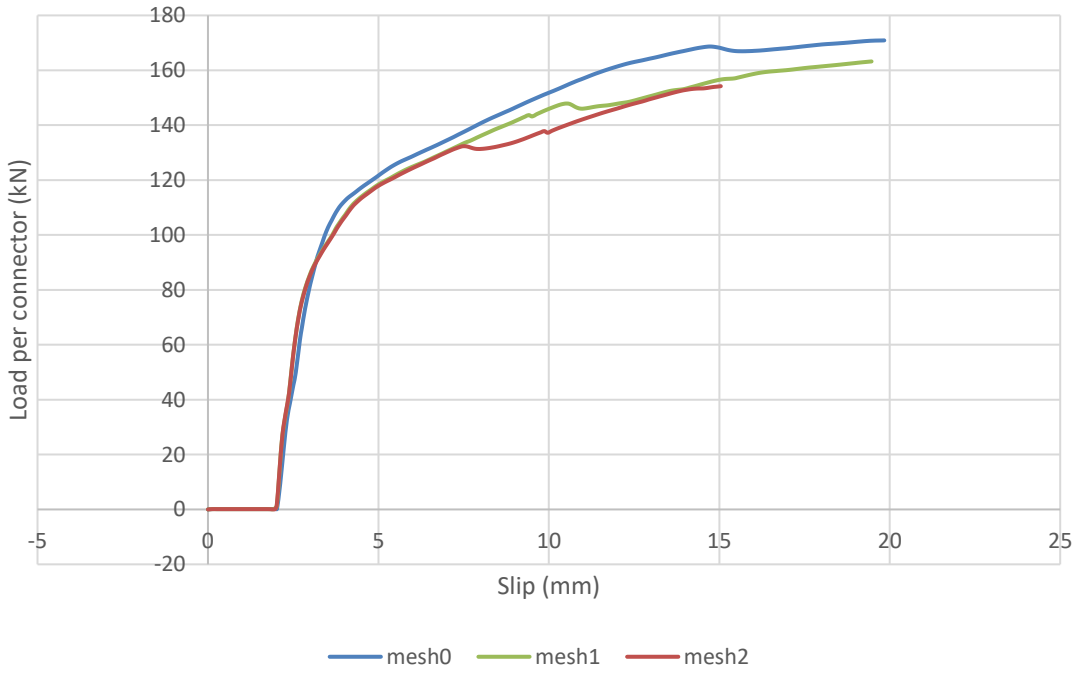

Fig. 4.14 Mesh sensitivity analysis

4.5.3 Validation study

The FE models of the steel–RAC composite slab was validated by comparing the simulated failure modes and load–slip curves with the corresponding experimental results. Graphical comparisons of the experimental and numerical failure modes for the representative specimen M20-200-RA30 showed a high level of agreement on (i) the patterns and locations of shear cracks on concrete – as exhibited in Figs. 4.15(a) and 4.15(b), and (ii) the deformed shape of the bolted shear connectors – as exhibited in Fig. 4.15(c). Quantitative comparisons were then conducted. The obtained load–slip curves from both experimental and numerical studies for the representative specimens M20-200-RA70 and M24-400-NA are compared in Fig. 4.16, in which the experimental load–slip responses were successfully captured by the FE models. The challenges encountered in numerical modelling arise from the complexity of the modelling itself, exacerbated by irregular concrete and decking geometries, particularly due to the recess in the concrete created for the bolt with the bolt head lodged within. Even with an appropriate mesh size established through mesh sensitivity analysis, the total number of elements exceeds 20,000, prolonging the computation time to several hours. The analysis results are significantly contingent upon the assigned concrete damage model; the degree of correlation between analysis and testing outcomes is largely influenced by the meticulous calibration of the concrete damage model. In other words, the finite element model must be refined to identify an appropriate concrete damage model that aligns with the results for specific structural behaviour. Moreover, although the results can be accurately determined, such a modelling setup cannot be applied to more complex models, such as beam bending tests, which necessitate significantly larger models comprising over ten times the number of elements, resulting in convergence issues; thus, a simplified and equivalent modelling approach is essential to facilitate the analysis. In summary, the established FE models were validated, since the structural response observed in the push-off tests conducted on steel–RAC composite slab specimens were well replicated in this numerical investigation.

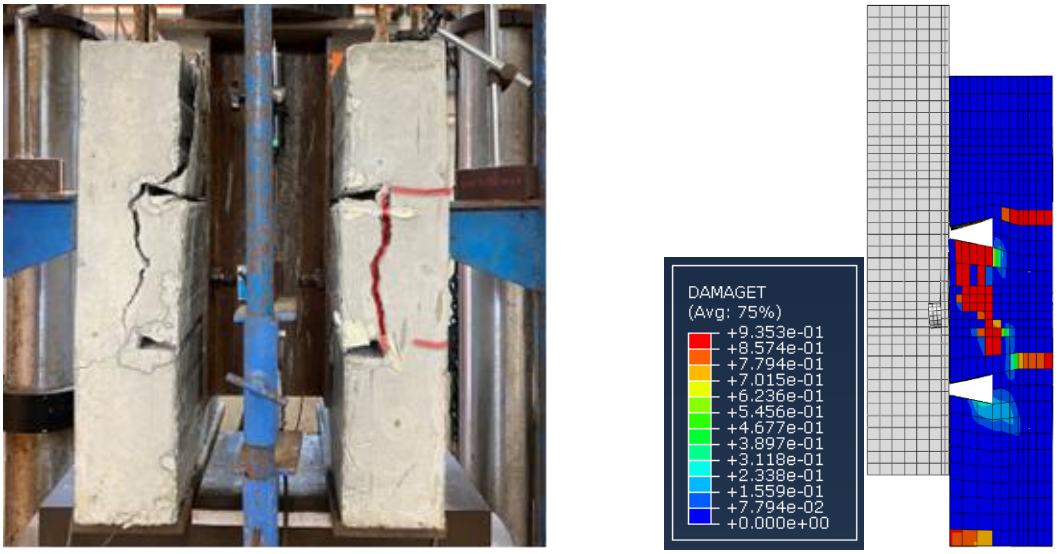

(a) Push-off specimen

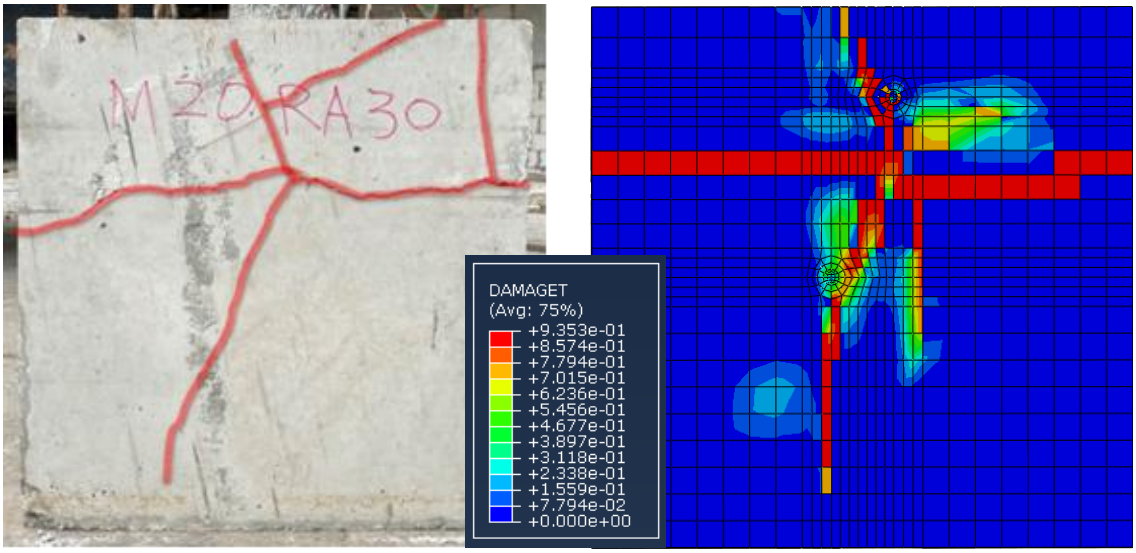

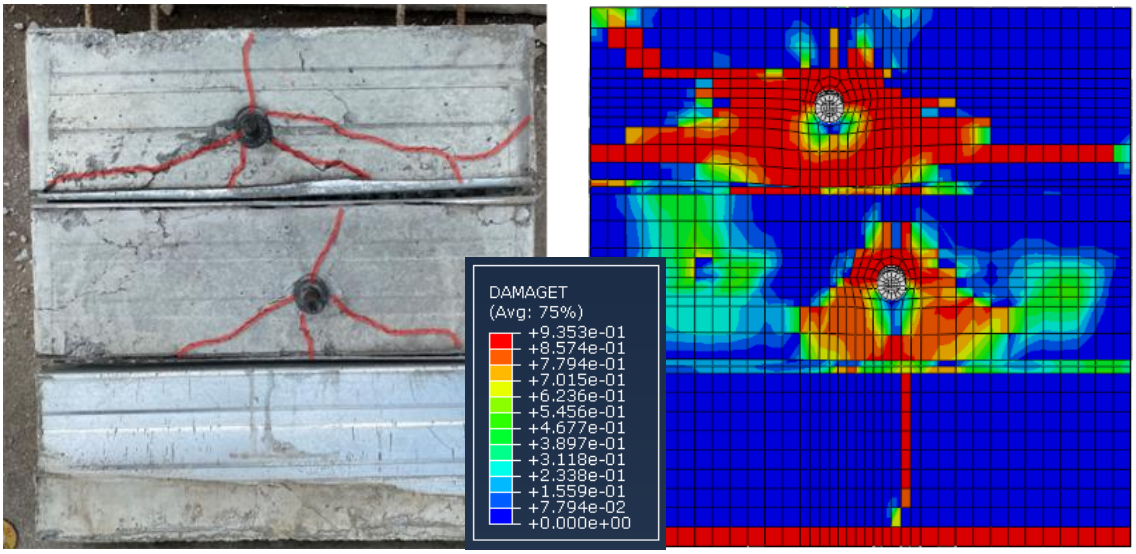

(b) Concrete slab

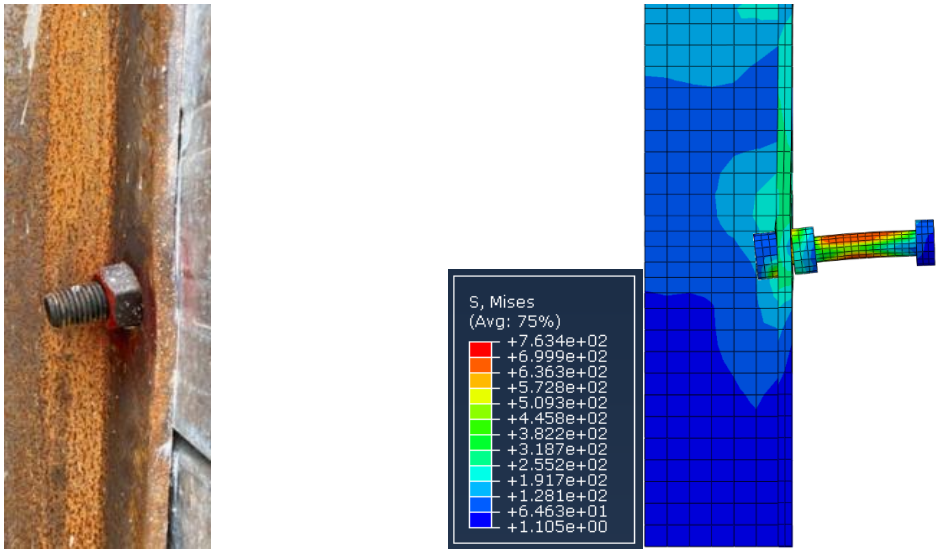

(c) Connector

Fig. 4.15 Test and FE failure modes

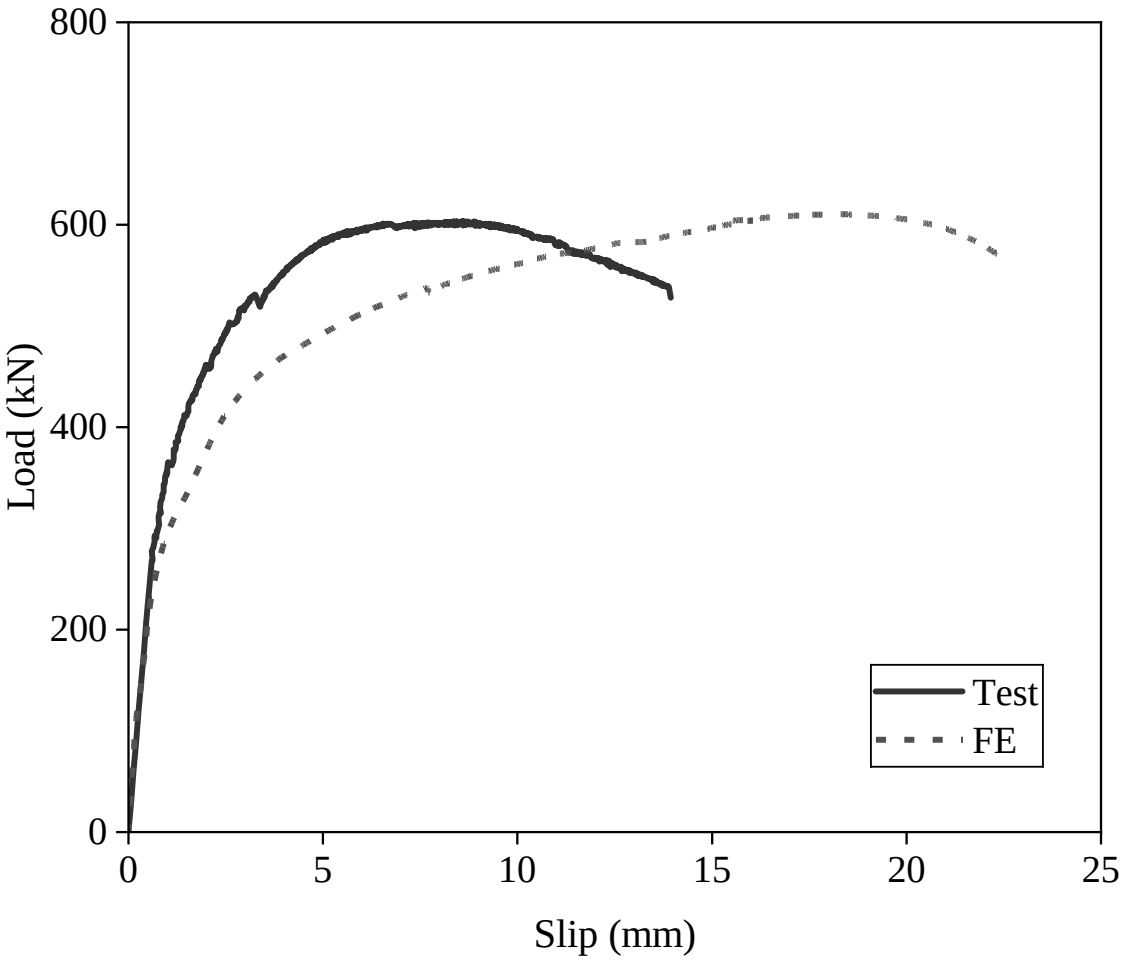

(a) M20-200-RA70

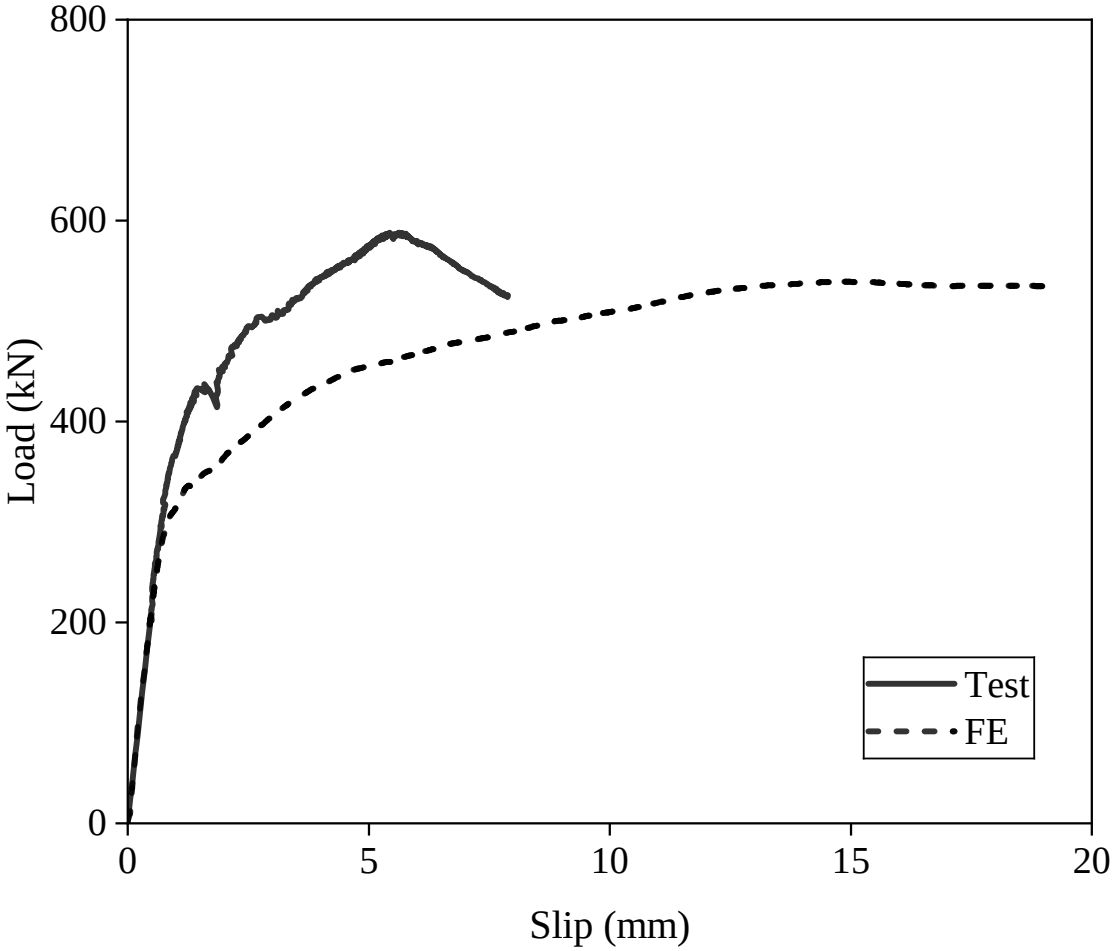

(b) M24-400-NA

Fig. 4.16 Test and FE load–slip curves

4.6 Evaluation on design codes

4.6.1 Overview

Following the laboratory experiments and numerical simulations, design analyses were performed. Owing to the lack of design provisions for steel–RAC composite slabs with demountable bolted shear connectors, the relevance of the existing codified design rules for conventional steel–NAC composite slabs with welded shear connectors, as prescribed in EN 1994-1-1 (2004) and ANSI/AISC 360-16 (2016), were described and evaluated for their applicability by comparing the experimentally acquired ultimate loads and failure modes against the unfactored codified predictions.

4.6.2 Evaluation on EN 1994-1-1 (EC4) and EN 1993-1-8 (2005)

The European code EN 1994-1-1 (2004) is used for the design of composite steel and concrete structures; however, it only covers welded shear connectors. Therefore, EN 1993-1-8 (2005) has also been referenced to evaluate the steel resistance of the bolted connector, which is given in Eq. (4.10), where F_{ub} is ultimate tensile strength of bolts and partial factor γ_{M2} is taken as 1 instead of 1.25 for the research comparison. For the conventional steel–NAC composite slabs with welded shear connectors, the European code EN 1994-1-1 (2004) specifies two possible failure modes – shear fracture of the connector (denoted as 'B') and concrete crushing (denoted as 'C'). The shear resistance of the welded shear connector is taken as the lower value of two ultimate load predictions associated with the two failure modes. The formula of the steel shear resistance per connector, denoted by $P_{Rd,S,EC4}$, is given in Eq. (4.7), where f_u denotes the material ultimate strength of bolts, d signifies the diameter of the shank of the bolt and partial factor γ_v is taken as 1 instead of 1.25 for the research comparison. The formula of the concrete shear resistance per connector, denoted by $P_{Rd,C,EC4}$, is given in Eq. (4.8), where α is a factor set to 1.0 for the connector with the length-to-diameter ratio larger than 4.0. Furthermore, since the push-off specimens were prepared with profiled steel decking that has ribs transverse to the steel beam, a reduction factor k_t must be considered in addition to the concrete resistance calculated in a solid slab, as given in Eq. (4.9), where n_r represents the number of connectors on one rib, b_0 denotes the minimum pan width for the inverted trapezoidal rib, h_p indicates the rib height and h_{sc} refers to the connector height inside the slab. This reduction factor k_t should not exceed 0.75 for profiled decking with predrilled holes.

$$P_{Rd,S,EC4} = 0.8 f_u \frac{\pi d^2}{4} / \gamma_v \tag{4.7}$$

$$P_{Rd,C,EC4} = 0.29 \alpha d^2 \sqrt{f_{ck} E_{cm}} / \gamma_v \tag{4.8}$$

$$k_t = \frac{0.7}{\sqrt{n_r}} \frac{b_0}{h_p} \left(\frac{h_{sc}}{h_p} - 1\right) \tag{4.9}$$

$$F_{v,Rd,EC3} = 0.6 f_{ub} A / \gamma_{M2} \tag{4.10}$$

The experimental results, P_u, and EC3/EC4 predictions on the ultimate load per connector, $P_{Rd,EC}$, and the associated failure mode for all the specimens are tabulated in Table 4.7. Furthermore, the ratio $P_u/P_{Rd,EC}$ is calculated for each specimen to assess the accuracy of EC3/EC4 design provisions. Note that a ratio of $P_u/P_{Rd,EC}$ greater than 1.0 indicates that the EC3/EC4 prediction is on the safe side, and vice versa. As shown in Table 4.7, the mean and COV of $P_u/P_{Rd,EC}$ are 1.27 and 0.15, respectively, suggest that EC3/EC4 yields safe ultimate load predictions for steel–RAC concrete composite slabs utilising bolted shear connectors. Bolted shear connectors may demonstrate lower strength in comparison to welded counterparts. This is evidenced by the significant deformation observed in the bolted connectors after the push-off tests, indicating that the steel structural capacity is being approached. The steel shear resistance derived from EC3, which is comparable to and slightly exceeds the concrete resistance, seems more reliable, whereas the steel resistance calculated using EC4, which only utilises about 50% of the steel capacity, deviates greatly from the experimental results. This suggests that the EC4 design formula, intended for welded shear connectors, could not be directly applied to demountable bolted connectors. Nevertheless, for all the test specimens, the predicted concrete shear resistance is lower than the predicted steel shear connector resistance derived from both EC3 and EC4. As a result, the concrete crushing failure mode is predicted for all the specimens which aligns with the experimental results.

The calculated shear resistance of the connector is determined using geometric configuration and material parameters, including the strength of steel, the strength of concrete, and the corresponding concrete secant modulus. Despite identical geometric configurations and comparable material properties, the code-predicted shear resistances fall within a similar range. In contrast to experimental results, which indicate that a higher recycled aggregate replacement ratio correlates with increased tested shear resistance for the same shear connector geometry, this phenomenon cannot be accounted for by the current design formula. Upon re-evaluation of the concrete component, which serves as the sole variable in the specimen configuration with same shear connector geometry, a reduced water-to-cement ratio (indicating increased cement content) was utilised to attain comparable target characteristic compressive strength. Thus, these results can be attributed to a denser cement matrix resulting from the lower

water-to-cement ratio. At the microstructural level, while the overall strength of concrete is influenced by the weakest portion of the cement matrix, the aggregate, and the interfacial transition zone (ITZ) between the cement matrix and aggregate, the size of the bolt is comparable to that of the aggregate. In turn, the adhesion between the concrete and the bolt may exhibit characteristics similar to the bond between the cement matrix and the bolt. Therefore, a denser cement matrix may enhance the bonding behaviour between the concrete and the bolt, resulting in improved resistance of shear connectors in the overall context. However, such conjectures could not be addressed using either code calculation formulas or FEM, which models the concrete itself as a nonlinear homogenous material.

Table 4.7 Comparison of test failure loads and modes with predicted results from EN 1994-1-1 (2004) and EN 1993-1-8 (2005)

Specimen ID	Experiment	EC3/EC4 Prediction					
	P_u (kN/connector)	P_{Rd} (kN/connector)				$P_u/P_{Rd,EC}$	Failure mode
		$P_{Rd,C,EC4}$	$P_{Rd,S,EC4}$	$F_{v,Rd,EC3}$	$P_{Rd,EC}$		
M20-200-NA	110.1	103.3	201.1	117.6	103.3	1.07	C
M20-200-RA30	133.3	95.4	201.1	117.6	95.4	1.40	C
M20-200-RA70	150.9	100.2	201.1	117.6	100.2	1.51	C
M20-200-RA100	157.6	106.9	201.1	117.6	106.9	1.47	C
M24-400-NA	147.0	148.7	289.5	169.4	148.7	0.99	C
M24-400-RA30	176.5	137.4	289.5	169.4	137.4	1.29	C
M24-400-RA70	167.6	144.2	289.5	169.4	144.2	1.16	C
M24-400-RA100	195.5	153.9	289.5	169.4	153.9	1.27	C
Average						1.27	C
COV						0.15	C

4.6.3 Evaluation on ANSI/AISC 360-16 (AISC) and ACI 318-19 (ACI)

The American specification ANSI/AISC 360-16 (2016) offers comprehensive design guidelines specifically for structural steel buildings. With regard to conventional steel–NAC composite slabs with welded shear connectors, ANSI/AISC 360-16 (2016) employs the same framework as EN 1994-1-1 (2004) in predicting the shear resistance of the shear connector by considering two failure modes - shear fracture of the connector (denoted as 'B') and concrete crushing (denoted as 'C'). The formula of the steel shear resistance per connector, denoted by $P_{Rd,S,AISC}$, is given in Eq. (4.11), where the factors R_g and R_p are taken as 1.0 and 0.6, respectively for composite slabs oriented perpendicular to the steel beam with one connector on each rib. The formula of the concrete shear resistance per connector, denoted by $P_{Rd,C,AISC}$, is given in Eq. (4.12).

$$P_{Rd,S,AISC} = R_g R_p A_{sa} f_u \tag{4.11}$$

$$P_{Rd,C,AISC} = 0.5 A_{sa} \sqrt{f_c E_c} \tag{4.12}$$

ACI 318-19 also covers anchor strength, which, although not explicitly aimed at composite slab design, is relevant because the behaviour of bolted connectors in concrete is similar to that of anchors in concrete. Hence, ACI is also referenced for comparison. Similarly, ACI specifies the same two failure modes as AISC: bolt failure (denoted as 'B') and concrete failure (denoted as 'C'). The bolt strength is given in Eq. (4.13), yielding the same result as Eq. (4.11). The concrete breakout strength is given by Eq. (4.14) and Eq. (4.15). In these equations, V_b represents the basic concrete breakout strength, c_{a1} is the concrete edge distance and $P_{Rd,C,ACI}$ represents the design concrete breakout strength after considering various factors due to the concrete profile, i.e. A_{vc} denotes the projected area for the anchor related to edge distance, $\psi_{ed,V}$ represents the breakout edge effect factor, $\psi_{c,V}$ signifies the breakout cracking factor and $\psi_{h,V}$ indicates the breakout thickness factor.

$$P_{Rd,S,ACI} = 0.6 A_{se} f_{ut} \tag{4.13}$$

$$V_b = \left(8\left(\frac{h_{ef}}{d_a}\right)^{0.2}\sqrt{d_a}\right)\sqrt{f_c}\,(c_{a1})^{1.5} \tag{4.14}$$

$$P_{Rd,C,ACI} = \frac{A_{vc}}{A_{vc0}} \psi_{ed,V} \psi_{c,V} \psi_{h,V} V_b \tag{4.15}$$

The predictions from AISC and ACI regarding the ultimate load per connector, $P_{Rd,AISC}$ and $P_{Rd,ACI}$, along with the associated failure modes, are tabulated in Table 4.8. The ratios $P_u/P_{Rd,AISC}$ and $P_u/P_{Rd,ACI}$ are also calculated for each specimen to assess the precision of the AISC and ACI design provisions. As shown in Table 4.8, the mean and coefficient of variation (COV) of both are 1.09 and 0.15, respectively. This indicates that both AISC and ACI design provisions provide more accurate, though less conservative, predictions of the ultimate load than EC3/EC4. Especially for NAC, the results derived from welded shear connectors give unsafe predictions.

One important point to highlight is that the way AISC calculates the shear resistance of shear connectors differs from EC4. Although AISC considers both concrete and steel resistances, the reduction factor due to profiled decking and connector arrangement are applied to the steel resistance rather than the concrete resistance. In other words, the concrete resistance serves more as a lower bound for the design check, while the steel resistance not only accounts for the steel cross-sectional area but also considers the influence of the concrete profile. This results in an overestimation of the concrete resistance. Similarly, the concrete resistance calculated using ACI is also extremely high compared to EC4. While this approach generally provides a predicted resistance at an acceptable level, the inaccuracy in the concrete resistance prevents a clear understanding of the failure mode.

Table 4.8 Comparison of test failure loads and modes with predicted results from ANSI/AISC 360-16 (2016) and ACI 318-19 (2019)

Specimen ID	Experiment	ANSI/AISC Prediction					ACI Prediction				
	P_u (kN/connector)	P_{Rd} (kN/connector)			$P_u/P_{Rd,AISC}$	Failure Mode	P_{Rd} (kN/connector)			$P_u/P_{Rd,ACI}$	Failure Mode
		$P_{Rd,C,AISC}$	$P_{Rd,S,AISC}$	$P_{Rd,AISC}$			$P_{Rd,C,ACI}$	$P_{Rd,S,ACI}$	$P_{Rd,ACI}$		
M20-200-NA	110.1	145.4	117.6	117.6	0.94	B	595.3	117.6	117.6	0.94	B
M20-200-RA30	133.3	134.3	117.6	117.6	1.13	B	581.9	117.6	117.6	1.13	B
M20-200-RA70	150.9	141.0	117.6	117.6	1.28	B	596.0	117.6	117.6	1.28	B
M20-200-RA100	157.6	150.5	117.6	117.6	1.34	B	603.8	117.6	117.6	1.34	B
M24-400-NA	147.0	209.5	169.4	169.4	0.87	B	628.7	169.4	169.4	0.87	B
M24-400-RA30	176.5	193.5	169.4	169.4	1.04	B	614.6	169.4	169.4	1.04	B
M24-400-RA70	167.6	203.2	169.4	169.4	0.99	B	629.6	169.4	169.4	0.99	B
M24-400-RA100	195.5	216.8	169.4	169.4	1.15	B	637.7	169.4	169.4	1.15	B
Average					1.09					1.09	
COV					0.15					0.15	

4.7 Summary

This chapter presents tests and numerical simulations aimed at examining the structural behaviour and capacity of steel–RAC composite slabs with demountable bolted shear connectors. The experimental programme commenced with material testing to acquire parameters for concrete, steel beam and profiled decking, followed by a total of eight push-off tests on full-scale steel–RAC composite slab specimens. The experimental failure modes and loads as well as load–slip curves were obtained and discussed in detail. Subsequently, FE models were established to replicate the push-off test, and the numerical results were corroborated with the experimental data. In light of the lack of established design codes for steel–RAC composite slabs with demountable bolted shear connectors, the corresponding design provisions for steel–NAC composite slabs with welded shear connectors, as set out in EN 1994-1-1 (2004), EN 1993-1-8 (2005), ANSI/AISC 360-16 (2016) and ACI 318-19 (2019), were evaluated for their applicability. Based on the evaluation results, the subsequent conclusions were derived from the design analyses: (i) EC4 provides an accurate prediction of the shear resistance of bolted shear connectors in NAC and offers a safe but conservative prediction for RAC. However, the steel shear resistance derived from EC4 overestimates the steel resistance, and the results from EC3 are much more accurate and closer to experimental results.; and (ii) AISC and ACI provide more accurate predictions on average but give unsafe predictions for the shear resistance of bolted shear connectors in NAC. Furthermore, AISC and ACI cannot accurately predict the failure mode. Therefore, modifications to the design codes are needed to accurately predict both the shear resistance of bolted connectors and the failure mode while ensuring safety.

5 EXPERIMENTAL INVESTIGATION AND ANALYSIS OF FULL-SCALE BENDING TEST

5.1 Introduction

This chapter reports experiments on the flexural behaviour and resistances of composite beams with RAC composite slab utilising bolted shear connectors. A total of five beam tests were carried out in the four-point bending configuration. The test observations, encompassing failure modes, load–mid-span deflection curves, slips between the steel beam and composite slab and strain distributions at the mid-span cross-section, were reported and discussed. The experimental data were subsequently compared with the flexural resistances predicted by EN 1994-1-1 (2004) and ANSI/AISC 360-16 (2016).

5.2 Full-scale four-point bending tests

Five four-point bending tests were carried out on full-scale composite beam specimens using bolted shear connectors to investigate their flexural behaviour and bending resistances. The testing specimens were prepared using the same batch of concrete and steel materials used in the push-off tests covered in Chapter 4. Concrete cylinder tests were performed concurrently with the bending tests to obtain the concrete properties. Table 5.1 presents the average material properties for each concrete type, which includes the 28-day compressive strength derived from three concrete cube tests, the compressive strength from two concrete cylinder tests conducted on the testing day, and the measured secant modulus, which was collaborated with BS EN 12390–13 (2013). Coupon tests on steel materials have been elaborated in section 4.2.1 and will not be repeated here again.

Table 5.1 Key material properties of concrete

Concrete type	f_{cu} (N/mm^2) at 28 days	f_c (N/mm^2)	E_{cm} (N/mm^2)
NA	50.0	41.7	36890
RA30	51.5	40.7	32932
RA100	53.8	46.5	38400

The four point bending tests were conducted utilising a hydraulic testing frame with a loading capacity of 1000 kN at a fixed loading rate of 3 mm/min. Before testing, the composite beam specimen was simply supported between two steel rollers, spanning a total of 5.6 m, while a spreader beam was employed to distribute load at two points, spaced 2 m apart.

Fig. 5.1 displays the four-point bending test setup, where a load cell is positioned between the hydraulic jack and spreader beam to record the applied loads, three vertically installed line transducers (LT-V1, LT-V2 and LT-V3) are used to record the vertical deflections of the beam at the mid-span and two loading points, eight linear variable displacement transducers (LVDT-H1 to LVDT-H8) are horizontally installed to measure the relative slips between the steel I-beam and the composite slab. Moreover, strain gauges were attached along the mid-span cross-section to measure the normal strains across the section. Fig. 5.2 illustrates the placement of four concrete strain gauges (SG1 to SG4) on the top surface of the concrete slab at mid-span and ten steel strain gauges (SG5 to SG14) adhered onto the profiled steel decking and steel I-section beam at the mid-span cross-section to measure the strains at specific locations.

(a) Test setup

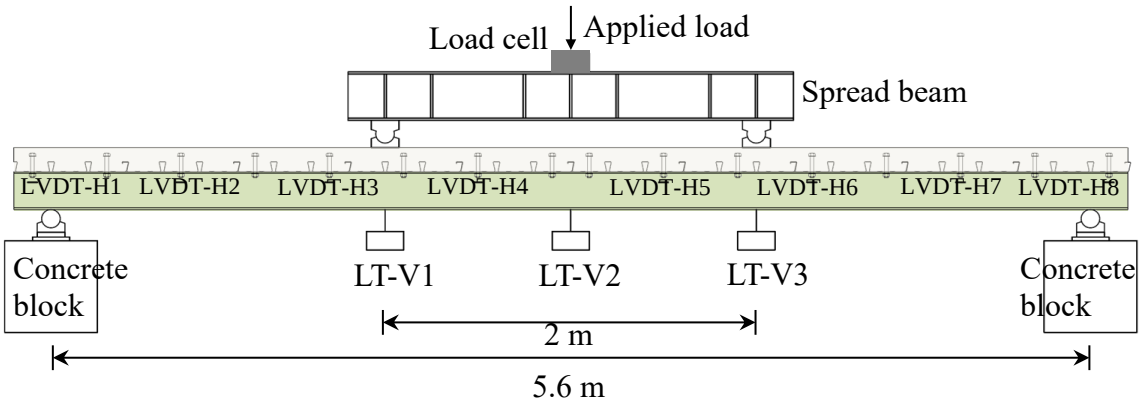

(b) Schematic diagram

Fig. 5.1 Composite beam four-point bending test setup

(a) Concrete strain gauges

(b) Steel strain gauges

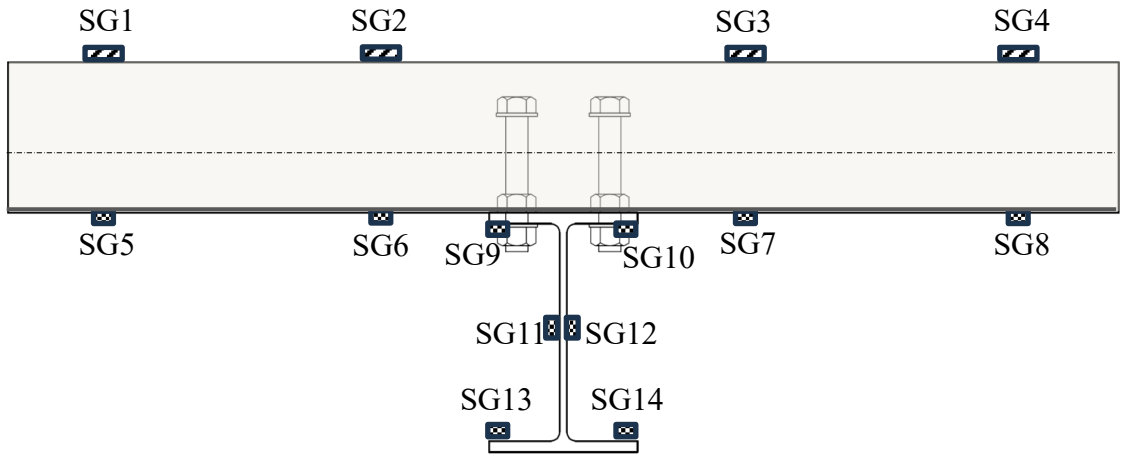

(c) Schematic diagram

Fig. 5.2 Locations of strain gauges across the mid-span beam section

5.3 Discussions on test results

5.3.1 Failure modes

In general, similar deformed shapes were observed for all the composite beam specimens, as shown in Fig. 5.3(a), where the vertical bending displacements symmetrically took place and neither out-of-plane rotations nor fracture of bolted shear connectors occurred. For all the test specimens, cracks were initiated in the concrete slab and propagated from bottom to top – see Fig. 5.3(c). However, the composite beam specimens continued to resist the applied loads until (i) crushing occurred at the top surface of the concrete slab of the M20-200 composite beam specimens, as displayed in Fig. 5.3(b), and (ii) cracks developed around the bolted shear connectors of the M24-400 composite beam specimens, as shown in Fig. 5.3(d). Note that the cracks around the bolted shear connectors were invisible during the test and could only be observed through post-processing after the test (i.e. cutting off the profiled steel decking).

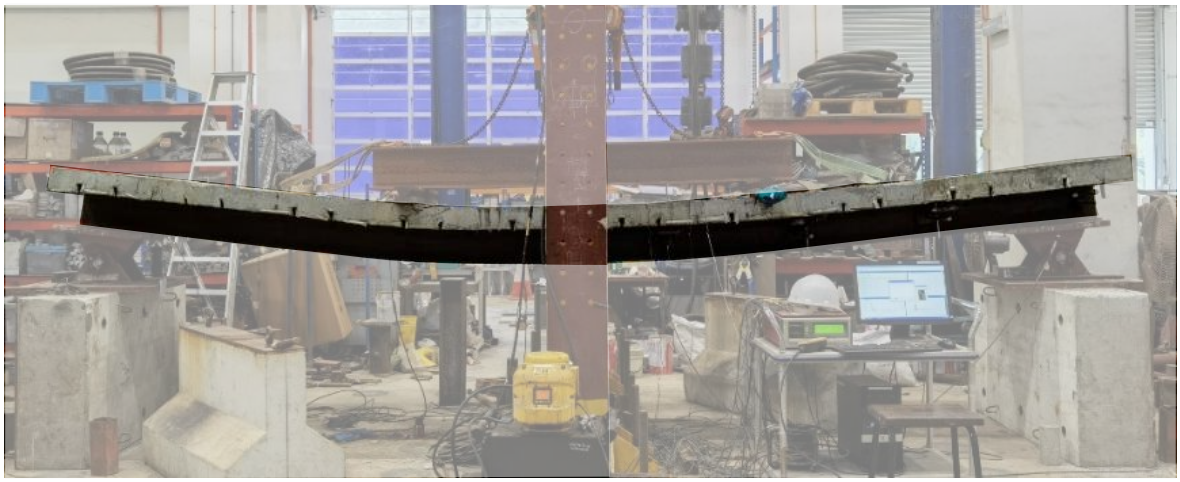

M20-200-NA

M20-200-RA30

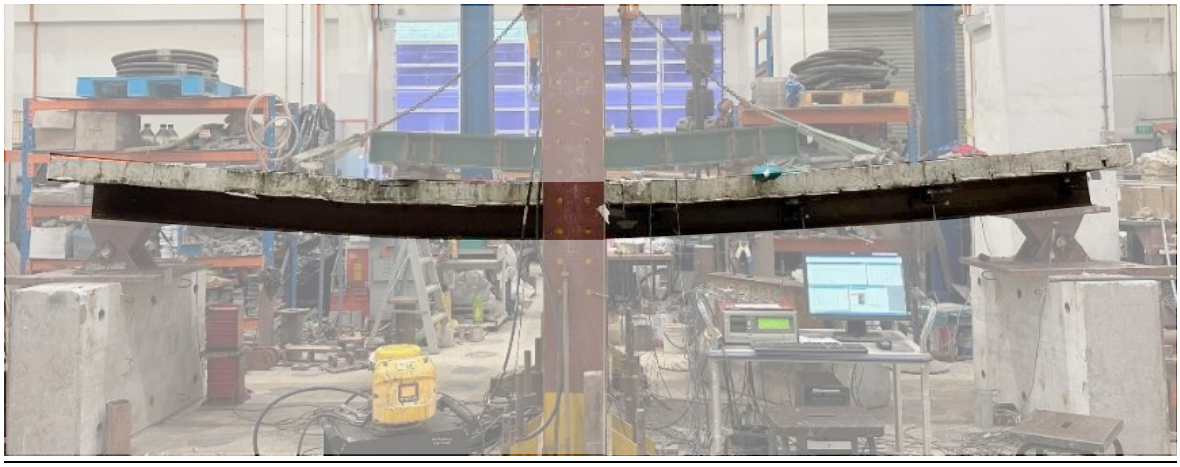

M20-200-RA100

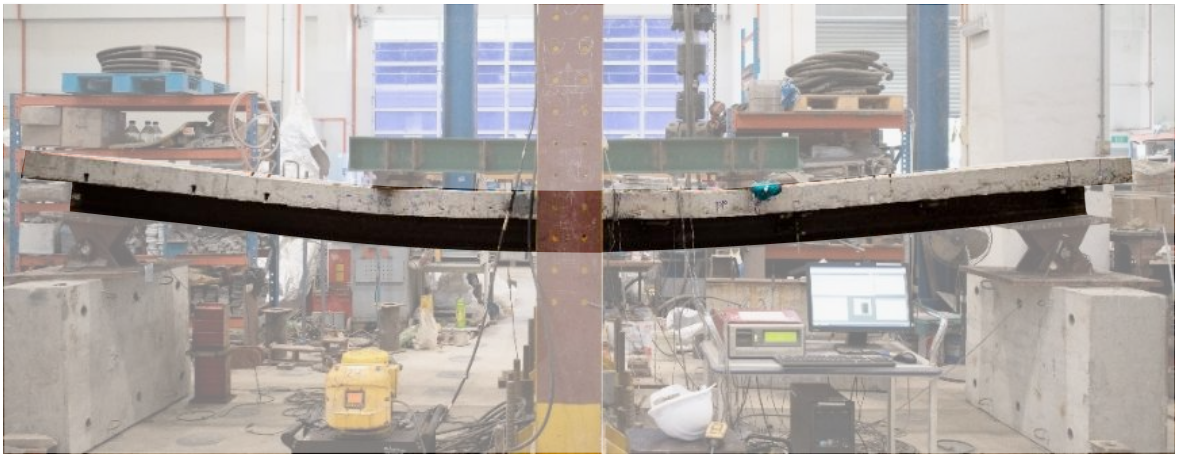

M24-400-RA30

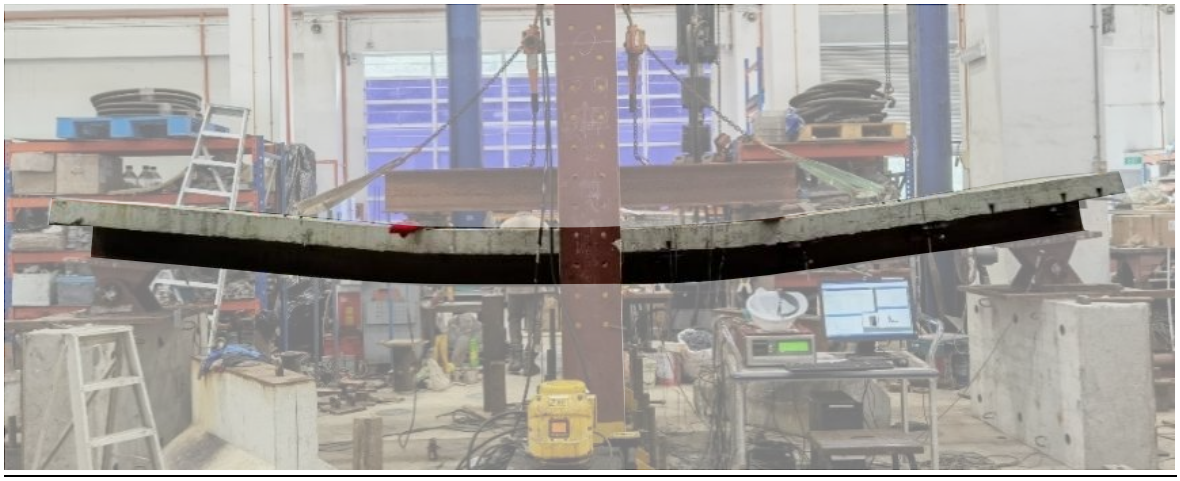

M24-400-RA100

(a) Deformed shapes

(b) Concrete crushing on M20-200

(c) Concrete crack on M24-400

(d) Cracks around shear connectors

Fig. 5.3 Failure modes of composite beam specimens

5.3.2 Load–deflection curves

The applied loads are plotted against the measured mid-span deflections for two series of composite beam specimens – M20-200 and M24-400, as shown in Figs 5.4 (a) and 5.4(b), respectively. The yielding points depicted in the figures indicate the onset of yielding at the bottom flange of the steel I-beam. Fig. 5.4 illustrates that the load–mid-span deflection curves of all test specimens exhibited nonlinearity subsequent to the yielding points.

Table 5.1 presents the principal test results, encompassing the yield loads N_y and the corresponding mid-span deflections δ_y, the ultimate loads N_u and the corresponding ultimate mid-span deflections δ_u and the ultimate moment M_u, defined as the sum of the ultimate applied moment during tests and the moment induced by the self-weight of each composite beam specimen. Regarding the composite beam specimens with the same connector size and spacing, an increase in the recycled aggregate replacement ratio results in an enhanced flexural capacity but reduced ductility. Moreover, the M20-200 composite beam specimens have slightly higher ultimate moment capacities and smaller deflections than the M24-400 composite beam specimens made from the same concrete type, resulting from a higher degree of shear connection in these M20-200 specimens in comparison with their M24-400 counterparts.

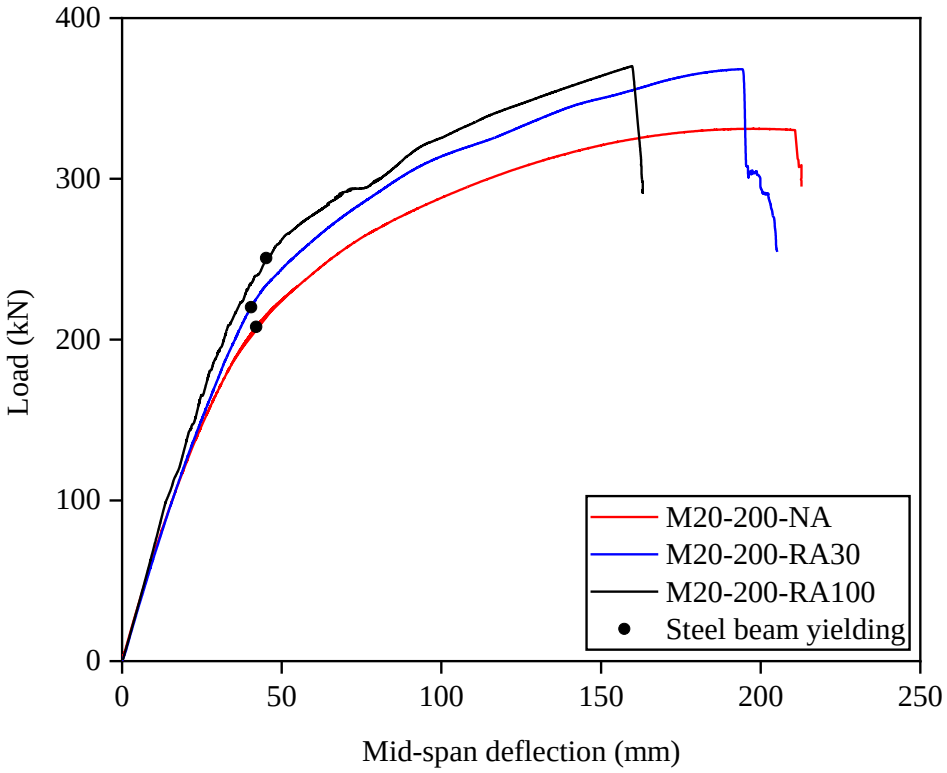

(a) M20-200

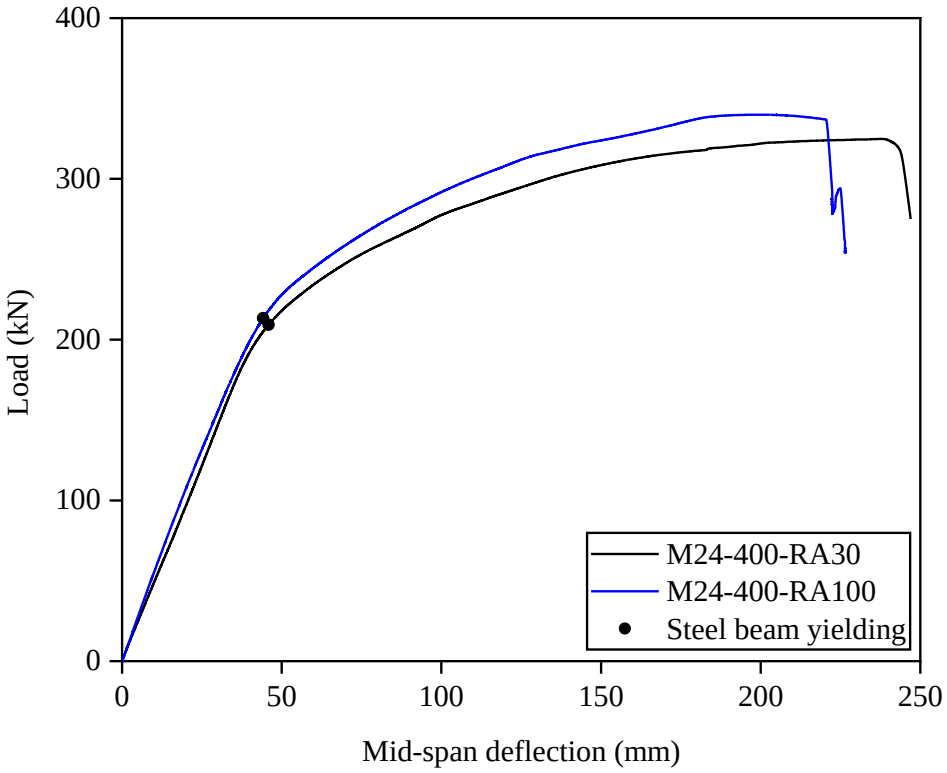

(b) M24-400

Fig. 5.4 Load–mid-span deflection curves of composite beam specimens

Table 5.2 Four-point bending test results

Specimen ID	N_y (kN)	δ_y (mm)	N_u (kN)	δ_u (mm)	M_u (kNm)
M20-200-NA	207.9	42.0	331.1	197.6	310.5
M20-200-RA30	220.2	40.4	368.2	193.4	343.8
M20-200-RA100	250.7	45.1	370.3	160.0	345.7
M24-400-RA30	209.3	45.9	320.0	235.0	304.7
M24-400-RA100	213.3	44.2	340.3	199.2	327.6

5.3.3 Slips

In order to investigate the shear-slip behaviour at the interface between the composite slab and steel I-beam, the applied loads are plotted against the relative slips at different locations along the beam length, as shown in Fig. 5.5. Note that for all the specimens, debonding occurred at the beam ends, which affected the corresponding end slip (i.e. LVDT-H1). Therefore, the slips at beam ends are not presented in the figures. From Fig. 5.5 it is observed that, unlike the conventional composite beam, slippage developed at the beginning of the test, which can be attributed to the 2 mm clearance of the bolt holes in the steel I-beam and profiled steel decking. Generally, the longitudinal slip increased with the applied load, and the slip within two loading points (as measured by LVDT-H4) was significantly lower than the slip between the loading point and support (as measured by LVDT-H2 and LVDT-H3). For specimens with the same connector size and arrangement, at the same loading level, a reduction in the slip was observed as the recycled aggregate replacement ratio increased.

The comparison results for the composite beam specimens with the same concrete type but varied arrangements of bolted shear connectors indicate that less slippage was developed in the composite beam with a higher degree of shear connection. Moreover, the longitudinal slips were found to be closely related to the vertical deflections and thus the curvature of the composite beam, as shown in Fig. 5.6, where the mid-span deflections are plotted against the slips measured by LVDT-H2, LVDT-H3 and LVDT-H4 and roughly linear increasing trends were observed.

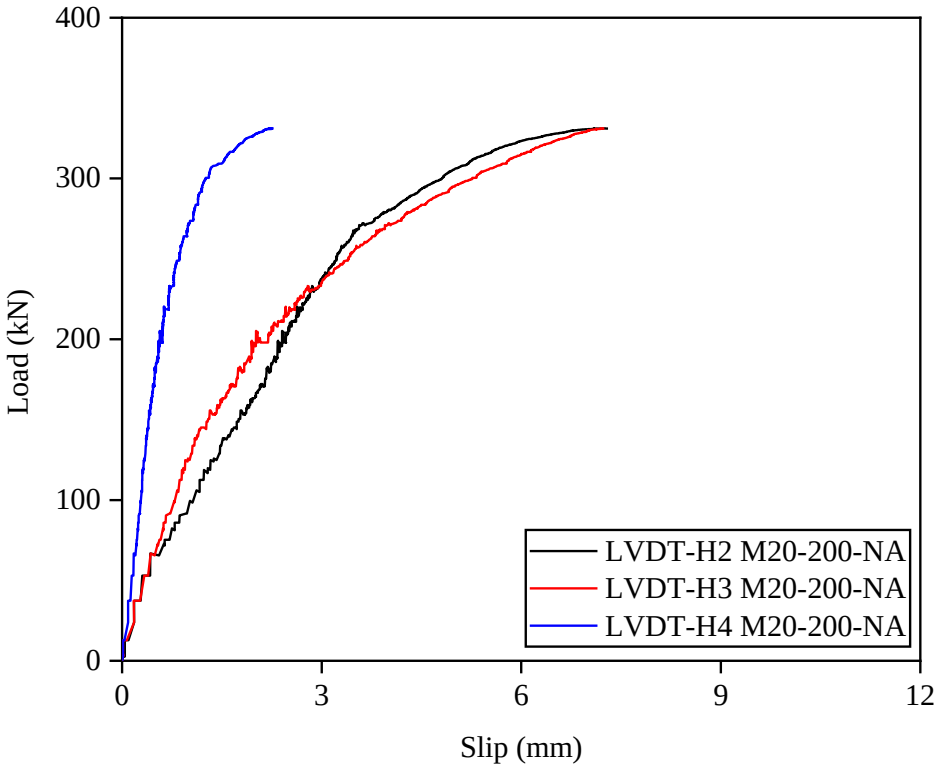

(a) M20-200-NA

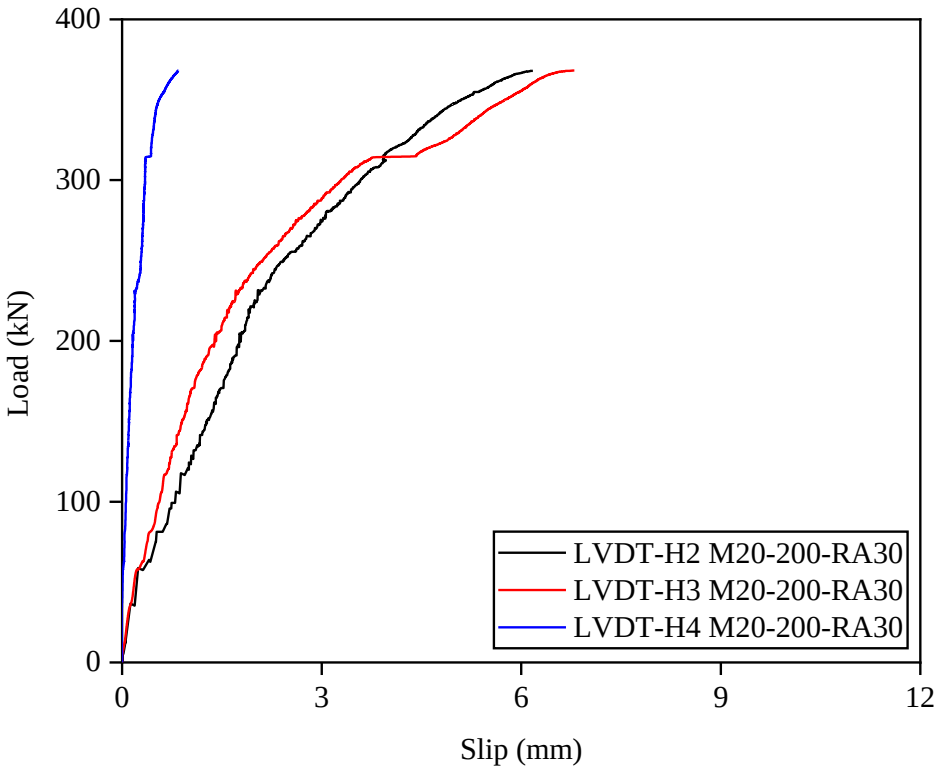

(b) M20-200-RA30

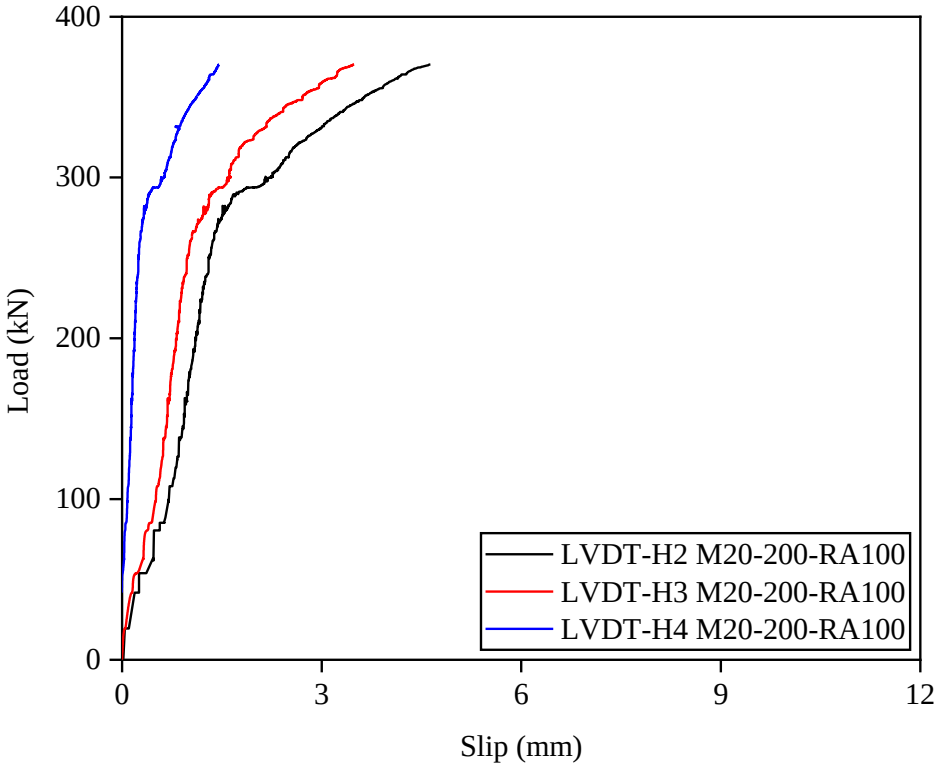

(c) M20-200-RA100

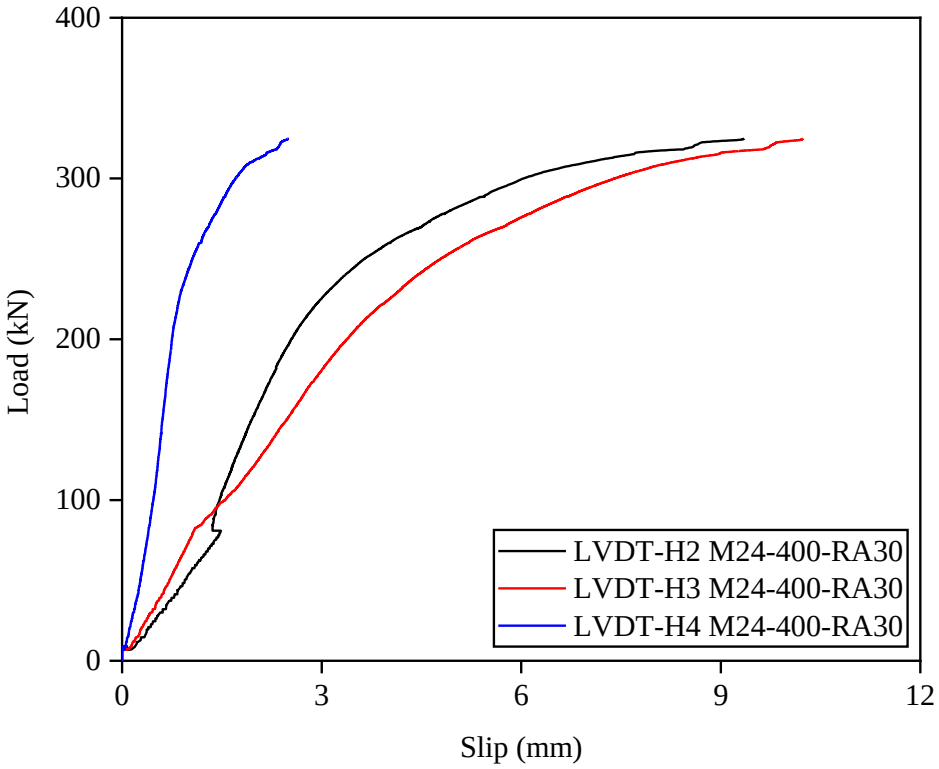

(d) M24-400-RA30

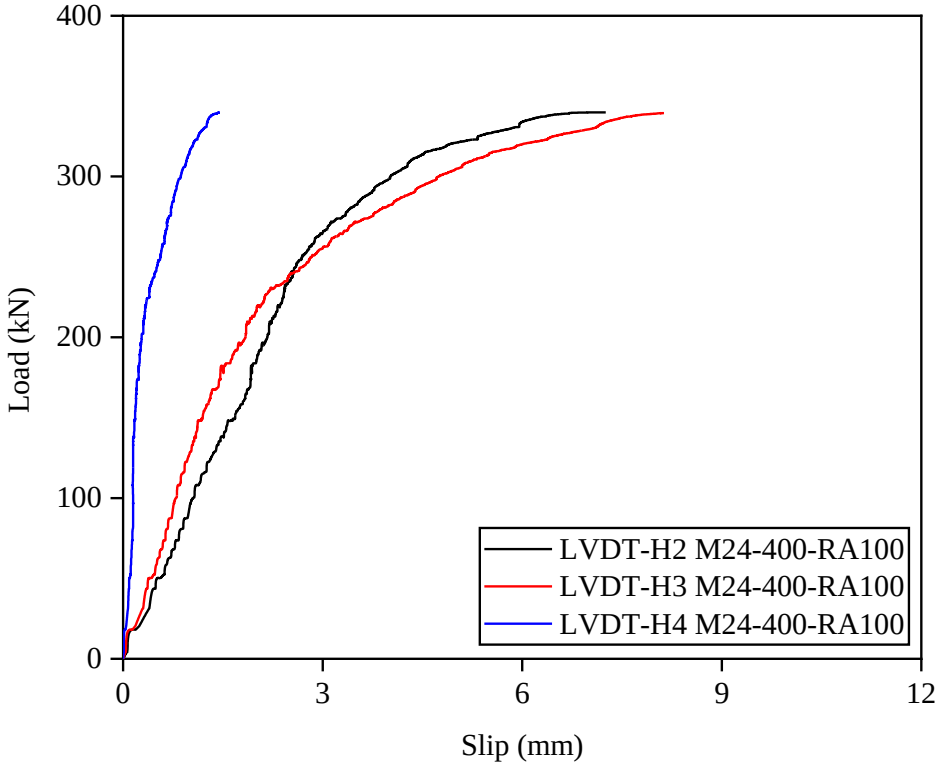

(e) M24-400-RA100

Fig. 5.5 Load–slip curves of composite beam specimens

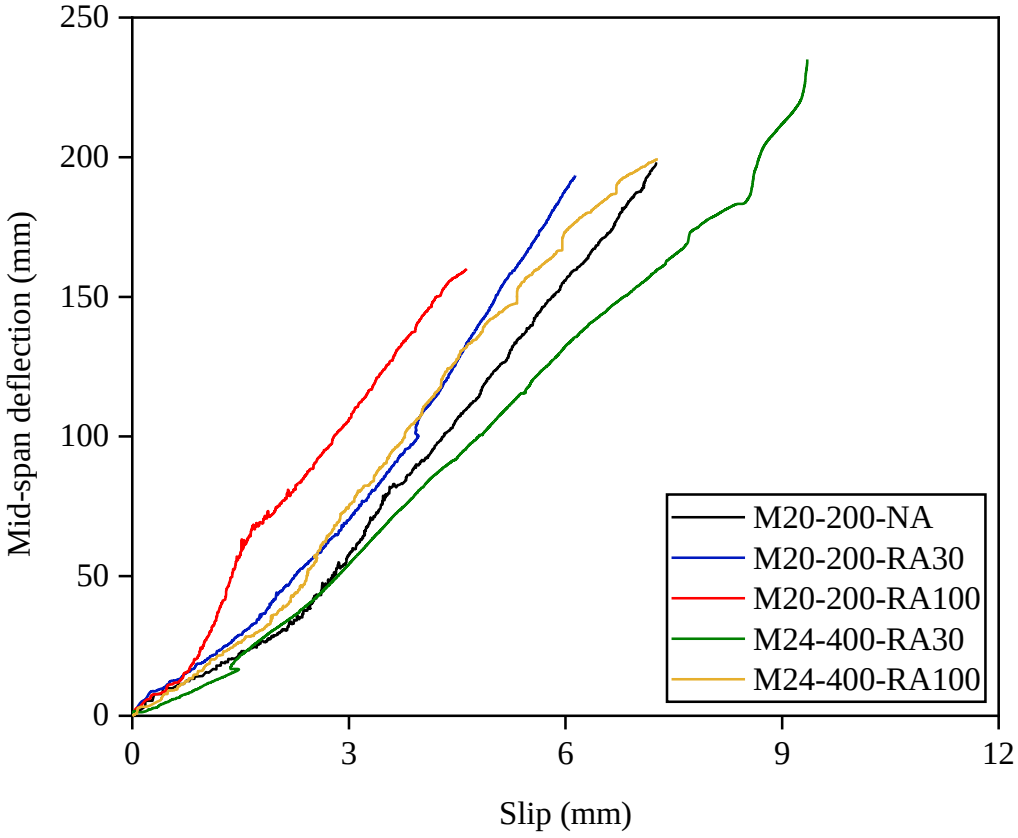

(a) LVDT-H2

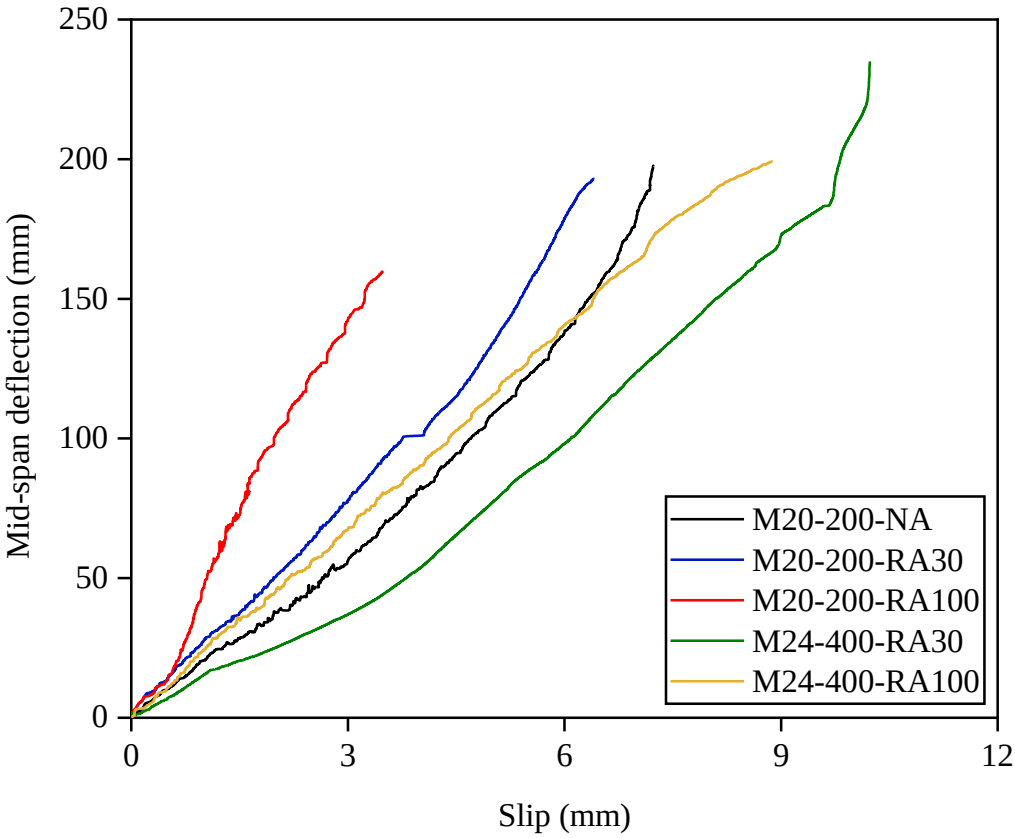

(b) LVDT-H3

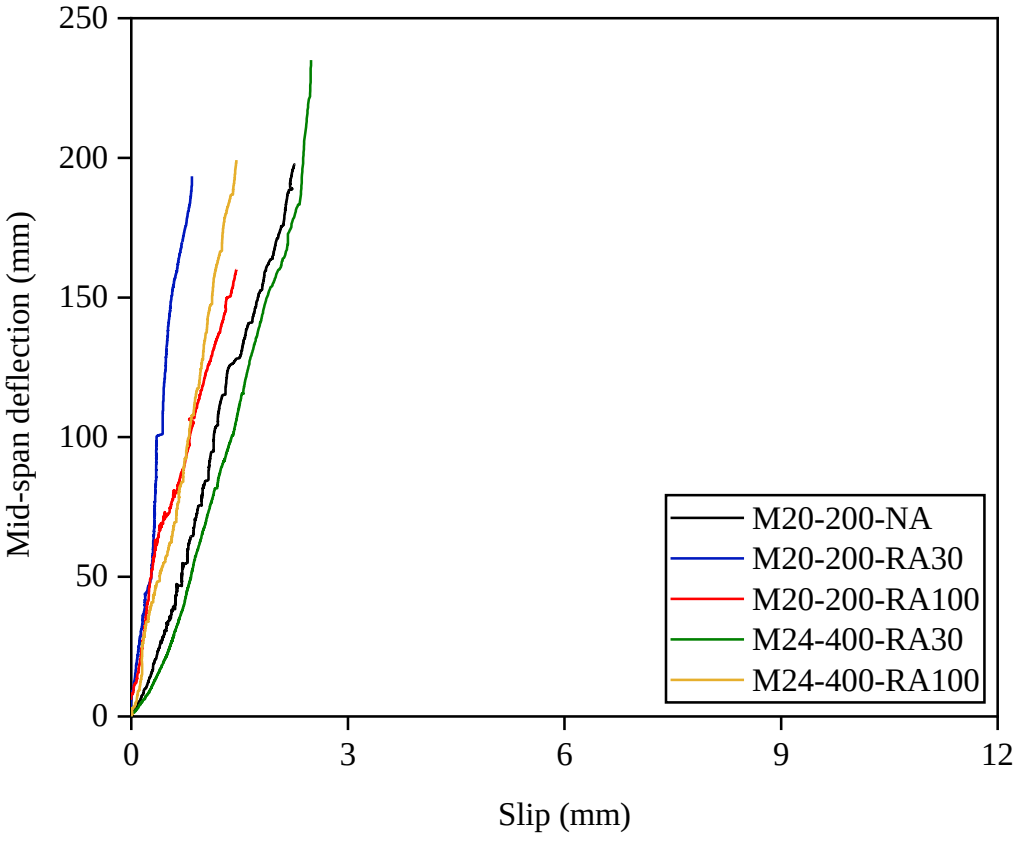

(c) LVDT-H4

Fig. 5.6 Mid-span deflection–slip curves of composite beam specimens

5.3.4 Strain distributions

The longitudinal strain distributions at the mid-span cross-section of the composite beam specimens are discussed herein. In view of the symmetric geometry of the composite beam specimen, only strains on the half of each cross-section were presented herein. The measured load–strain curves of all the composite beam specimens are presented in Fig. 5.7, indicating the yield loads, where positive values denote tensile stresses and negative values denote compressive stresses. It is evident that the longitudinal strains became nonlinear upon the onset of yielding.

The compressive strains developed across the top surface of the concrete slab (as measured by SG3 and SG4) were uniform, verifying the effective width over the whole cross-section. In contrast, the tensile strains on the bottom flange of the steel I-beam (as measured by SG14) were much larger than those on the web of the steel I-beam (as measured by SG12). The tensile strains on both positions continuously increased with the applied load, revealing that the cracking in the concrete and yielding in the steel beam did not interrupt the load transfer. The strains on the profiled steel decking were constantly relatively small during tests (as measured by SG 7 and SG8). Moreover, in order to show the location of the neutral axis and the distribution of strains, the strains along the height of the cross-section have been plotted at five load levels (i.e. 50 kN, 100 kN, 150 kN, 200 kN and yield load) in Fig. 5.8.

For the composite beam specimens M20-200-NA, M20-200-RA30, M24-400-RA30 and M24-400-RA100, the top flange of the steel I-beam were in compression until the onset of yielding, upon which tensile strains started to develop in the top flange, indicating that the neutral axis was shifted higher up in the post-yielding stage due to the yielding of steel section. However, for the composite beam specimen M20-200-RA100, only tensile strains were observed during testing, indicating that the neutral axis remained within the concrete slab.

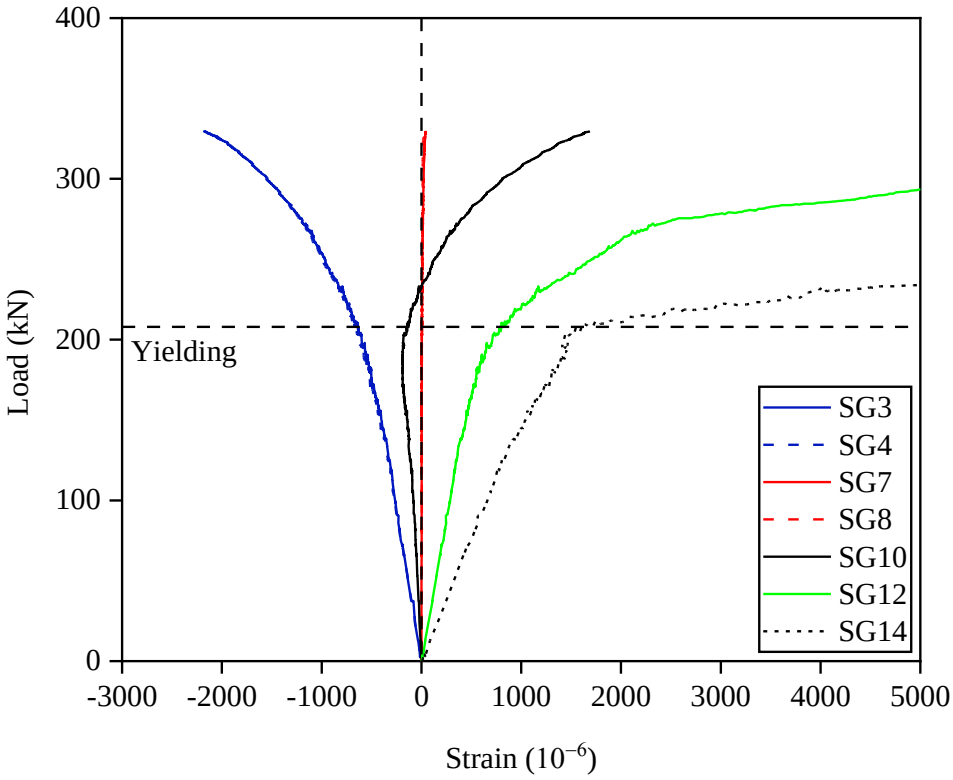

(a) M20-200-NA

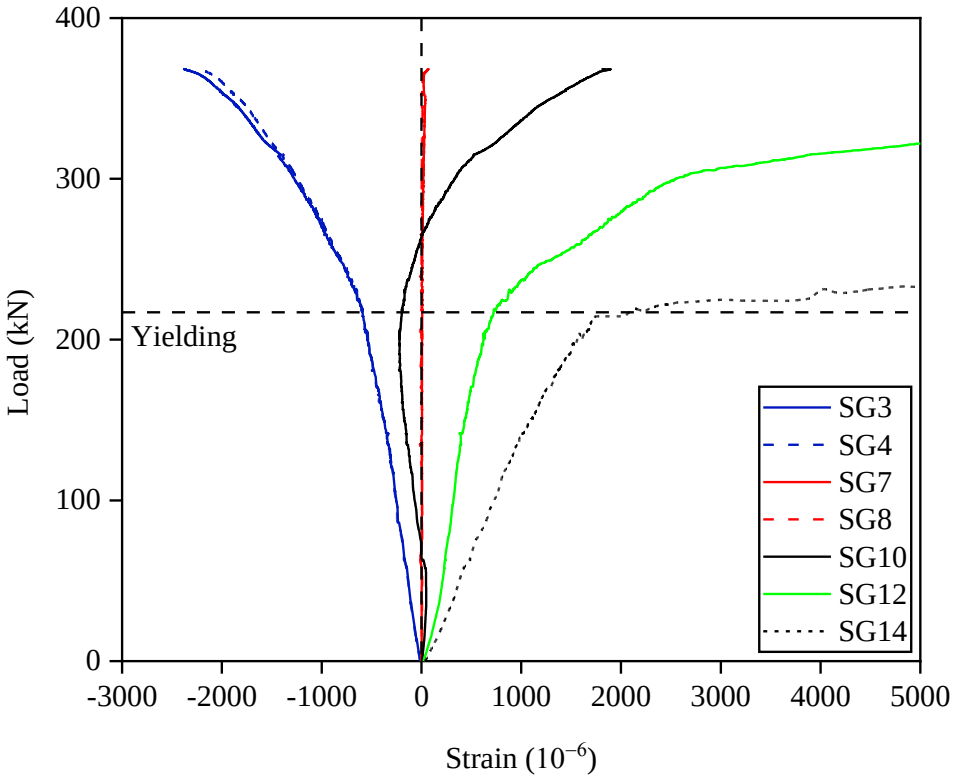

(b) M20-200-RA30

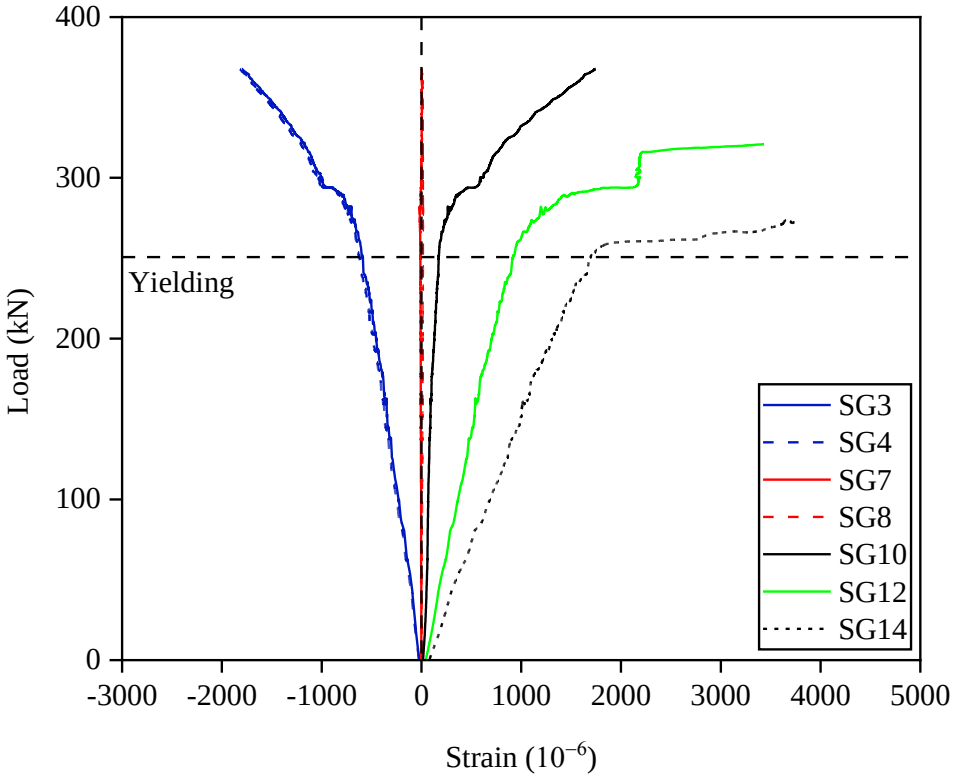

(c) M20-200-RA100

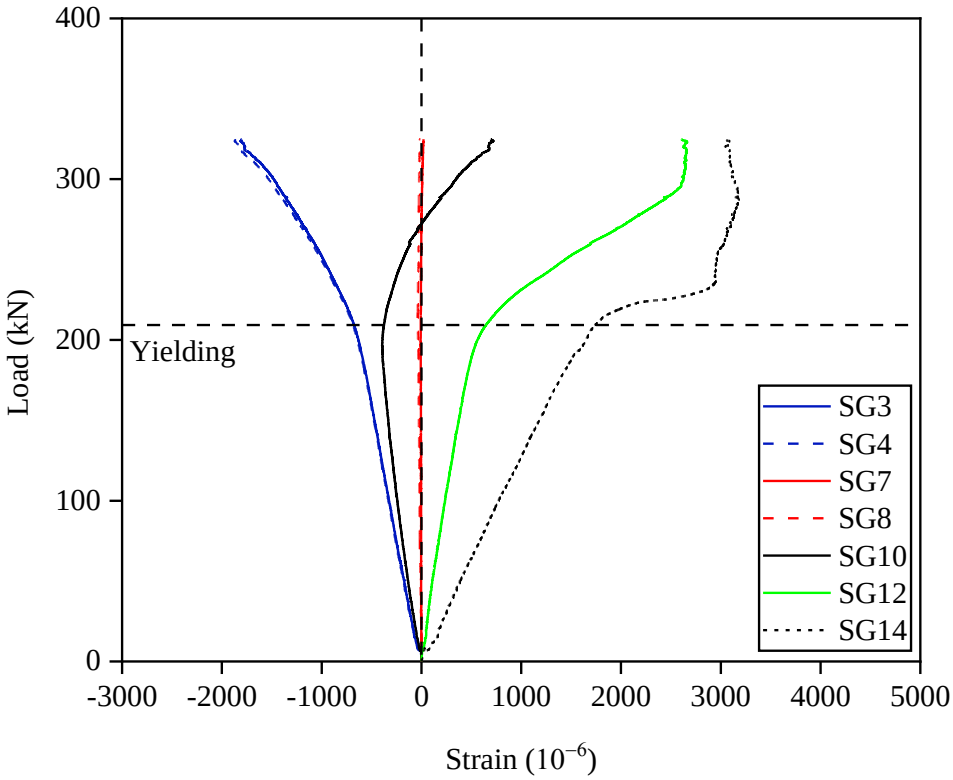

(d) M24-400-RA30

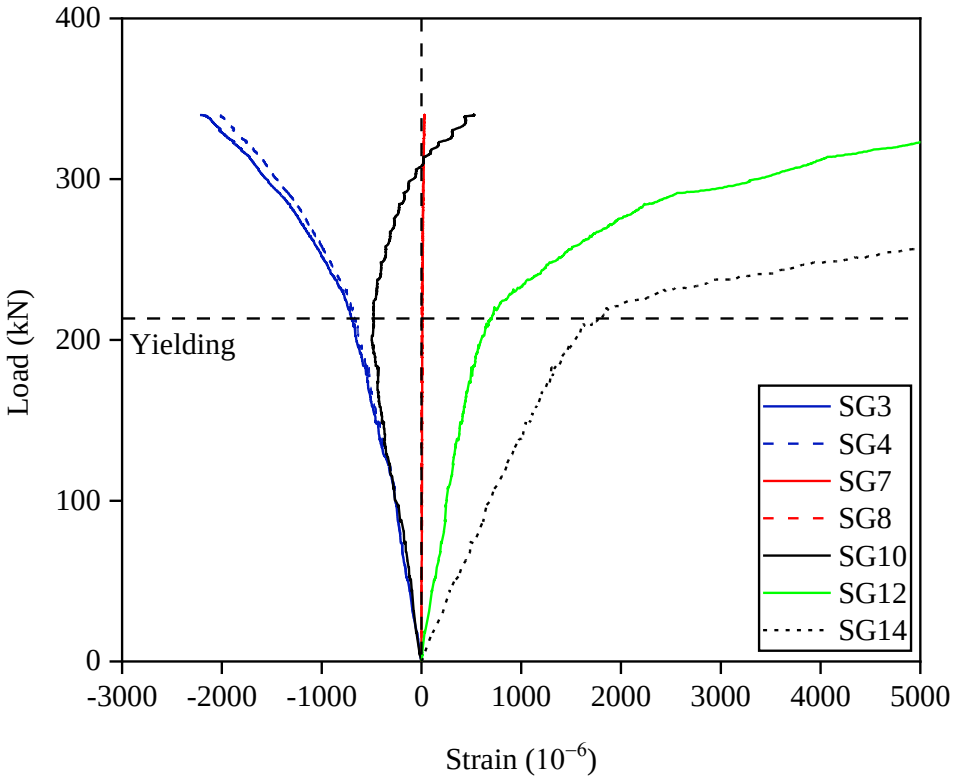

(e) M24-400-RA30

Fig. 5.7 Load-strain curves of composite beam specimens

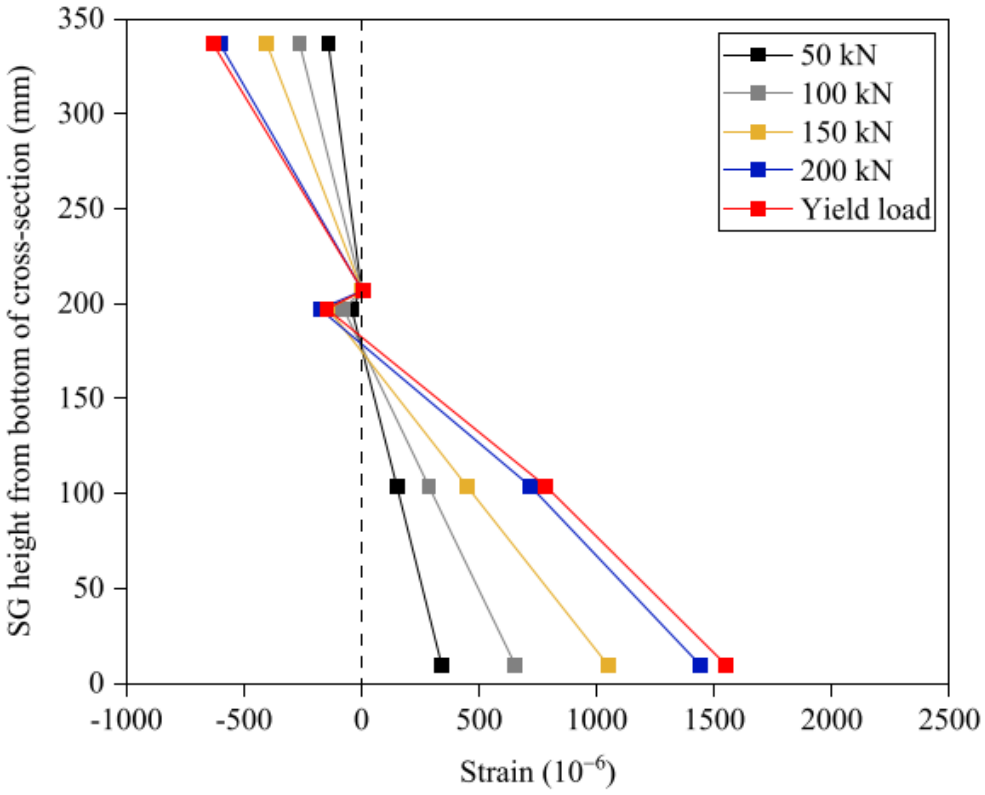

(a) M20-200-NA

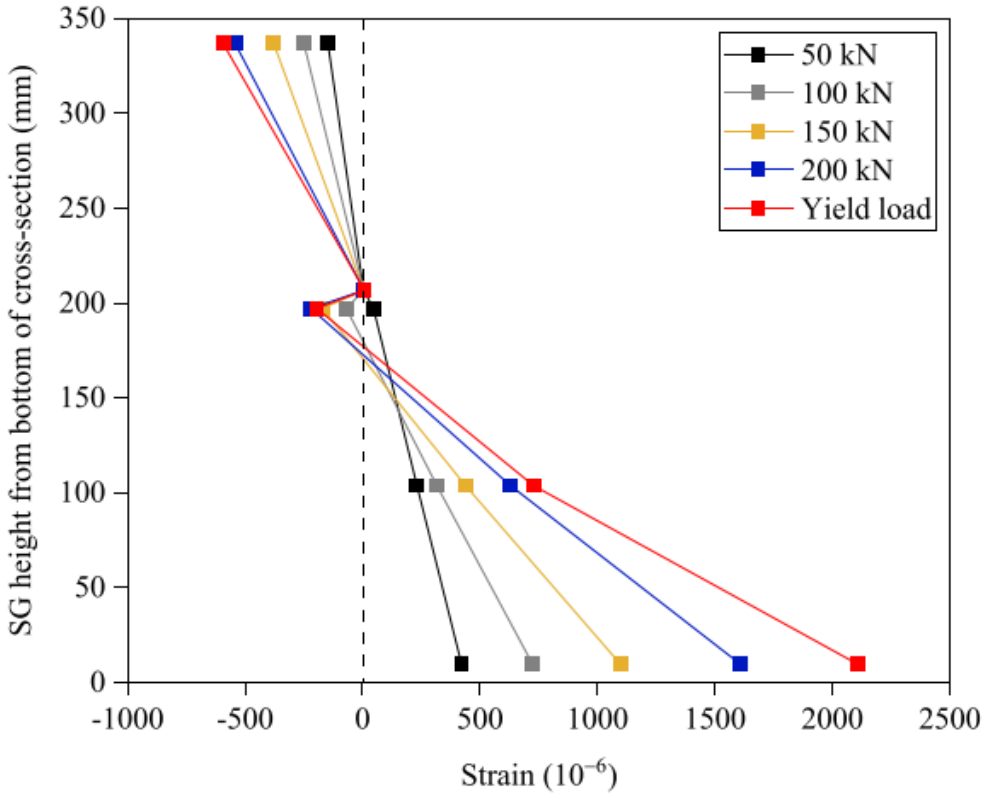

(b) M20-200-RA30

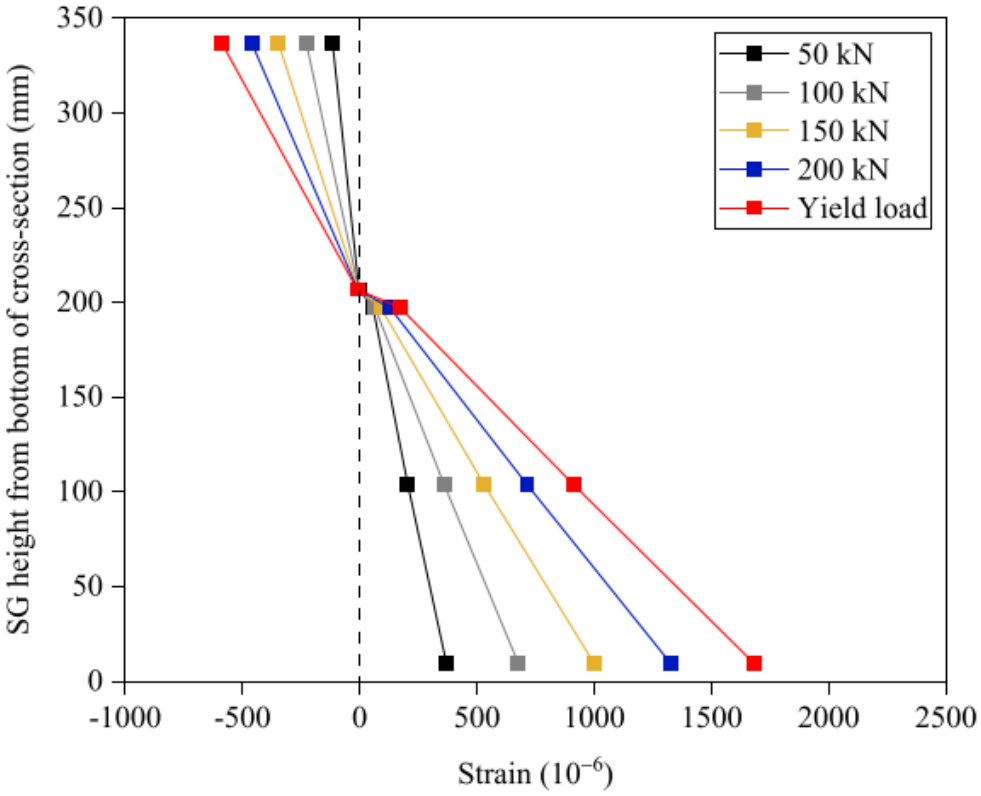

(c) M20-200-RA100

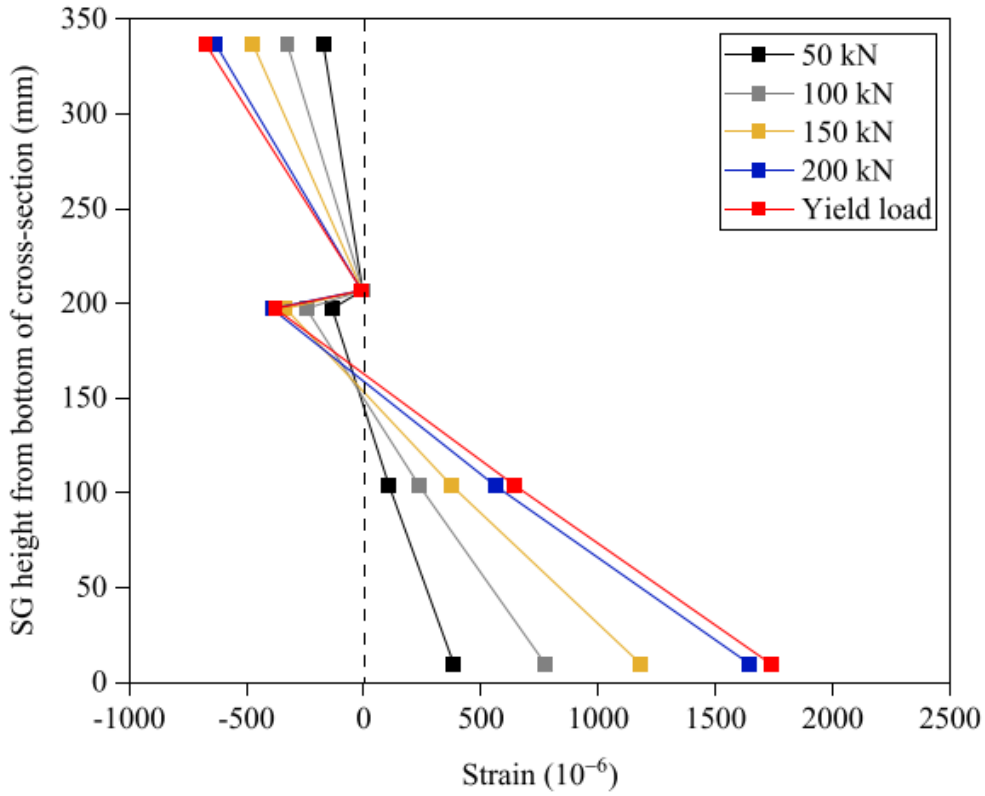

(d) M24-400-RA30

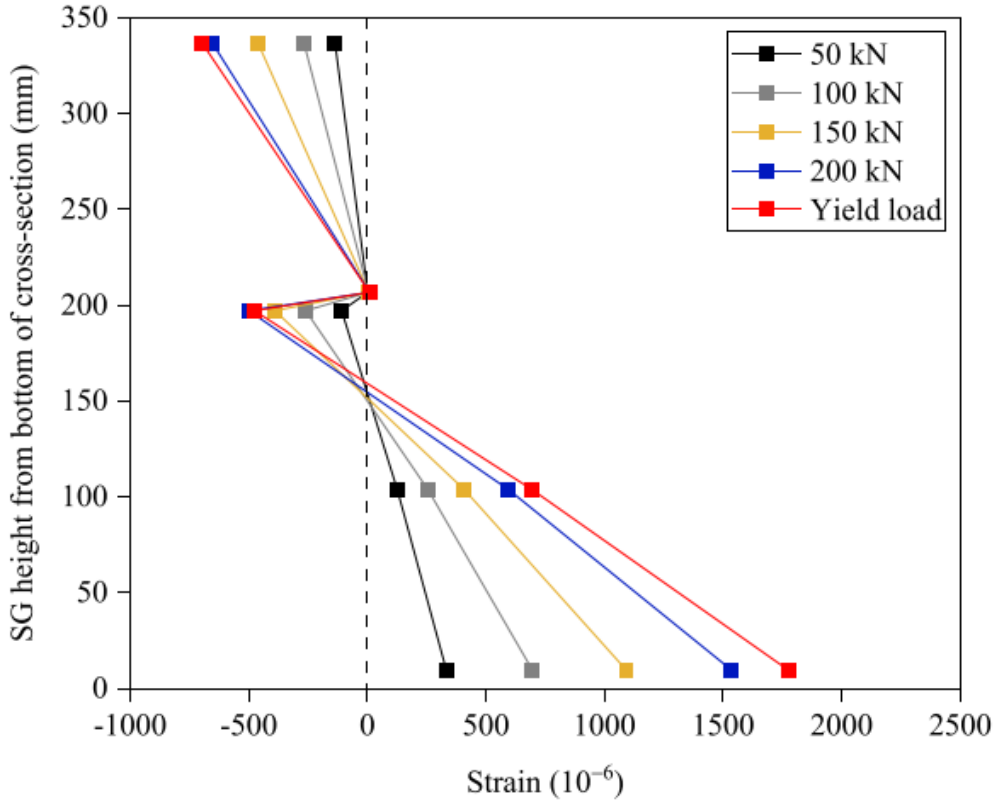

(e) M24-400-RA30

Fig. 5.8 Cross-sectional strain distributions

5.3.5 Demountability

Following the four-point bending tests performed on the composite beams with demountable shear connectors, an evaluation was undertaken regarding the detachability of the slab from the steel beam. The findings demonstrated that, despite significant deformation during testing, the slab could be separated from the steel beam with remarkable ease, as shown in Fig. 5.9. This result illustrates the efficacy and durability of demountable shear connectors under harsh conditions, preserving functionality despite significant structural distortion.

The demountable beam system is designed for operation under service loads in practical applications, as opposed to the extreme loading levels encountered in laboratory testing. Consequently, the structure would generally not undergo substantial deflection or damage. Under service stresses, the integrity of the demountable shear connectors would be maintained, and their removal would likely be more uncomplicated than witnessed in the testing environment. The system's simplicity of disassembly under standard working settings underscores its appropriateness for realistic reuse applications.

The ramifications of these findings are substantial for sustainable construction methodologies. The suggested floor system can be conveniently disassembled, facilitating the removal and future reutilization of the steel beams. This capability correlates with circular economy ideas, providing a sustainable solution for construction by minimising waste and enabling the reuse of structural components. This technology significantly mitigates the environmental impact of construction and demolition by extending the lifespan and reusability of essential structural components.

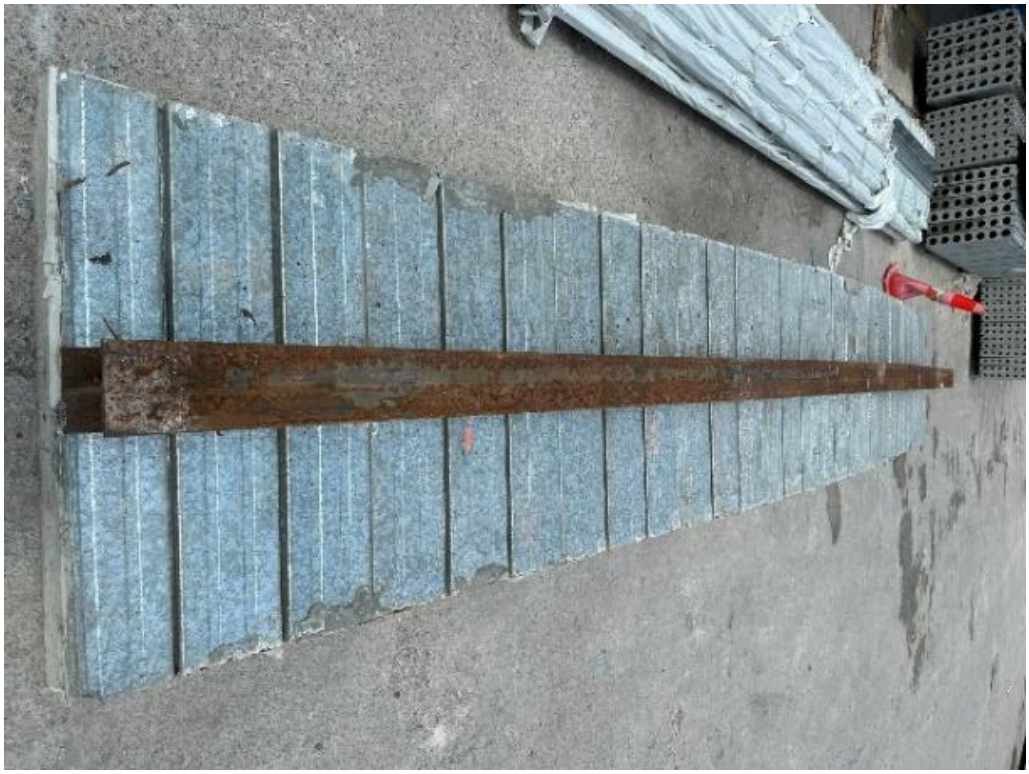

(a) flipped sample after the bending test

(b) Demount bolted shear connector

(c) Demounting steel I-beam from slab below

(d) Demounted composite slab

(e) Demounted steel I-beam

Fig. 5.9 Demountability

5.4 Evaluation on design codes

5.4.1 Overview

In the design of composite beams, current design rules utilise a consistent framework: (i) determining the extent of shear connection and (ii) computing the flexural resistance based on the plastic stress distribution within the composite section. In the absence of established design codes for steel–RAC composite beams with bolted shear connectors, the design provisions for steel–NAC composite beams with welded shear connectors, as prescribed in EN 1994-1-1 (2004) and ANSI/AISC 360-16 (2016), were described and evaluated for their applicability by comparing the experimentally acquired ultimate moments against the unfactored code predictions.

5.4.2 Degree of connection

The degree of shear connection η_{pred} of the composite beam was defined in Eq. (5.1), where n_r denotes the number of bolted shear connectors within a half span of the composite beam, $V_{b,pred}$ represents the shear resistance of an individual bolted shear connector, and V_s is taken as the minimum of the maximum possible tensile resistance of the steel beam and the maximum possible compression resistance of concrete slab, as given in Eq. (5.2), where A_s denotes the gross cross-sectional area of the steel beam, b_{eff} represents the effective width of the concrete slab and h_c indicates the thickness of the composite slab. Owing to the absence of the design formulation for the shear resistance prediction of a bolted shear connector, the codified design equation of a welded shear connector was adopted herein.

$$\eta_{pred} = \frac{n_r V_{b,pred}}{V_s} \tag{5.1}$$

$$V_s = min(A_s \sigma_{0.2}, 0.85 b_{eff} h_c f_c) \tag{5.2}$$

Both the European standard EN 1994-1-1 (2004) and American specification ANSI/AISC 360-16 (2016) consider two possible failure modes – shear fracture of the connector and concrete crushing. The design formulations to determine the

shear resistance of an single connector, as specified in EN 1994-1-1 (2004) and ANSI/AISC 360-16 (2016), were given by Eqs (4.7) and (4.8) in Chapter 4. The predicted degrees of shear connection η_{pred} for all composite beam specimens are reported in Table 5.3 and 5.4, where both EN 1994-1-1 (2004) and ANSI/AISC 360-16 (2016) lead to the full shear connection for all M20-200 composite beam specimens and the partial shear connection for M24-400 composite beam specimens.

5.4.3 Flexural resistance

Both EN 1994-1-1 (2004) and ANSI/AISC 360-16 (2016) prescribe the use of the plastic theory to obtain the plastic moment resistance of a composite beam M_{pred}, with the typical plastic stress distributions for full and partial shear connections illustrated in Figs 5.10(b) and 5.10(c), respectively. For the composite section with the full shear connection (i.e. M20-200 composite beam specimens), the plastic moment resistance of the composite section M_{pred} is calculated from Eq. (5.3), where T_s represents the tensile resistance of the steel beam and taken equal to $A_s\sigma_{0.2}$ for the scenario of full shear connection, h denotes the depth of the steel beam and x_c indicates the depth of the plastic neutral axis (PNA) to the most compressed fibre of the concrete slab and obtained from the force equilibrium between the compressive resistance of the concrete slab C_c and tensile resistance of the steel beam T_s, as given by Eq. (5.4).

$$M_{pred,full} = T_s(\frac{h}{2} + h_c - \frac{x_c}{2}) \tag{5.3}$$

$$x_c = \frac{C_c}{0.85 b_{eff} f_c} \tag{5.4}$$

Regarding the composite section with the partial shear connection (i.e. M24-400 composite beam specimens), the plastic moment resistance of the composite section M_{pred} is calculated from Eq. (5.5). The compressive resistance of the concrete slab C_c is taken as the minimum of the shear resistance provided by shear connectors, the maximum possible tensile resistance of the steel beam and the maximum possible compression resistance of concrete slab, as given by Eq. (5.6). The PNA was found to locate within the top flange of the steel beam. The depth

of the concrete compressive stress block x_c is then calculated from Eq. (5.4). The resistance of the top flange in compression C_s is obtained from the force equilibrium, as shown in Eq. (5.7), with the corresponding depth of the PNA to the top of the flange x_s given by Eq. (5.8). y_s is the distance from the bottom of the steel section to the centroid of the steel section in tension.

$$M_{pred,partial} = C_c(h + h_c - \frac{x_c}{2} - y_s) + C_s(h - \frac{x_s}{2} - y_s) \quad (5.5)$$

$$C_c = min(n_r V_{b,pred}, A_s\sigma_{0.2}, 0.85 b_{eff} h_c f_c) \quad (5.6)$$

$$C_s = \frac{1}{2}(A_s\sigma_{0.2} - C_c) \quad (5.7)$$

$$x_s = \frac{C_s}{b_f \sigma_{0.2}} \quad (5.8)$$

Moreover, given the complexity of the plastic theory, EN 1994-1-1 (2004) provides an alternative simplified method to predict the flexural resistance of a composite beam $M_{pred,S}$, where the linear interpretation between the plastic moment capacity of steel beam section $M_{pl,a}$ and the plastic moment capacity of the composite section with the full shear connection $M_{pred,full}$ is conducted, as given by Eq. (5.9).

$$M_{pred,S} = M_{pl,a} + \eta_{pred}(M_{pred,full} - M_{pl,a}) \quad (5.9)$$

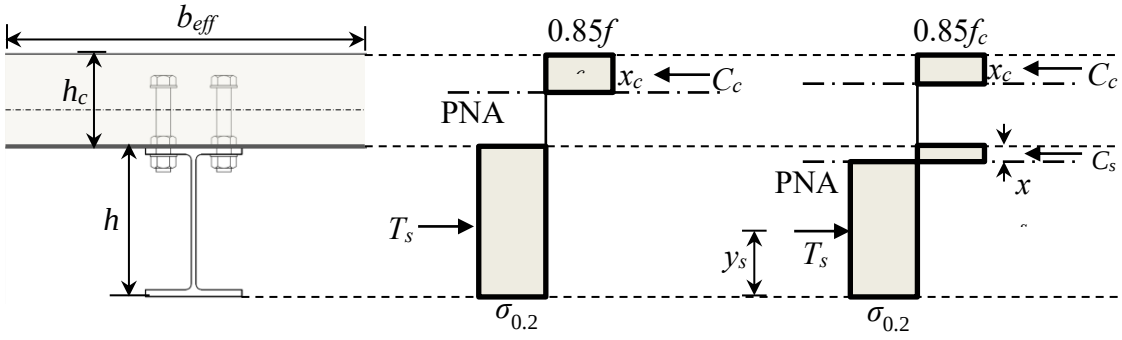

(a) Composite section (b) Full shear connection (c) Partial shear connection

Fig. 5.10 Plastic stress distribution of composite section

The codified design flexural capacities were assessed by comparing with the test results. Both the EC4 and AISC predicted plastic moment resistances, according to

the plastic theory and simplified method, for all composite beam specimens are reported in Table 5.6. It can be concluded that both EN 1994-1-1 (2004) and ANSI/AISC 360-16 (2016) generally yielded conservative flexural resistance predictions for steel–RAC composite beams with bolted shear connectors. In comparison to EN 1994-1-1 (2004), ANSI/AISC 360-16 (2016) demonstrated a reduction in conservatism while providing more precise forecasts of the flexural resistance for steel–RAC composite beams with partial shear connections. Furthermore, the simplified method yielded more conservative predictions of flexural resistance compared to those derived from plastic theory.

Table 5.3 Comparison of test failure loads with predicted results from EN 1994-1-1 (2004)

Specimen ID	M_u (kNm)	η_{EC4}	M_{EC4} (kNm)	M_u/M_{EC4}	$M_{EC4,S}$ (kNm)	$M_u/M_{EC4,S}$
M20-200-NA	310.5	1.00	315.4	0.98	315.4	0.98
M20-200-RA30	343.8	1.00	314.7	1.09	314.7	1.09
M20-200-RA100	345.7	1.00	318.6	1.08	318.6	1.08
M24-400-RA30	304.7	0.78	284.4	1.07	272.6	1.12
M24-400-RA100	327.6	0.90	304.8	1.07	299.4	1.09

Table 5.4 Comparison of test failure loads with predicted results from ANSI/AISC 360-16 (2016)

Specimen ID	M_u (kNm)	η_{AISC}	M_{AISC} (kNm)	M_u/M_{AISC}	$M_{AISC,S}$ (kNm)	$M_u/M_{AISC,S}$
M20-200-NA	310.5	1.00	315.4	0.98	315.4	0.98
M20-200-RA30	343.8	1.00	314.7	1.09	314.7	1.09
M20-200-RA100	345.7	1.00	318.6	1.08	318.6	1.08
M24-400-RA30	304.7	0.91	303.1	1.01	297.9	1.02
M24-400-RA100	327.6	0.91	306.4	1.07	301.5	1.09

Furthermore, rather than employing code-based calculations to ascertain the shear resistance of the steel connector, the shear resistance values derived from the push-off tests in Chapter 4 were utilised to compute the bending resistance. This method facilitated a direct comparison with the experimental bending test outcomes. The comparisons are presented in Table 5.5 below. The results

demonstrate that the projected bending resistance, derived from push-off test data, correlates more closely with experimental bending test outcomes, indicating that push-off tests can serve as a reliable indirect approach for evaluating bending resistance with enhanced precision.

Table 5.5 Comparison of test failure loads with predicted results from push-off tests

Specimen ID	M_u (kNm)	η_{AISC}	$M_{push\text{-}off}$ (kNm)	$M_u/M_{push\text{-}off}$	$M_{push\text{-}off,S}$ (kNm)	$M_u/M_{push\text{-}off,S}$
M20-200-NA	310.5	1.00	315.39	0.98	315.39	0.98
M20-200-RA30	343.8	1.00	314.65	1.09	314.65	1.09
M20-200-RA100	345.7	1.00	318.63	1.08	318.63	1.08
M24-400-RA30	304.7	0.95	311.82	0.98	309.01	0.99
M24-400-RA100	327.6	1.00	318.63	1.03	318.63	1.03

The computed shear resistance of the connector is contingent upon its geometric configuration and material characteristics, as outlined in Section 4.6.2. Nonetheless, it fails to consider the differences in shear resistance resulting from differing water-to-cement ratios at varied levels of recycled aggregate substitution. In this instance, push-off testing offers a more dependable approach for directly assessing the shear resistance of the connector.

The bending resistance of a RAC-steel composite beam with a demountable shear connector is determined by the sectional resistance of both concrete and steel, along with the degree of shear connection η, which is directly influenced by the shear resistance of the connector. Incorporating empirically derived shear resistance from push-off tests might mitigate the shortcomings of existing design regulations, which fail to particularly address demountable shear connectors in RAC. This facilitates a more precise computation of the degree of shear connection η, resulting in a more accurate evaluation of the composite beam's overall bending resistance.

5.5 Summary

In this chapter, the flexural behaviour and resistances of steel–RAC composite beams with bolted shear connectors have been investigated through experiments. The experimental programme adopted five composite beam specimens, which were made from concrete with different recycled aggregate replacement ratios (0%, 30% and 100%) and designed with different arrangements of bolted shear connectors, and incorporated tensile coupon tests, concrete compression tests and four-pointing bending tests. The test configuration, methodologies, and recorded outcomes were fully reported. The experimental failure modes, load–mid-span deflection curves, load–slip and mid-span–slip curves and strain distributions were discussed and analysed. It can be found that the specimens with a higher recycled aggregate replacement ratio and higher degree of shear connection exhibited improved flexural capacity and a lower level of ductility and horizontal slip between the steel beam and composite slab. In the absence of established design codes for steel–RAC composite beams with bolted shear connectors, the corresponding design provisions for steel–NAC composite beams with welded shear connectors, as specified in EN 1994-1-1 (2004) and ANSI/AISC 360-16 (2016), were evaluated for their applicability to steel–RAC composite beams with bolted shear connectors. Based on the assessment results, it can be suggested that both EN 1994-1-1 (2004) and ANSI/AISC 360-16 (2016) generally provided an acceptable level of design accuracy and consistency for steel–RAC composite beams with bolted shear connectors, while ANSI/AISC 360-16 (2016) was shown to yield less conservative but more accurate flexural resistance predictions than EN 1994-1-1 (2004).

6 CONCLUSIONS AND SUGGESTIONS FOR FUTURE WORK

6.1 Conclusions

This chapter summarises the principal research findings and conclusions of the thesis, with more comprehensive concluding notes presented at the end of each chapter. Subsequent sections delineate recommendations for future research.

Chapter 1 delineates the context and rationale for the research, highlighting sustainable construction methodologies via recycling, reuse, and waste minimisation. It presents RAC, a composite formed by substituting natural aggregates with recycled aggregates, highlighting its mechanical deficiencies relative to NAC. RAC is typically employed in non-structural applications due to its diminished strength, stiffness, and durability. This is examined in temporary or short-term lease structures, where durability requirements are diminished. An innovative, sustainable composite flooring solution utilising RAC and demountable shear connectors is presented to enable the reuse of steel beams. According to circular economy principles, this technique facilitates straightforward construction and disassembly by enabling material reutilization. At the end of the chapter, the research goals are laid out. These include measuring shear resistance, bending behaviour, and the performance of RAC with different aggregate replacements and using numerical models to back up the results.

Chapter 2 comprehensively examines previous studies on RAC, its microstructural properties, and mechanical performance. The dual ITZ of RAC, arising from the combination of old and fresh cement mortars, results in diminished durability, tensile strength, and elastic modulus relative to NAC. The review discusses the pros and cons of using RAC in structural elements like slabs, composite beams, and concrete-filled steel tubes. It focuses on only a little research that has been done on composite beams using RAC. This chapter also talks about different demountable shear connectors, focusing on bolted and Nelson connectors and how well they work to provide shear resistance equal to welded studs. Various forms of profiled steel decking are analysed for their contributions to improving composite action and minimising concrete use, including specifics on prevalent decking goods utilised in the construction industry. The chapter points out a need

for more research on how RAC can be used in composite beams with demountable connections and suggests looking into how well RAC works at a specific strength grade.

Chapter 3 introduces the proposed RAC composite floor system, which includes demountable shear connectors and is designed for short-term construction applications. The flooring solution comprises an RAC slab featuring profiled steel decking and systematically organised demountable shear connectors. Bolted and Nelson connectors are compared, with bolted connectors selected for their practicality. The chapter outlines the arrangement and installation of these components, specifying connector spacing according to decking geometry, and the strategy for disassembly after testing to facilitate material reutilization. The testing plan includes push-off tests to assess shear-slip behaviour and four-point bending tests on full-scale beams to evaluate structural performance. Different types of RAC mixtures and connector configurations are used to make specimens. Testing plans are laid out in tables, which makes it easy to check the system's durability and mechanical properties.

Chapter 4 presents an experimental and numerical investigation of the shear resistance and load-slip behaviour of demountable bolted shear connectors in a steel–RAC composite slab. In the experimental programme, compressive cylinder tests on concrete materials and tensile coupon tests on steel materials were first executed, followed by push-off tests on eight full-scale steel–RAC composite slab specimens. The experimental failure modes, resistance and load–slip curves were represented and discussed in detail. Thereafter, FE models were established and validated in accordance with the test results. In light of the absence of designated design codes for steel–RAC composite slab with demountable bolted shear connectors, the current design provisions for steel–NAC composite slabs with welded shear connectors, as prescribed in EN 1994-1-4 (2004) and ANSI/AISC 360-16 (2016), as well as the current design provision for bolt as prescribed in EN 1993-1-8 (2008) and cast in bolt anchor as prescribed in ACI 318-19 (2019) were assessed for their applicability. Based on the comparison results, (i) EC4 accurately predicts the shear resistance of bolted shear connectors in NAC and conservatively for RAC, but overestimates steel resistance compared to EC3, which aligns more closely with experimental results; and (ii) AISC and ACI provide generally accurate

predictions but offer unsafe estimates for NAC and do not correctly identify the failure mode.

Chapter 5 analyses the flexural behaviour and resistance of steel–RAC composite beams with bolted shear connectors through experimental analysis. The experimental programme consists of five composite beam specimens made from concrete with different recycled aggregate replacement ratios and designed with different bolted shear connector configurations. Similarly, concrete compression tests and tensile coupon tests were conducted to ascertain the material property, followed by four-pointing bending tests. The experimental failure modes, load–mid-span deflection curves, load–slip and mid-span–slip curves and strain distributions were summarised and examined. Given the fixed design concrete strength irrespective of the recycled aggregate replacement ratio, the specimens with the higher recycled aggregate replacement ratio and a higher degree of shear connection showed improved flexural capacity and a lower level of ductility and horizontal slip between the steel beam and composite slab. Similar to the push-off test, the corresponding design provisions for steel–NAC composite beams with welded shear connectors, as outlined in EN 1994-1-4 (2004) and ANSI/AISC 360-16 (2016), were used to verify their applicability to steel–RAC composite beams with bolted shear connectors. According to the calculated results, both EN 1994-1-4 (2004) and ANSI/AISC 360-16 (2016) generally provided an acceptable level of design accuracy and consistency for steel–RAC composite beams with bolted shear connectors. However, ANSI/AISC 360-16 (2016) demonstrates less conservative yet more precise predictions of flexural resistance compared to EN 1994-1-4 (2004).

Overall, the push-off test effectively represents the shear behaviour due to the direct interface shear force applied and can be utilised to indirectly predict the flexural behaviour of a composite beam under bending. The four-point bending test directly assesses the flexural behaviour of the composite beam, influenced by the shear response at the shear connectors between the concrete and steel beam. Both types of tests indicate that composite beams utilising demountable shear connectors show comparable structural performance for a given design strength of concrete. Additionally, a rise in the recycled aggregate replacement ratio corresponds to an enhancement in the ultimate capacity. Although both EN 1994-1-4 (2004) and ANSI/AISC 360-16 (2016) provided a marginally unsafe

prediction on the shear resistance of the bolted shear connector in NAC, they still can be adopted to design such structural applications in RAC similar to conventional NAC composite beams with welded shear studs. Notably, ANSI/AISC 360-16 (2016) provides less conservative but more precise resistance estimations compared to EN 1994-1-4 (2004). The proposed structural system resembles a traditional composite floor system but is slightly more economical due to the reduced expense of shear connections relative to welded shear studs, particularly when factoring in labour expenses. The utilisation of recycled aggregate diminishes the embodied carbon footprint, mitigates environmental harm, and lessens dependence on foreign resources. The system's demountability, evidenced by push-off and bending tests, facilitates the reuse of steel beams post-building lifespan, hence fostering a competitive and circular economy in the construction sector.

6.2 Suggestions for future work

Based on the findings described in earlier sections, recommendations for future studies on RAC–steel composite beams utilising demountable shear connectors are given herein.

Driven by the goal of applying research outcomes to engineering applications, the testing plan primarily focused on achieving either full shear connection or a high degree of shear connection. The study results demonstrate that demountable bolt shear connectors can be equivalent replacements for welded shear connectors, irrespective of the recycled aggregate replacement percentages. Notably, all observed failure modes involved concrete failure rather than shear connector failure, aligning with the initial testing plan. Future research could explore using more miniature shear connectors (e.g., M10) to study different failure modes.

Furthermore, this study on RAC focuses primarily on a fixed design compressive strength rather than variable design compressive strengths with a consistent water-to-cement ratio, as previous researchers have done. This approach is also motivated by engineering applications, where the design strength of the concrete is predetermined before determining the percentage of recycled aggregate

replacement. The research findings indicate that, for a given design strength, the structural behaviour of RAC is superior to that of NAC — showing improvements of up to approximately 20% in push-off tests and up to around 10% in bending tests. This trend was consistently observed across all test specimens for both push-off and bending tests, challenging the common belief that RAC is inherently weaker than NAC. However, this difference in resistance cannot be verified using current design codes and FEM models, which are based solely on compressive strength. The water-to-cement ratio may also influence structural response beyond compressive strength. Future research should include more testing to investigate further and validate this hypothesis.

Lastly, in order to promote the utilisation of the RAC composite beam in structures, it will be worthwhile to conduct long-term bending tests and investigate the influence of recycled aggregate replacement percentage on long-term deflection of the beam. It will be equally important to verify the demountability of the RAC slab and reusability of the steel beam under service loads. While the dynamic performance of bolted shear connectors has been validated in prior investigations on NAC over 5 million loading cycles, no studies have been undertaken on RAC. Conducting analogous tests on RAC is essential to evaluate its fatigue loading resistance and to ascertain if its capacity is influenced by microstructural variations when compared to NAC.

List of references

ABAQUS (2017) *ABAQUS/standard user's manual*. Version 6.17. Dassault Systems Simulia 500 Corp. USA.

ACI 318-19 (2019) *Building code requirements for structural concrete*. American Concrete Institute.

ANSI/AISC 360-16 (2016) *Specification for Structural Steel Buildings*. American Institute of Steel Construction.

Ataei, A. & Zeynalian, M. (2021) 'A study on structural performance of deconstructable bolted shear connectors in composite beams', *Structures*, 29, pp. 519–533.

Ban, H., Uy, B., Pathirana, S.W., Henderson, I., Mirza, O. and Zhu, X. (2015) 'Time-dependent behaviour of composite beams with blind bolts under sustained loads', *Journal of Constructional Steel Research*, 112, pp. 196–207.

Betonwerk Büscher (2023) 'The Büscher Wall – Building sustainably with concrete containing recycled constituents', *BFT International*, Issue 06. Available at: https://www.bft-international.com/en/artikel/the-buescher-wall-building-sustainably-with-concrete-containing-recycled-constituents-3897796.html

Brito, J. de & Saikia, N. (2013) *Recycled Aggregate in Concrete*. London: Springer.

BS EN 12390-13:2013 (2013) *Testing Hardened Concrete – Part 13: Determination of Secant Modulus of Elasticity in Compression*. Brussels: European Committee for Standardization (CEN).

Burnet, M.J. & Oehlers, D.J. (2001) 'Rib shear connectors in composite profiled slabs', *Journal of Constructional Steel Research*, 57, pp. 1267–1287.

Cai, M., Ke, X. and Su, Y. (2020) 'Axial compressive performance of RAC-encased RACFST composite columns', *Engineering Structures*, 210, p. 110393.

Cai, M., Ke, X. and Xu, D. (2021) 'Study on axial compressive stiffness of RAC-encased RACFST composite columns', *Thin-Walled Structures*, 162, p. 107570.

Chen, J., Wang, Y., Roeder, C.W. and Ma, J. (2017) 'Behaviour of normal-strength recycled aggregate concrete filled steel tubes under combined loading', *Engineering Structures*, 130, pp. 23–40.

Chen, Q., Zhang, J., Wang, Z., Zhao, T. and Wang, Z. (2024) 'A review of the interfacial transition zones in concrete: Identification, physical characteristics, and mechanical properties', *Engineering Fracture Mechanics*, 300, p. 109979.

Chen, Y.T., Zhao, Y., West, J.S. and Walbridge, S. (2014) 'Behaviour of steel–precast composite girders with through-bolt shear connectors under static loading', *Journal of Constructional Steel Research*, 103, pp. 168–178.

Chen, Z., Xu, J., Chen, Y. and Lui, E.M. (2016) 'Recycling and reuse of construction and demolition waste in concrete-filled steel tubes: A review', *Construction and Building Materials*, 126, pp. 641–660.

Ciao, J.L., Yang, T.Y., Nie, X., Li, B.Y., Fan, J.S. and Shu, B.A. (2022) 'Experimental and numerical investigation on mechanical performance of continuous steel-UHPC composite slabs', *Engineering Structures*, 270, p. 114804.

Dai, X.H., Lam, D. and Saveri, E. (2015) 'Effect of concrete strength and stud collar size to shear capacity of demountable shear connectors', *Journal of Structural Engineering*, 141(11), p. 04015025.

de Azevedo, V.D.S., de Lima, L.R., Vellasco, P.C.D.S., Tavares, M.E.D.N. and Chan, T.M. (2021) 'Experimental investigation on recycled aggregate concrete filled steel tubular stub columns under axial compression', *Journal of Constructional Steel Research*, 187, p. 106930.

Domingo-Cabo, A., Lázaro, C., López-Gayarre, F., Serrano-López, M.A., Serna, P. and Castaño-Tabares, J.O. (2009) 'Creep and shrinkage of recycled aggregate concrete', *Construction and Building Materials*, 23, pp. 2545–2553.

Du, T., Wang, W.H., Lin, H.L., Liu, Z.X. and Liu, J. (2010) 'Experimental study on interfacial strength of the high performance recycled aggregate concrete', in *Earth and Space 2010: Engineering, Science, Construction, and Operations in Challenging Environments*. ASCE, pp. 2821–2828.

E8/E8M-15a (2015) *Standard test methods for tension testing of metallic materials*. West Conshohocken, PA: American Society for Testing and Materials (ASTM).

EN 1992-1-1 (2004) *Eurocode 2: Design of concrete structures – Part 1-1: General rules and rules for buildings*. CEN.

EN 1993-1-8 (2005) *Eurocode 3: Design of steel structures – Part 1.8: Design of joints*. CEN.

EN 1994-1-1 (2004) *Eurocode 4: Design of composite steel and concrete structures – Part 1-1: General rules and rules for buildings*. CEN.

EN ISO 6892-1 (2016) *Metallic materials: Tensile testing – Part 1: Method of test at room temperature*. CEN.

Etxeberria, M., Vázquez, E. and Marí, A. (2006) 'Microstructure analysis of hardened recycled aggregate concrete', *Magazine of Concrete Research*, 58(10), pp. 683–690.

Etxeberria, M., Vázquez, E., Marí, A. and Barra, M. (2007) 'Influence of amount of recycled coarse aggregates and production process on properties of recycled aggregate concrete', *Cement and Concrete Research*, 37, pp. 735–742.

Faella, C., Martinelli, E. and Nigro, E. (2010) 'Steel-concrete composite beams in partial interaction: Closed-form "exact" expression of the stiffness matrix and

the vector of equivalent nodal forces', *Engineering Structures*, 32, pp. 2744–2754.

Guo, H., Shi, C., Guan, X., Zhu, J., Ding, Y., Ling, T.C., Zhang, H. and Wang, Y. (2018) 'Durability of recycled aggregate concrete – a review', *Cement and Concrete Composites*, 89, pp. 251–259.

He, A., Su, A., Liang, Y. and Zhao, O. (2021) 'Experimental and numerical investigations of circular recycled aggregate concrete-filled stainless steel tube columns', *Journal of Constructional Steel Research*, 179, p. 106566.

Henderson, I.E.J., Zhu, X.Q., Uy, B. and Mirza, O. (2017) 'Dynamic behaviour of steel-concrete composite beams retrofitted with various bolted shear connectors', *Engineering Structures*, 131, pp. 115–135.

Kildashti, K., Katwal, U., Tao, Z. and Tam, V. (2024) 'Numerical simulation of steel-concrete composite beams and slabs at elevated temperatures', *Engineering Structures*, 315, p. 118297.

Kwon, G., Engelhardt, M.D. and Klingner, R.E. (2010) 'Behaviour of post-installed shear connectors under static and fatigue loading', Journal of Constructional Steel Research, 66, pp. 532–541.

Lam, D., Dai, X., Ashour, A. and Rahman, N. (2017) 'Recent research on composite beams with demountable shear connectors', *Steel Construction*, 10(2), pp. 125–134.

Lam, D., Yang, J., Wang, Y., Dai, X., Sheehan, T. and Zhou, K. (2021) 'New composite flooring system for the circular economy', *Steel and Composite Structures*, 40, pp. 649–661.

Li, C., Shi, Y., Xiao, H., Tan, L. and He, L. (2024) 'Experimental and numerical investigation on flexural behaviour of steel-UHPC composite slabs with PBL shear connectors', *Journal of Building Engineering*, 95, p. 110109.

Li, D., Uy, B., Wang, J. and Song, Y. (2020) 'Behaviour and design of high-strength Grade 12.9 bolts under combined tension and shear', *Journal of Constructional Steel Research*, 174, p. 106305.

Li, W., Li, Q., Jiang, W. and Jiang, L. (2011) 'Seismic performance of composite reinforced concrete and steel moment frame structures – state-of-the-art', *Composites Part B: Engineering*, 42, pp. 190–206.

Li, W., Luo, Z., Tao, Z., Duan, W.H. and Shah, S.P. (2017) 'Mechanical behaviour of recycled aggregate concrete-filled steel tube stub columns after exposure to elevated temperatures', *Construction and Building Materials*, 146, pp. 571–581.

Liu, B., Bai, G.L., Xu, Z.H., Ma, J.F. and Han, Y.Y. (2019) 'Experimental study and finite element modelling of bond behaviour between recycled aggregate concrete and the shaped steel', *Engineering Structures*, 201, p. 109840.

Liu, Q., Xiao, J. and Sun, Z. (2011) 'Experimental study on the failure mechanism of recycled concrete', *Cement and Concrete Research*, 41, pp. 1050–1057.

Liu, X., Bi, Z., Hu, J., Hao, H., Lin, Z., Li, H., Xie, Y., Zhao, K., Jing, Y. and Yang, G. (2023) 'Bolted shear connectors in steel–concrete composite structures: Shear behaviour', *Structures*, 58, p. 105524.

Liu, X., Bradford, M.A. and Abdolreza, A. (2017) 'Flexural performance of innovative sustainable composite steel-concrete beams', *Engineering Structures*, 130, pp. 282–296.

Lu, L., Ding, Y., Guo, Y., Hao, H. and Ding, S. (2022) 'Flexural performance and design method of the prefabricated RAC composite slab', *Structures*, 38, pp. 572–584.

Lysaght-Bondek-II (2013) *Structural steel decking system: Design and construction manual to Eurocodes*.

Lyu, W.Q., Han, L.H. and Hou, C. (2021) 'Axial compressive behaviour and design calculations on recycled aggregate concrete-filled steel tubular (RAC-FST) stub columns', *Engineering Structures*, 241, p. 112452.

McNeil, K. & Kang, T.H.-K. (2013) 'Recycled concrete aggregates: A review', *International Journal of Concrete Structures and Materials*, 7(1), pp. 61–69.

Mehta, P.K. & Monteiro, P.J.M. (2006) *Concrete: Microstructure, properties, and materials*, 3rd edn. New York: McGraw-Hill.

Moynihan, M.C. & Allwood, J.M. (2014) 'Viability and performance of demountable composite connectors', *Journal of Constructional Steel Research*, 99, pp. 47–56.

Neves, R. & Brito, J. de (2022) 'Estimated service life of ordinary and high-performance reinforced recycled aggregate concrete', *Journal of Building Engineering*, 46, p. 103769.

Padmini, A.K., Ramamurthy, K. and Mathews, M.S. (2009) 'Influence of parent concrete on the properties of recycled aggregate concrete', *Construction and Building Materials*, 23, pp. 829–836.

Pathirana, S.W., Uy, B., Mirza, O. and Zhu, X. (2015) 'Strengthening of existing composite steel-concrete beams utilising bolted shear connectors and welded studs', *Journal of Constructional Steel Research*, 114, pp. 417–430.

Pavlović, M., Marković, Z., Veljković, M. and Buđevac, D. (2013) 'Bolted shear connectors vs. headed studs behaviour in push-out tests', *Journal of Constructional Steel Research*, 88, pp. 134–149.

Polus, Ł. & Szumigała, M. (2019) 'Laboratory tests vs. FE analysis of concrete cylinders subjected to compression', *AIP Conference Proceedings*, [online] Available at: https://pubs.aip.org

Qureshi, J., Lam, D. and Ye, J. (2011) 'Effect of shear connector spacing and layout on the shear connector capacity in composite beams', *Journal of Constructional Steel Research*, 67, pp. 706–719.

Rahal, K. (2007) 'Mechanical properties of concrete with recycled coarse aggregate', *Building and Environment*, 42, pp. 407–415.

Ramberg, W. & Osgood, W.R. (1943) *Description of stress-strain curves by three parameters*. Technical Note (902). Washington, DC: National Advisory Committee for Aeronautics.

Ravindrarajah, R.S. & Tam, C.T. (1985) 'Properties of concrete made with crushed concrete as coarse aggregate', *Magazine of Concrete Research*, 37(130), pp. 29–38.

Rehman, N., Lam, D., Dai, X. and Ashour, A.F. (2016) 'Experimental study on demountable shear connectors in composite slabs with profiled decking', *Journal of Constructional Steel Research*, 122, pp. 178–189.

Rehman, N., Lam, D., Dai, X. and Ashour, A.F. (2018) 'Testing of composite beam with demountable shear connectors', *Proceedings of the Institution of Civil Engineers-Structures and Buildings*, 171, pp. 3–16.

Sagoe-Crentsil, K.K., Brown, T. and Taylor, A.H. (2001) 'Performance of concrete made with commercially produced coarse recycled concrete aggregate', *Cement and Concrete Research*, 31, pp. 707–712.

SS EN 12620 (2008) *Specification for aggregates for concrete*. Singapore: Building and Construction Standards Committee.

Suwaed, A.S.H. & Karavasilis, T.L. (2020) 'Demountable steel-concrete composite beam with full-interaction and low degree of shear connection', *Journal of Constructional Steel Research*, 171, p. 106152.

Tam, V.W., Soomro, M. and Evangelista, A.C.J. (2018) 'A review of recycled aggregate in concrete applications (2000–2017)', *Construction and Building Materials*, 172, pp. 272–292.

Tam, V.W., Soomro, M., Evangelista, A.C. and Haddad, A. (2021) 'Deformation and permeability of recycled aggregate concrete – A comprehensive review', *Journal of Building Engineering*, 44, p. 103393.

Tam, V.W., Wang, Z.B. and Tao, Z. (2014) 'Behaviour of recycled aggregate concrete filled stainless steel stub columns', *Materials and Structures*, 47(1), pp. 293–310.

Topcu, I.B. & Sengel, S. (2004) 'Properties of concretes produced with waste concrete aggregate', *Cement and Concrete Research*, 34, pp. 1307–1312.

Wang, Y., Chen, J. and Geng, Y. (2015) 'Testing and analysis of axially loaded normal-strength recycled aggregate concrete filled steel tubular stub columns', *Engineering Structures*, 86, pp. 192–212.

Wang, Y., Wang, Q., Geng, Y. and Ranzi, G. (2016) 'Long-term behaviour of simply supported composite slabs with recycled coarse aggregate', *Magazine of Concrete Research*, 68(24), pp. 1278-1293.

Wang, Z., Zhong, Y. and Zhao, O. (2024) 'Circular recycled aggregate concrete-filled stainless steel tube stub columns after exposure to fire: Experiments, simulations, and design', *Engineering Structures*, 302, p. 117418.

Wang, Z., Zhong, Y., Jiang, K., Su, M. and Zhao, O. (2024a) 'Post-fire behaviour and resistances of square recycled aggregate concrete-filled stainless steel tube stub columns', *Thin-Walled Structures*, 197, p. 111564.

Wang, Z., Zhong, Y., Liang, Y. and Zhao, O. (2025) 'Global buckling and residual capacities of circular recycled aggregate concrete-filled stainless steel tube (RACFSST) columns after exposure to fire', *Engineering Structures*, 322, p. 119166.

Wang, Z., Zhong, Y., Su, A., Su, M. and Zhao, O. (2024b) 'Post-fire flexural buckling and resistances of square recycled aggregate concrete-filled stainless steel tube (RACFSST) columns', *Thin-Walled Structures*, 205, p. 112490.

Xiamuxi, A., Aosimanjiang, A. and Yang, B. (2023) 'Loading performance of reinforced and recycled aggregate concrete-filled circular steel tube short column with different steel ratios', *Construction and Building Materials*, 399, p. 132486.

Xiamuxi, A., Chen, H. and Liu, C. (2024) 'Flexural behaviour of reinforced and recycled aggregate concrete-filled square steel tubes', *Journal of Constructional Steel Research*, 221, p. 108891.

Xiao, J. & Falkner, H. (2007) 'Bond behaviour between recycled aggregate concrete and steel rebars', *Construction and Building Materials*, 21, pp. 395–401.

Xiao, J., Huang, Y., Yang, J. and Zhang, C. (2012) 'Mechanical properties of confined recycled aggregate concrete under axial compression', *Construction and Building Materials*, 26(1), pp. 591–603.

Xiao, J., Li, J. and Zhang, C. (2005) 'Mechanical properties of recycled aggregate concrete under uniaxial loading', *Cement and Concrete Research*, 35(6), pp. 1187–1194.

Xiao, J., Li, W., Fan, Y. and Huang, X. (2012a) 'An overview of study on recycled aggregate concrete in China (1996–2011)', *Construction and Building Materials*, 31, pp. 364–383.

Xiao, J., Wang, C., Ding, T. and Akbarnezhad, A. (2018) 'A recycled aggregate concrete high-rise building: Structural performance and embodied carbon footprint', *Journal of Cleaner Production*, 199, pp. 868–881.

Yang, D., Liu, F. and Wang, Y. (2023) 'Axial compression behaviour of rectangular recycled aggregate concrete-filled steel tubular stub columns', *Journal of Constructional Steel Research*, 201, p. 107687.

Yang, Y.F. & Han, L.H. (2006) 'Compressive and flexural behaviour of recycled aggregate concrete filled steel tubes (RACFST) under short-term loadings', *Steel and Composite Structures*, 6(3), p. 257.

Yang, Y.F. & Han, L.H. (2006a) 'Experimental behaviour of recycled aggregate concrete filled steel tubular columns', *Journal of Constructional Steel Research*, 62(12), pp. 1310–1324.

Yang, Y.F. & Hou, R. (2012) 'Experimental behaviour of RACFST stub columns after exposed to high temperatures', *Thin-Walled Structures*, 59, pp. 1–10.

Yang, Y.F. & Ma, G.L. (2013) 'Experimental behaviour of recycled aggregate concrete filled stainless steel tube stub columns and beams', *Thin-Walled Structures*, 66, pp. 62–75.

Yang, Y.F., Hou, C. and Liu, M. (2021) 'Tests and numerical simulation of rectangular RACFST stub columns under concentric compression', *Structures*, 27, pp. 396–410.

Yong, P.C. & Teo, D.C.L. (2009) 'Utilisation of recycled aggregate as coarse aggregate in concrete', *UNIMAS E-Journal of Civil Engineering*, 1(1), August.

Zhang, H., Geng, Y., Wang, Y. and Li, X. (2022) 'Experimental study and prediction model for bond behaviour of steel-recycled aggregate concrete composite slabs', *Journal of Building Engineering*, 53, p. 104585.

Zhang, H., Geng, Y., Wang, Y.Y. and Wang, Q. (2020) 'Long-term behaviour of continuous composite slabs made with 100% fine and coarse recycled aggregate', *Engineering Structures*, 212, p. 110464.

Zhang, H., Wang, Y., Wang, Q. and Geng, Y. (2022a) 'Experimental study and prediction model for non-uniform shrinkage of recycled aggregate concrete in composite slabs', *Construction and Building Materials*, 329, p. 127142.

Zhang, W.H., Wang, R., Zhao, H., Lam, D. and Chen, P. (2022b) 'Axial-load response of CFST stub columns with external stainless steel and recycled aggregate concrete: Testing, mechanism analysis and design', *Engineering Structures*, 256, p. 113968.

Zhao, H., Wang, Z., Zhang, W., Wang, R., Yang, D. and Lam, D. (2024) 'Performance of round-ended recycled aggregate CFST stub columns after fire exposure', *Journal of Constructional Steel Research*, 212, p. 108311.

Zhao, H., Zhang, W.H., Wang, R., Hou, C.C. and Lam, D. (2023) 'Axial compression behaviour of round-ended recycled aggregate concrete-filled steel tube stub columns (RE-RACFST): Experiment, numerical modelling and design', *Engineering Structures*, 276, p. 115376.

Zhong, Y. & Zhao, O. (2022) 'Behaviour of eccentrically loaded circular recycled aggregate concrete-filled stainless steel tube stub columns', *Journal of Constructional Steel Research*, 198, p. 107568.

Zhong, Y., Zhao, O. and Young, B. (2022) 'Experimental and numerical investigations of recycled aggregate concrete-filled stainless steel tube stub columns under combined compression and bending', *Engineering Structures*, 266, p. 114502.